

POLITECNICO DI TORINO

Master Degree
in Mathematical Engineering

Master's Thesis

**Uncertainty quantification of mechanical stiffnesses
in a base-shake sine test of a spacecraft**



Supervisors

Prof. Andrea Tosin
Prof. Mattia Zanella
Dr. Pietro Nali

Candidate

Matteo Defilippi

Academic Year 2019 - 2020

Acknowledgements

I would like to thank Prof. Andrea Tosin for the help and inspiration he has given me in these months of work on my thesis, Prof. Mattia Zanella for the availability and advice he has given me to improve my work. Both of them, with their experience, have accompanied me in this new and stimulating journey that has allowed me to understand the importance of the professional figure of the Mathematical engineer in the workplace. Moreover, I would like to thank Dr. Pietro Nali for his availability and his engineering skills in the aerospace world. I have been very lucky to work with helpful and highly competent people who have allowed me to achieve my goals. Thanks to my family who have always been by my side during the difficult moments of my university career, always pushing me to improve and aspire to the best for me and my future career. Mom and Dad if when I grow up I will be 1/10 of what you are now, then I can consider myself satisfied, Cristina if it wasn't for you, I would be alone.

A special thanks to Irene who has been by my side inspiring me with her tenacity and making me calm, happy and carefree, a necessary and sufficient condition for me to face everyday life and achieve my goals.

I would also like to thank Giulio Lucci, friend and esteemed colleague, all my friends of De Candidas, the Gin Tonic Boys and my colleagues at JEToP who have always been supportive and motivating to me and who have managed to make my university career happy and enjoyable. Thanks to my brothers and teammates from Collegno Rugby for making my evenings of escape from the studio hilarious and for the indestructible connection between us, among them I would like to mention Jacopo, Alessio and Stefano who have been a great inspiration for me.

Last but not least, my historical friends the PLTO who have been by my side since the first math test at the High School until the last university exam.

To be honest there would still be a lot of people to thank who have been by my side and have transmitted me positivity helping me, even if involuntarily, to do better and better. So with a sincere THANK YOU, I hope I can enclose you all.

Contents

1	Physical Model	1
1.1	The physical system	1
1.2	Geometry description	2
2	Uncertainty Quantification	5
2.1	Introduction to Stochastic Systems	5
2.1.1	Input Parameterization	6
2.2	Monte Carlo method	6
2.3	Generalized Polynomial Chaos	8
2.4	Stochastic Galerkin Method	9
2.5	Stochastic Collocation method	11
2.5.1	Lagrangian Interpolation approach	12
2.5.2	Pseudospectral approach	12
2.6	Benchmark case	13
2.6.1	Uniform case	14
2.6.2	Gaussian case	17
2.6.3	Exponential case	18
3	2-Degrees of Freedom	21
3.1	The Mathematical Model	21
3.1.1	Basic introduction of Modal Analysis	24
3.1.2	Application of the modal approach to the 2-dof satellite problem	28
3.2	Numerical Analysis	31
3.2.1	Initial Condition	32
3.3	2-DOF Stochastic System	33
3.3.1	Monte Carlo method	33
3.3.2	Collocation method	35
4	3-Degrees of Freedom	40
4.1	The Mathematical Model	40
4.1.1	Sweep approximation	44
4.1.2	Application of the modal approach to the 3-dof satellite problem	45
4.2	Numerical Analysis	46
4.2.1	Initial Conditions	47
4.3	3-DOF Stochastic System	49
4.3.1	Monte Carlo method	49
4.3.2	Collocation Method	51

5	Outcomes and future developments	55
A	Analytical Mechanics	58
A.1	Free coordinates and virtual displacements	58
A.1.1	Work	59
A.2	Static and virtual work principle	59
A.3	Kinetic Energy	60
A.4	Lagrangian Mechanics	61
A.4.1	The Lagrange Equations	61
A.4.2	Lagrangian Determinism	62
A.5	Linearization of the motion equations	63
B	Essentials of Probability Theory	65
B.1	Random variable	65
B.2	Probability Distributions	66
B.2.1	Discrete Distributions	66
B.2.2	Continuous Distributions	67
B.2.3	Expectation and Moments Theory	68
B.2.4	Convergence of Random Variables and Limit Theorems	69
B.3	Simulation of Random Variables	71
B.4	Statistical Tools	72
C	Integral calculus and Orthogonal Polynomials	73
C.1	Introduction to numerical integral calculus	73
C.2	Orthogonal Polynomials	75
C.3	Gaussian quadrature	77
C.4	Error estimation	78
D	Miscellaneous Topics	80
D.1	Runge-Kutta Method	80
D.2	Beta distribution and Gauss-Jacobi formula	80
D.3	1-Degree of Freedom	81
D.4	Equivalent oil meatus stiffness	82

Introduction

In the aerospace company, base-shake sine testing is a well-known technique used to study and analyze the dynamic characteristics of the spacecraft. Often, analyses of this kind are very expensive for the companies, so it is preferable to combine the analysis in the laboratory together with numerical simulations that can highlight trends not visible in the experimental tests.[18]

This type of simulations are based on finite element analysis with deterministic approaches, in which the properties of the shaking structure (shaker and seismic mass) are assigned a priori [13]. The latter are obtained with a retrospective approach, in phases prior to spacecraft testing with the so-called "dummy tests", i.e. vibrational tests in which the dynamic quantities of the target test (e.g. the spacecraft) are known. However, as accurate as this phase is, the deduction of these parameters is subject to unpredictable perturbations and the use of perturbed parameters can affect the numerical simulations made on the spacecraft.

These disturbances in the parameters can be due to a variety of causes. It is important to remember that the structure used for base-shake sine testing is located in a sterile place where quantities such as humidity and temperature are constantly monitored to allow the test to be as accurate as possible. On the other hand there are components of the shaking structure that are difficult to control and the dynamic characteristics of the latter may vary during testing.

Many components of the structure have the task of decoupling the vibrations of the satellite from the vibrations of the structure itself; in fact it has been demonstrated, through Virtual Shaker Testing (VST) [18]-[19], that the accelerations given as input to the structure do not correspond to those declared in the sine test specification. One of the most important effects is given by the dynamic coupling between shaker and test article.

It is, therefore, understood that there is unpredictable variability in the test and so a deterministic approach in the mathematical modelling and simulations of the vibration problem may be incomplete. The mathematical literature provides tools based on the uncertainty quantification in mathematical models with parameters perturbed by stochastic phenomena. [2]-[8]-[15]

Activities in the area of uncertainty quantification analysis for spacecraft do exist but are relatively limited and lack additional development and practical guidelines and procedures in order to be used in industrial practice. Recently, the European Space Agency (ESA) proposed two studies, EDIS (Enhancements of Dynamic Identification for Spacecraft), on stochastic correlation and validation of structural dynamic models, and ARVAN (Application of the Reliability Version of ASKA and NASTRAN), on probabilistic coupled dynamic analysis and structural reliability of satellites. Both studies, based on Monte Carlo Methods, are in progress under the technical management of the European Space Agency [9].

The aim of this thesis is to present a more accurate method of uncertainty quantification analysis than the Monte Carlo method (MC). In fact, as explained in more detail below, the number of sample M strongly influenced the accuracy of MC, in fact the rate convergence is equal to $O(M^{-1/2})$ [8]. In the literature, however, there are methods with a stronger accuracy such as

generalized polynomial chaos Stochastic Galerkin methods [4] and Stochastic Collocation Methods (SC) [2]. These approaches require a rather advanced mathematical treatment compared to Monte Carlo method. For this reason, we apply the SC to a simplified physical system. The complex consisting of the shaker, the seismic mass and the satellite is approximated as a system of rigid bodies.

The stiffness (and the corresponding damping) of the oil meatus represents the uncertain quantity on which we place the interest, approximated with a torsional spring. In the real physical system it is an under-pressure oil with the purpose of isolating the vibrating base, called slip table, from the seismic mass, i.e. a reinforced concrete structure where the shaker and the spacecraft rest.

The physical properties of the oil meatus are difficult to monitor precisely and their variation may not be detected, so the meatus assumes random characteristics. In addition, the unpredictable perturbations of the properties of the pressurized oil can influence the vibrations and the dynamic characteristics of the satellite. The most interesting datum in spacecraft analysis is the vibration resonance frequency, this depends on the structural properties of the test article.

The European Space Agency (ESA) imposes constraints on the resonance frequency to the manufacturers. As it can easily be imagined, the costs of building a spacecraft are far from superfluous and for this reason several tests are performed both experimental and numerical to ensure the ESA requirements. It is important for an aerospace company to know whether uncertainties about mechanical components can distort the test and influence the final result.

This thesis is organized in four main chapters: in the first we describe the physical system under examination with its geometrical approximations, while in the second chapter we introduce the methods of uncertainty quantification by comparing the results obtained on a benchmark case of aggregation/dispersion of a particle system identified by their speed in space. The use of a case-example like this one, is preparatory to understand some choices and hypotheses made through the thesis. In fact, in this benchmark case it is possible to calculate analytically the quantities of interest, e.g. the average, which are then compared with the numerical quantities obtained. The third and fourth chapters present the construction of the mathematical model and its motion equations using a rigorous formalism of Analytical Mechanics. Then numerical results of systems of deterministic parameter equations are presented. Finally, the stochastic methods presented within chapter 2 are applied to the physical system, assuming the stiffness of the oil meatus perturbed by a random variable with an assigned probability distribution.

Chapter 1

Physical Model

1.1 The physical system

The physical system studied in this thesis consists mainly of three elements: the seismic mass, the shaker body and the satellite. Figure 1.1 illustrates the FEM domain system useful to simulate the base-shake sine vibration test.

The *seismic mass* corresponds to a wide reinforced concrete structure, while the *shaker body* is an electrodynamic shaker, inside which there is a coil. The latter is often bought from external manufacturers who take care of the assembly and testing phase of the product; following the manual prepared by the manufacturer, the customer is able to obtain the various mechanical properties of the shaker body.

In this thesis we consider the LDS V994 shaker body, used by Thales Alenia Space (TAS) [23], it is represented in Fig 1.2.

The V994 is tied to a magnesium base called the *slip table*. The material is chosen for its

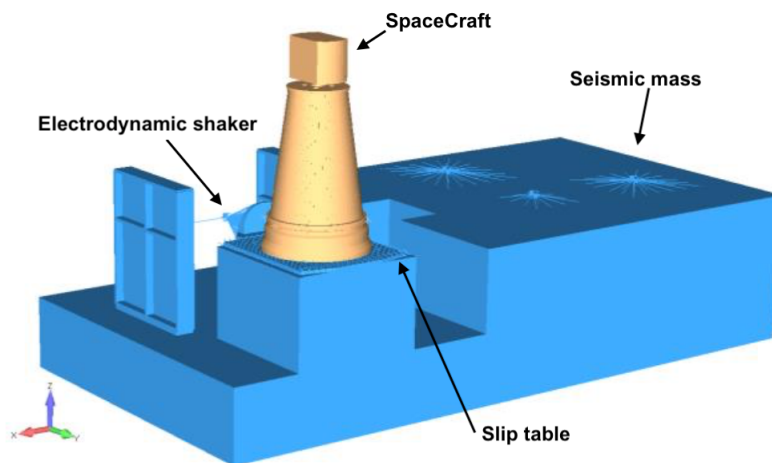


Figure 1.1: FEM domain representing the S/C+VTA assembly on TAS v994 shaker assembly, lateral configuration



Figure 1.2: The High force shaker LDS V994 made by Brüel and Kjær Sound and Vibration Measurement A/S[21].

lightness in order to avoid an overload on the coil.

The slip table is responsible for transmitting the movement made by the coil to the object placed on it, e.g. the spacecraft. However, it should be noted that the spacecraft is fixed to the table through the VTA, the Vibration Test Adapter.

Beneath the slip table there are bearings and the *oil meatus*, i.e. pressured oil which allows the slipping without friction between the solids. A marble base is placed under the slip table, the marble has a hardness and surface finish that allows the slipping through the oil. Finally, under the marble base there is a steel plate, which interfaces with the rest of the seismic mass in reinforced concrete.

The operation of a base-shake sine test is straightforward. The movement is impressed by the shaker body: the horizontal sinusoidal movement of the coil produces on the slip table an oscillating force, which causes the vibrations of the test item placed on it. The force applied is decided beforehand by the tester and is imposed in the form of a *sine sweep acceleration*, with the property of varying its oscillation frequency from an initial f_0 with a sweep rate R_f expressed in octaves/minutes [20].

The spacecraft (S/C) placed on the shaker assembly can have various shapes and dimensions, in this discussion we deal with medium-high S/C size (from 2.5 tons or $2.5 \cdot 10^3$ kg).

1.2 Geometry description

In the previous section the real physical system has been described. However, at a mathematical-mechanical level is useful to introduce some hypotheses and approximations in order to work and analyze the dynamic behavior of the spacecraft.

The first assumption consists in approximating the whole complex composed by the shaker assembly and the spacecraft to a system of rigid bodies; this allows us to considerably reduce the number of degrees of freedom (dofs). Moreover, the geometric characteristics of the S/C are not taken into account, indeed the VTA + S/C + slip table assembly is condensed into a rectangular object with inertia and whose mass is the sum of the three components.

From a mathematical-modelling point of view this is allowed, since the weight force is neglected. Note that all displacements are taken from the static equilibrium configuration, which means that the weight force does not have to be taken into account as it is balanced by the springs' static elastic return force [11]. Further, the forces that should be applied to the slip table, are exerted on the centre of gravity (CoG) of the condensed mass thus maintaining a modelling

consistency.

Let us introduce $\{\mathbf{i}_1, \mathbf{i}_2, \mathbf{i}_3\}$ a fixed system with origin in the CoG of the seismic mass, the point O ; then we indicate with m_1 the mass of the space craft and the Vibration Test Adapter (VTA), while the slip table (SL) is represented by m_2 . Therefore, the sum $m = m_1 + m_2$ is the condensed rigid body analysed in this thesis. We refer to the mass m as the *test-target* (or test-article) and to the mass M as the seismic mass.

The V994 shaker body, except the SL, is supposed to have neglected mass; however the coil function is approximated to a damped spring (k_b, c_b) and an external force, applied to the CoG of the slip table represented by the point B in Fig. 1.3.

The inertial properties of the seismic mass M are approximated by a damped spring (k_{st}, c_{st}) fixed in its CoG, the point O . The spring is introduced in order to avoid the excessive rotation of the mass.

The longitudinal distance between the CoG of the S/C and the CoG of the seismic mass is h_{2d} , while h_{1d} is the longitudinal distance between the CoG of the S/C+VTA and the CoG of the slip table. However, we will use the vertical CoG coordinate of the condensed mass, which is the point C , with the parameter Δh , see Fig. 1.4. In Fig. 1.1 - 1.3 it is observed that the slip table and the spacecraft are not positioned centrally with respect to O , this horizontal distance is represented by the parameter h_3 .

The oil meatus is represented in Fig. 1.3 by a grey coloured bearing, to which a stiffness and relative damping (k_{te}, c_{te}) is assigned (see Appendix D.4). However, at the mathematical modeling level it is approximated by a torsional spring with damping with one end tied to the mass m and the other to the seismic mass M . The stiffnesses k_b and k_{st} have been obtained from the numerical simulations of the partner company of this thesis. While k_{te} is the parameter that is supposed to be affected by random perturbations, later on. The rotational inertia of the

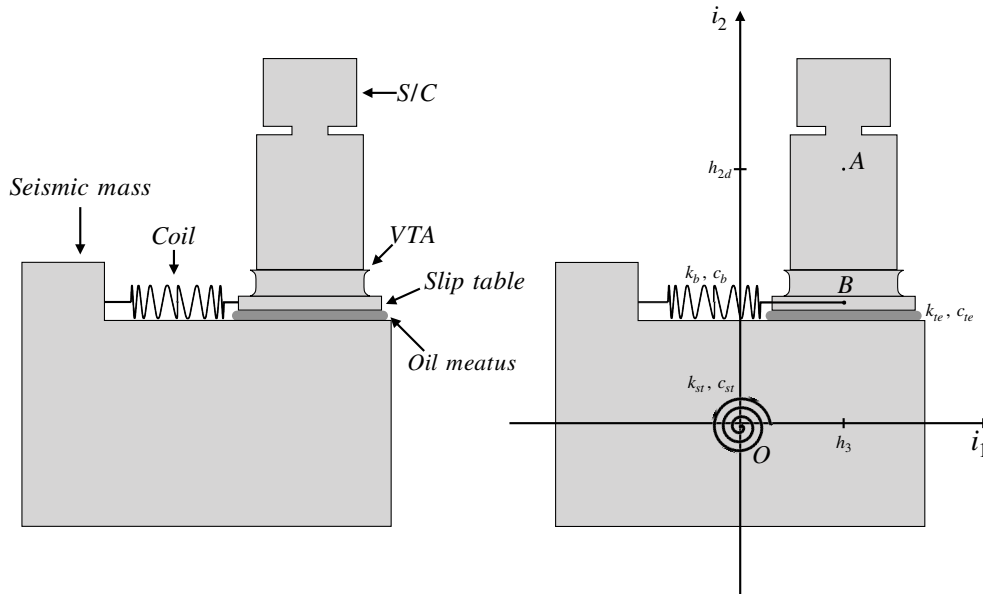


Figure 1.3: *The physical system in Fig. 1.1 in the y - z plane with the indicated components (on the left). The system with fixed cartesian reference system and the mechanical approximations (on the right).*

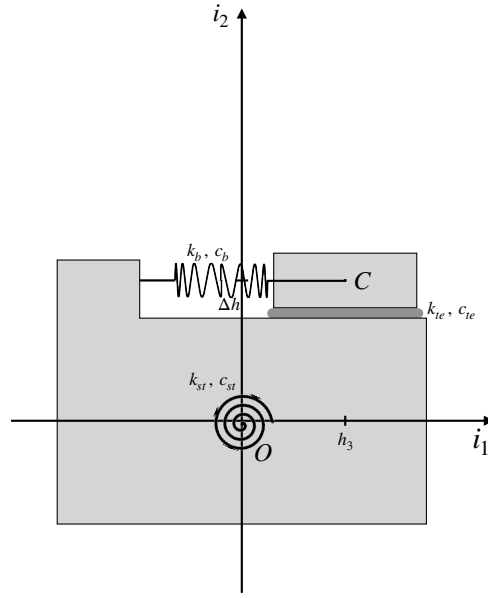


Figure 1.4: *The condensed physical system analysed, where C is the CoG of the S/C+VTA+ST assembly.*

	Description	Values	Unit of measure
k_{te}	Torsional oil meatus	$2.1535 \cdot 10^8$	N·m
k_b	Coil	10	N/m
k_{st}	Torsional M	10	N·m
m	Test-item mass	2730.337	kg
M	Seismic mass	$2.1439 \cdot 10^5$	kg
I_m	Inertia moment m	8086.645	kg·m ²
I_M	Inertia moment M	470229.1	kg·m ²
Δh	Vertical: $\overline{C - O}$	2.388718	m
h_3	Horizontal: $\overline{C - O}$	1.3438	m
R_f	Sweep rate	4	octave/min
f_0	Initial sweep frequency	5	Hz

Table 1.1: *Table of parameters*

seismic mass is I_M , while I_m is the moment of inertia of the test article.

Chapter 2

Uncertainty Quantification

This chapter is devoted to the formulation of ordinary differential equations (ODE) systems with random inputs/parameters and the solving approaches present in the literature. This type of differential equations are the basic tools for the uncertainty quantification (UQ). The UQ is concerned with estimating the impact of the uncertain input data on the model's outputs. It aims to enhance the model's usefulness by presenting an output in a probabilistic framework. This propagation of uncertainty through the model allows additional uncertainty analyses such as determining and/or reducing the principal contributors to the output uncertainties. Some of the most popular numerical methods for ODE in UQ studies will be presented, following [8] and [2]-[3]. Moreover, in order to clarify the concept we present a benchmark example, which will be particularly useful to emphasize some properties of the presented methods. A review of the basic theories of probability and numerical integration is in the Appendices B and C respectively.

2.1 Introduction to Stochastic Systems

Let (Ω, \mathcal{F}, P) be a complete probability space and $\omega \in \Omega$ is an event. Consider a d -dimensional boundary domain $\mathcal{D} \subset \mathbb{R}^d$, $d = 1, 2, 3$, with boundary $\partial\mathcal{D}$. The time domain is $[0, T]$ with $T > 0$. The problem is to find a solution as

$$u(x, \omega, t) : \bar{\mathcal{D}} \times [0, T] \times \Omega \rightarrow \mathbb{R} \quad (2.1)$$

of the differential system

$$\mathcal{L}(x, \omega, t; u) = f(x, \omega, t), \quad x \in \mathcal{D} \quad (2.2)$$

subject to the boundary condition

$$\mathcal{B}(x, \omega, t; u) = g(x, \omega, t), \quad x \in \partial\mathcal{D} \quad (2.3)$$

where (x_1, \dots, x_d) are the coordinate in \mathbb{R}^d . In details that \mathcal{L} is a differential operator, while \mathcal{B} is a boundary operator and $\partial\mathcal{D}$ is sufficiently regular to allow the differential problem to be well posed.

Let us consider an ordinary differential equation (ODE) defined as follows:

$$\begin{cases} \frac{d}{dt}u(\omega, t) = -\alpha(\omega)u \\ u(\omega, 0) = \beta(\omega) \end{cases} \quad (2.4)$$

where α, β are two random variables, and α is the uncertain rate and β is the uncertain initial condition. If the distribution function of α and β is known, i.e. $F_{(\alpha, \beta)}$, it is possible to evaluate statistical quantities; note that if they are independent $F_{(\alpha, \beta)} = F_\alpha F_\beta$. Therefore, the solution of the system (2.4) is a random quantity

$$u(\omega, t) : [0, T] \times \Omega \rightarrow \mathbb{R} \quad (2.5)$$

whose exact solution is

$$u(\omega, t) = \beta(\omega)e^{-\alpha(\omega)t} \quad (2.6)$$

Since the solution u of the problem (2.4) depends on random variables, we are interested in the so-called quantities of interest of the problem, i.e. the expectation of the solution defined as

$$\begin{aligned} \mathbb{E}(u(\omega, t)) &= \mathbb{E}(\beta e^{-\alpha t}) \\ &= \mathbb{E}(\beta)\mathbb{E}(e^{-\alpha t}), \quad (\text{if } \alpha, \beta \text{ independent}) \end{aligned} \quad (2.7)$$

2.1.1 Input Parameterization

Prior to any numerical experiments, is essential to characterize the random input, i.e. reduce an infinite-dimensional probability space to a useful finite-dimensional space or, more crucial, require that the random variable are mutually independent.

We firstly introduce the *parameterization procedure* whereby it is possible to parameterize a set of variable $Y = (Y_1, \dots, Y_n)$, $n > 1$, with distribution function F_Y , as $Y = T(Z)$ where T is a transformation function and $Z = (Z_1, \dots, Z_d)$, $1 \leq d \leq n$ a set of mutually independent random variable.

Note that if α and β are independent $Y(\omega) = (\alpha, \beta) = Z(\omega) \in \mathbb{R}^2$ and the solution becomes

$$u(Z, t) : [0, T] \times \mathbb{R}^2 \rightarrow \mathbb{R} \quad (2.8)$$

while if they are not independent it is possible to find a $Z(\omega)$ such that

$$\alpha(\omega) = \alpha(Z(\omega)), \quad \beta(\omega) = \beta(Z(\omega))$$

or there is a function g such that $\beta = g(\alpha)$, and so $Y(\alpha, g(\alpha)) \in \mathbb{R}$, the solution can be expressed with a single random variable as

$$u(Z, t) : [0, T] \times \mathbb{R} \rightarrow \mathbb{R} \quad (2.9)$$

2.2 Monte Carlo method

Monte Carlo (MC) method is one of the widely used numerical method to compute statistical quantities. It is easy to implement and with a straightforward interpretation, although due to its robustness the MC method can be extremely slow. The MC method integration converges with a rate of $O(M^{-1/2})$, where M in the number of samples.

The reasons why MC method is so heavily exploited are: it does not require information of uncertainty distribution, so it can be used directly on experimental observations. Furthermore, the Monte Carlo method is able to manage well the increase of dimension of the uncertainty without any kind of complication in its formulation, finally, the Monte Carlo method always gives a qualitatively correct answer.

For example, the integral of a Lebesgue integrable function $h(Z)$ can be expressed as the average or the expectation of the function h as follows

$$\mathbb{E}(h(Z)) = I(h) = \int h(z)g_Z(z)dz \quad (2.10)$$

where Z is a random variable with probability density g_Z .

The Monte Carlo method is based on the probabilistic interpretation of an integral. Consider a sequence $\{z_n\}$ of realizations of a the random variable Z with the density g_Z . The empirical approximation of the expectation as

$$I_M(h) = \frac{1}{M} \sum_{k=1}^M h(z_k) \quad (2.11)$$

note it is unbiased, which means the average on $I_M(h)$ is exactly $I(h)$.

The Monte Carlo integration error is

$$\varepsilon_M(h) = I(h) - I_M(h) \quad (2.12)$$

and for the Central Limit Theorem (presented and demonstrated in the Appendix B) we have that

$$\varepsilon_M(h) \approx \sigma M^{-1/2} \nu \quad (2.13)$$

where ν is a $N(0,1)$, while σ is the standard deviation of $h(Z)$. In [8] there is an in-depth analysis of the Monte Carlo method, here we present a brief proof that proves that the error size is $O(M^{-1/2})$. This proof follows from the Central Limit Theorem (CLT).

Let we define $\zeta_i = (h(z_i) - \bar{h})/\sigma$ for z_i uniformly distributed, where \bar{h} is defined in (2.10). Then

$$\begin{aligned} \mathbb{E}(\zeta_i) &= 0, \\ \mathbb{E}(\zeta_i^2) &= \int_0^1 \sigma^{-2}(h(z_i) - \bar{h})^2 dz = 1, \\ \mathbb{E}(\zeta_i \zeta_j) &= 0, \quad \text{if } i \neq j \end{aligned}$$

Following the CLT, we now consider sum

$$S_M = \frac{1}{M} \sum_{i=1}^M \zeta_i = \sigma^{-1} \varepsilon_M$$

and its standard deviation is

$$\begin{aligned} \mathbb{E}(S_M^2)^{1/2} &= \mathbb{E} \left(\frac{1}{M^2} \left(\sum_{i=1}^M \zeta_i \right)^2 \right)^{1/2} \\ &= M^{-1} \left(\mathbb{E} \left(\sum_{i=1}^M \zeta_i^2 \right) + \mathbb{E} \left(\sum_{i=1}^M \sum_{j \neq i} \zeta_i \zeta_j \right) \right)^{1/2} \\ &= M^{-1} \left(\sum_{i=1}^M 1 \right)^{1/2} = M^{-1/2} \end{aligned}$$

Therefore

$$\mathbb{E}(\varepsilon_M^2) = \sigma M^{-1/2}$$

In conclusion, the general procedure of the Monte Carlo sampling method used to solve ordinary differential equations with uncertain parameters as (2.4) follows three basic steps

- Generate identically and independently distributed random (or pseudo-random) numbers $z_k = (\alpha_k, \beta_k)$, $k = 1, \dots, M$, according with the probability distribution $F_{(\alpha, \beta)}$ and density $f_{(\alpha, \beta)}$.
- For each $k = 1, \dots, M$ solve the problem (2.4) with a numerical method and obtain $u(z_k, t)$
- Estimate the required solution statistics, as mean or variance. For example, the solution of the mean is

$$\mathbb{E}(u(t)) \approx \bar{u}(t) = \frac{1}{M} \sum_{k=1}^M u(z_k, t) \quad (2.14)$$

that is an unbiased approximation of (2.7). While the variance is

$$\text{Var}(u(t)) \approx \frac{1}{M-1} \sum_{k=1}^M (u(z_k, t) - \bar{u}(t))^2$$

2.3 Generalized Polynomial Chaos

A fundamental principle in the construction of numerical methods alternative to the Monte Carlo Method is the concept of *Generalized Polynomials Chaos* (gPC) [4]-[15]. The material from here until the end of the chapter is largely based on [2] but we used the notation consistent with [10] to indicate polynomials. Let Z a continuous random variable with distribution $F_Z(z)$ and probability density $f_Z(z)$, then suppose that all the moment exist and they are finite. Let us define a Hilbert space

$$L^2(I_Z) = \{f : I_Z \subseteq \Omega \rightarrow \mathbb{R} : \mathbb{E}(f^2) < \infty\}$$

and a polynomial set as

$$\{P_0(Z), P_1(Z), \dots, P_n(Z), \dots\} \quad (2.15)$$

the gPC are orthogonal polynomials that satisfy the following definition

$$\mathbb{E}(P_m(Z)P_n(Z)) = \int P_m(Z)P_n(Z)f_Z(z)dz = h_n\delta_{nm}, \quad n, m = 1, 2, \dots \quad (2.16)$$

where δ_{nm} is the kronecker delta and

$$E(P_n(Z)^2) = \int P_n^2(Z)f_Z(z)dz = h_n, \quad n = 1, 2, \dots \quad (2.17)$$

It is observed that the theory just cited is equivalent to the definition of orthogonal polynomials in the numerical approximation of integral described in Appendix C. Note that $\{P_n(Z)\}$, with $n = 1, 2, \dots$ has the property of being a base made of orthogonal polynomials for $L^2(\Omega)$, in which the density of the random variable acts as a weight function. This establishes a correspondence between the distribution of the random variable Z and the type of *classical* orthogonal polynomial present in literature:

- *Legendre* Polynomial chaos if $Z \sim U(a, b)$ where

$$f_Z(z) = \frac{1}{b-a}\chi_{[a,b]}(z) \quad (2.18)$$

- *Laguerre* Polynomial chaos if $Z \sim \text{Exp}(\lambda)$ where

$$f_Z(z) = \lambda e^{-\lambda z} \quad (z > 0) \quad (2.19)$$

- *Hermite* Polynomial chaos if $Z \sim N(\mu, \sigma^2)$ where

$$f_Z(z) = \frac{1}{\sqrt{2\pi\sigma^2}} \exp\left[-\frac{(z-\mu)^2}{2\sigma^2}\right], \quad (z \in \mathbb{R}) \quad (2.20)$$

- *Jacobi* Polynomial chaos if $Z \sim \text{Beta}(\alpha, \beta)$ where

$$f_Z(z) = \frac{(b-z)^\alpha (z-a)^\beta}{(b-a)^{(\alpha+\beta+1)} B(\alpha+1, \beta+1)}, \quad z \in [a, b], \quad \alpha, \beta > -1 \quad (2.21)$$

In conclusion, functions of the random variable Z can be approximated using a basis function; this is ensured by the orthogonality property defined in (2.16). The approximation is guaranteed by the following to results.

Definition 2.1 (Strong gPC approximation). Let $h(Z)$ be a function of random variable Z with probability distribution $F_Z(z)$. A generalized polynomial chaos in a strong sense is $h_n(Z) \in \mathbb{P}_n(Z)$, where $\mathbb{P}_n(Z)$ is the polynomial space of Z of degree up to $n \geq 0$, such that

$$\|h(Z) - h_n(Z)\| \rightarrow 0, \quad n \rightarrow \infty \quad (2.22)$$

in a proper norm defined in \mathcal{I}_Z

Definition 2.2 (Weak gPC approximation). Let Y be a random variable with probability distribution $F_Y(y)$ and let S be a standard random variable in a set of gPC basis functions. A weak generalized polynomial chaos approximation is $Y_n \in \mathbb{P}_n(S)$ such that Y_n converges to Y in a weak sense, e.g.

$$Y_n \xrightarrow{P} Y \quad (2.23)$$

2.4 Stochastic Galerkin Method

The generalized polynomial chaos (gPC) stochastic Galerkin method is an extension of classical Galerkin approach for deterministic equations [2]. Let us use the ODE system defined in (2.4) where the initial condition is assumed deterministic then

$$\begin{cases} \frac{d}{dt}u(Z, t) = -\alpha(Z)u(Z, t) \\ u(Z, 0) = \beta \end{cases} \quad (2.24)$$

where Z is a random variable. If the u solution is sufficiently regular in $L^2(\Omega)$, a Hilbert space, then it admits a base of the type $\{P_k(Z)\}$, this is also called gPC base function satisfying (2.16). Then the gPC projection of the solution is

$$u_M(Z, t) = \sum_{k=0}^M \hat{u}_k(t) P_k(Z), \quad \forall t \geq 0 \quad (2.25)$$

the expansion coefficient is defined as

$$\hat{u}_k(t) = \frac{1}{h_k} E(u(Z, t) P_k(Z)) \quad (2.26)$$

where $h_k = \|P_k\|_{L^2}^2$ defined in (2.17).

Let us suppose that the constant function $\alpha(Z)$ of the random variable Z can be expressed as

$$\alpha_M(Z) = \sum_{m=0}^M a_m P_m(Z) \quad (2.27)$$

however, if it does not exist, one can use numerical quadrature rules with a sufficient number of points.

Exploiting the gPC M -th degree approximation $u_M(Z, t) \approx u(Z, t)$ is possible to replace it in (2.24) system obtaining

$$\begin{aligned} \frac{d}{dt} u_M(Z, t) &= -\alpha_M(Z) u_M(Z, t) \\ \frac{d}{dt} \sum_{k=0}^M \hat{u}_k(t) P_k(Z) &= - \sum_{m=0}^M a_m P_m(Z) \sum_{k=0}^M \hat{u}_k(t) P_k(Z) \\ \frac{d}{dt} \sum_{k=0}^M \hat{u}_k(t) P_k(Z) &= - \sum_{m=0}^M \sum_{k=0}^M a_m \hat{u}_k(t) P_k(Z) P_m(Z) \end{aligned} \quad (2.28)$$

The gPC Galerkin procedure provides that

$$E \left(\frac{d}{dt} u_M(Z, t) P_j(Z) \right) = E(-\alpha_M(Z) u_M(Z, t) P_j(Z)), \quad \forall j = 1, \dots, M \quad (2.29)$$

upon substituting the (2.28) expression for α_M and u_M in (2.29), we obtain

$$\begin{aligned} E \left(\frac{d}{dt} \sum_{k=0}^M \hat{u}_k(t) P_k(Z) P_j(Z) \right) &= -E \left(\sum_{m=0}^M \sum_{k=0}^M a_m \hat{u}_k(t) P_k(Z) P_m(Z) P_j(Z) \right) \\ \frac{d}{dt} \hat{u}_j(t) &= \frac{1}{h_j} \sum_{m=0}^M \sum_{k=0}^M e_{mkj} a_m \hat{u}_k(t), \quad \forall j = 1, \dots, M \end{aligned} \quad (2.30)$$

where $\hat{u}_k(t)$ is defined by the expression (2.26) and

$$e_{mkj} = E(P_m(Z) P_k(Z) P_j(Z)), \quad m, k, j = 1, \dots, M \quad (2.31)$$

The system (2.30) is a system of coupled deterministic ordinary differential equations (ode) in the variable $\{\hat{u}_j(t)\}$ with initial condition

$$\hat{u}_j(0) = b_j, \quad \forall j = 1, \dots, M, \quad \text{where} \quad \beta_M = \sum_{k=1}^M b_k P_k(Z) \quad (2.32)$$

the size of this system is $M+1$, it can be solve with classical numerical method, e.g. Runge-Kutta method.

The Stochastic Galerkin method approach in the calculation of the quantities of interest is clearly different from that used by the Monte Carlo method. In fact, is introduced the probability distribution chosen for the variable Z , the uncertainty, which was not present in the MC method. This introduction is far from trivial, in fact it allows to calculate more accurately the quantities of interest, making, however, the method less general; on the other hand, the great power of MC lies in its malleability and in the fact that, if we can not have any kind of information on the

distribution of uncertainty, but we have given experimental, through the empirical approach it is possible to calculate qualitatively correct quantities. The MC method can, with a bit of abuse, be considered a useful brute force method to be used in borderline situations, however it is not an accurate method as we describe previously and if it is possible to know the distribution of uncertainty then it is not recommended. In the literature there are some improvements of the MC methods, but are not taken into consideration in this thesis, see [8].

2.5 Stochastic Collocation method

The methods of solving systems of stochastic differential equations presented so far have shown, on one hand, a immediate implementation at the expense of a low convergence speed equal to $O(M^{-1/2})$ (Monte Carlo methods); on the other hand there is a very high convergence speed, although, the formulation and implementation require much greater mathematical complexity (Stochastic Galerkin methods). For these reasons, we present the Stochastic Collocation Method (SC), proposed in [3]. Exploiting the numerical theory on integral calculus, the stochastic collocation methods achieves fast convergence when the solutions is sufficient smooth, as Stochastic Galerkin methods. Nevertheless, collocation methods require solutions of the corresponding deterministic problems at each points (called *collocation nodes*), similar to Monte Carlo methods, this yields the implementations of SC simple. Such properties make these methods a good alternatives to those presented previously.

Let us take the system defined in (2.24) with deterministic initial condition

$$\begin{cases} \frac{d}{dt}u(Z, t) = -\alpha(Z)u(Z, t) \\ u(Z, 0) = \beta \end{cases} \quad (2.33)$$

where Z is a random variable in $I_Z \subset \mathbb{R}^d$, $d = 1, 2, 3$. Let $\{z_j\}_{j=1}^R \subset I_Z$ be a set of nodes, where $R > 1$ is the number of *collocation nodes*. Then for each $j = 1, \dots, R$ we have to solve at the node z_j the ode system

$$\begin{cases} \frac{d}{dt}u(z_j, t) = -\alpha(z_j)u(z_j, t) \\ u(z_j, 0) = \beta \end{cases} \quad (2.34)$$

since that value of Z is fixed the differential problem is deterministic and for this reason with the ensemble $\{u_j\}_{j=1}^R$ of the solutions, where $u_j = u(\cdot, z_j)$, it is possible to apply post-processing operations in order to obtain useful stochastic quantities. Moreover, if we find $w(Z) \in W(Z)$, where $W(Z)$ is a polynomial space, such that

$$\|w(Z) - u(Z)\| \rightarrow 0, \quad R \rightarrow \infty \quad (2.35)$$

which means $w(Z)$ is a good approximation of $u(Z)$, where the norm is typically a L^p norm with $p \geq 1$.

Note that the problem (2.34) for each j is naturally decoupled. This is in direct contrast to the stochastic Galerkin approaches, where the resulting expanded equations in the (2.30) are, in general, coupled.

There are two major approach for SC methods: *interpolation approach* and *pseudospectral approach*.

2.5.1 Lagrangian Interpolation approach

Let $\{z_j\}_{j=1}^R$ be the nodal set, the Lagrangian basis polynomials is defined as

$$l_j(Z) = \prod_{\substack{m=1 \\ m \neq j}}^R \frac{Z - z_m}{z_j - z_m} \quad (2.36)$$

where

$$l_j(z_i) = \delta_{ij}, \quad 1 \leq i, j \leq R \quad (2.37)$$

Solving the the ode system the ensemble of solutions $\{u_j\}_{j=1}^R$ is obtained. Then focal point of the Lagrangian interpolation approach for stochastic collocation method is to find the polynomial $w(Z) \in W(Z)$ that is a good approximation of $u(Z)$ such that $w(z_j) = u^{(j)}$ for each j and

$$w(Z) = \sum_{j=1}^R u(z_j) l_j(Z) \quad (2.38)$$

is important to observe that even if the method has a straightforward formulation, it can become nontrivial in practice.

Once all the collocation points are obtained, the statistics of the random solution can be evaluated, e.g.,

$$\mathbb{E}(w(Z)) = \sum_{j=1}^R w(z_j) \int_{I_Z} l_j(Z) f_Z(z) dz \quad (2.39)$$

2.5.2 Pseudospectral approach

The discrete projection or pseudospectral approach for the stochastic collocation methods is based on approximate, by an integration rule as the quadrature formulas, the expansion coefficient:

$$\hat{u}_k(t) = \frac{1}{h_k} \mathbb{E}(u(Z, t) P_k(Z)) \quad (2.40)$$

of the continuous generalized polynomial chaos (gPC) projection of the solution of the problem (2.34)

$$u_M(Z, t) = \sum_{k=0}^M \hat{u}_k(t) P_k(Z), \quad \forall t \geq 0. \quad (2.41)$$

Recall that a *quadrature rule* is an approximation of an integral by

$$\int_{I_Z} g(z, t) f_Z(z) dz \approx \sum_{i=1}^R p_i g(z_i, t) \quad (2.42)$$

It is an interpolation formula, where $\{z_i\}$ are the nodes obtained as the R zeros of the $P_R(Z)$, the orthogonal polynomial to the weight function $f_Z(z)$, and p_i are the corresponding weights. Therefore, the pseudospectral gPC projection of solution is

$$w_M(Z, t) = \sum_{k=0}^M \hat{u}_k(t) P_k(Z), \quad \forall t \geq 0 \quad (2.43)$$

where the expansion coefficient is approximated as

$$\hat{w}_k(t) = \frac{1}{h_k} \sum_{i=1}^R p_i u(z_i, t) P_k(z_i) \quad (2.44)$$

Moreover, if the quadrature rule is convergent, then $\hat{w}_k(t) \rightarrow \hat{u}_k(t)$, for all t, k and for $R \rightarrow \infty$, thereby w_n and u_n become identical $\forall Z$.

It is important to observe that in Stochastic Collocation method the distribution of collocation points is fixed deterministically a priori and is determined through the aid of existing theory polynomial interpolation (or integration). Furthermore, by constructing the appropriate polynomial interpolations, SC method can achieve fast convergence, even exponential convergence under sufficient smoothness conditions, similar to stochastic Galerkin methods. However, the method finds difficulties when the uncertainty dimensionality increases. In fact the error of the SC method is proportional to $O(R^{-\alpha/d})$ where R is the number of nodes, $\alpha > 0$ is a constant that depends on the smoothness of the solution and $d > 1$ is the size of the uncertainty. This brings a notable complication since every collocation point requires a deterministic system simulation, bringing a considerable increase of the computational times. And for $d \gg 1$ the rate of convergence deteriorates drastically. This is the well-known "*curse of dimensionality*".

In order to make the SC method a good alternative in high-dimensional to MC it necessary to reduce the number of collocation nodes. In [2] and [3] algorithms to build scattered grids of points to keep high order of accuracy by the SC, are presented. For example, in [3] it is shown that for random dimensions $d = 50$, the stochastic collocation methods (using both Stroud's methods and Smolyak methods for sparse grid) are more efficient than brute-force Monte Carlo methods.

2.6 Benchmark case

This section presents a simple system of ordinary differential equations in order to clarify the concepts just mentioned in the previous sections, following [16]. Moreover, this simple example will be particularly useful later on, when we will have to describe the dynamic behavior of the physical system at the core of this thesis; in fact, some hypotheses and assumptions that will be placed in the following chapters are, in part, justified in this section. Let us define a set of N particles their behavior is described by an ode system where v_i is the velocity of the i -th particle, $i = 1, \dots, N$. Although, the latter is a function of Z , a stochastic variable with probability density g_Z as

$$v_i = v_i(Z, t), \quad \forall i = 1, \dots, N \quad (2.45)$$

The governing equation of the system is

$$\frac{d}{dt} v_i(Z, t) = \frac{1}{N} \sum_{j=1}^N k(Z, t) [v_j - v_i] \quad (2.46)$$

with initial conditions

$$v_i(Z, t) = v_i^0, \quad \forall i = 1, \dots, N. \quad (2.47)$$

Let us define $V(Z) = N^{-1} \sum_{j=1}^N v_j(Z, t)$. We can prove that

$$\begin{aligned} \frac{d}{dt} \frac{1}{N} \sum_{i=1}^N k(Z, t) v_i(Z, t) &= \frac{1}{N} \sum_{i=1}^N k(Z, t) [V(Z) - v_i(Z, t)] \\ &= k(Z, t) V(Z) - \frac{1}{N} \sum_{i=1}^N k(Z, t) v_i(Z, t) \\ &= 0, \\ \frac{d}{dt} V(Z) &= 0 \quad \Rightarrow \quad V(Z) = V \end{aligned}$$

Therefore, we can rewrite the system as

$$\begin{aligned} \frac{d}{dt} v_i(Z, t) &= \frac{1}{N} \sum_{j=1}^N k(Z, t) [v_j - v_i] \\ &= k(Z, t) [V - v_i] \end{aligned} \tag{2.48}$$

Integrating in time the (2.48) we obtain the solution

$$v_i(Z, t) = V + (v_i^0 - V) e^{-\int_0^t k(Z, s) ds} \quad \forall i = 1, \dots, N \tag{2.49}$$

Let's now suppose that we can separate the stochastic part from the time depending part in $k(Z, t)$ as

$$k(Z, t) = k(Z)h(t) \tag{2.50}$$

and we assume that $k(Z) = Z$.

We would like to calculate the expected velocity of the i -th particle

$$\mathbb{E}(v_i(Z, t)) = \int_{I_Z} v_i(z, t) g_Z(z) dz \tag{2.51}$$

In conclusion, by substituting the (2.49) in (2.51) we obtain that

$$\mathbb{E}(v_i) = \int_{I_Z} (V + (v_i^0 - V) e^{-z \int_0^t h(s) ds}) g(z) dz \tag{2.52}$$

Therefore based on the probability distribution we will have different behaviors, let we describe a few case with different characteristics.

2.6.1 Uniform case

Let us define $Z \sim U[a, b]$ such that

$$g_Z(z) = \frac{1}{b-a} \chi_{[a,b]}(z) \tag{2.53}$$

upon substituting the probability density in (2.52) we obtain:

$$\begin{aligned} \mathbb{E}(v_i) &= V + (v_i^0 - V) \int_{I_Z} \exp \left[-z \int_0^t h(s) ds \right] \frac{1}{b-a} \chi_{[a,b]}(z) dz \\ &= V + \frac{(v_i^0 - V)}{(b-a)} \int_a^b \exp \left[-z \int_0^t h(s) ds \right] dz \\ &= V + \frac{(v_i^0 - V)}{(b-a)} \frac{\exp \left[-a \int_0^t h(s) ds \right] - \exp \left[-b \int_0^t h(s) ds \right]}{\int_0^t h(s) ds} \end{aligned} \tag{2.54}$$

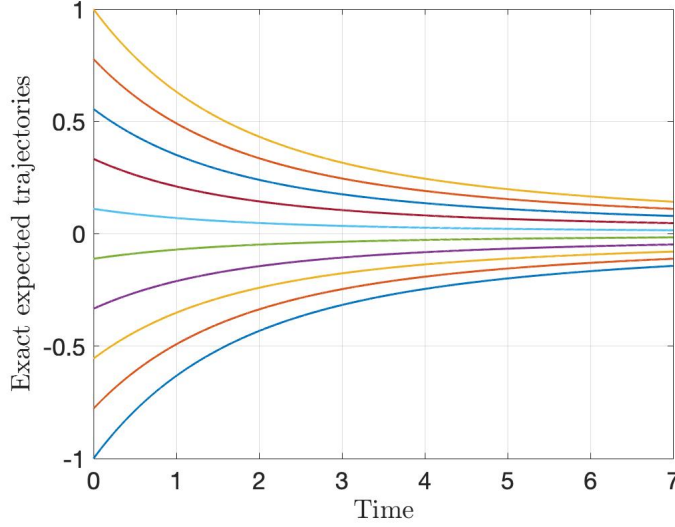


Figure 2.1: *Uniform case: The evolution of the exact expected trajectories $v_i(t)$ (2.56).*

Assuming that the stochastic parameter of the system is time-independent, i.e. $h(t) = 1$. We have

$$\mathbb{E}(v_i) = V + (v_i^0 - V) \frac{e^{-at} - e^{-bt}}{(b-a)t} \quad (2.55)$$

The standard case is with $a = 0$ and $b = 1$; thereby, the equation (2.55) becomes

$$\mathbb{E}(v_i) = V + \frac{(v_i^0 - V)}{t} (1 - e^{-t}) \quad (2.56)$$

The equations (2.55)-(2.56) represent the analytical expression of the mean velocity obtain by the ode system (2.48). However, this system can be solved by numerical integrating methods as Runge-Kutta, but this type of methods have to be tailored to ordinary differential equations (ODE) with random input/parameter.

Let we start with the traditional methods, the Monte Carlo sampling, following the three steps cited above

- Generate i.i.d random (or pseudo-random) numbers z_1, \dots, z_M , according with the probability distribution G_Z and density g_Z .
- For each $k = 1, \dots, M$ solve the problem (2.48) with a numerical method (Runge-Kutta) and obtain $v_i(z_k, t)$ for each i -th particle
- Estimate the required solution statistics, as mean or variance.

Then the mean velocity of the i -th particle obtained with MC is

$$\bar{v}_i(t) = \frac{1}{M} \sum_{k=1}^M v_i(z_k, t), \quad \forall t \geq 0 \quad (2.57)$$

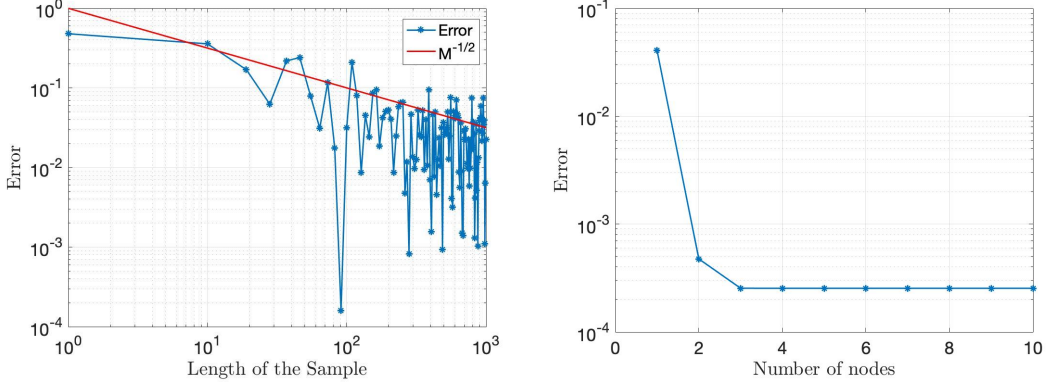


Figure 2.2: *Uniform case: The convergence of the error in the MC in loglog scale (on the left), compared with the error in SC in semilog scale (on the right). Calculated at $t = 1.5$.*

and the variance is

$$\text{Var}(v_i(t)) = \frac{1}{M-1} \sum_{k=1}^M (v_i(z_k, t) - \bar{v}_i(t))^2, \quad \forall t \geq 0 \quad (2.58)$$

where $\bar{v}_i(t)$ in (2.58) is obtained with (2.57).

As already mentioned in the previous sections, MC is extremely simple, at a practical level; but it only exploits a sequence of realizations of a random variable and its mathematical treatment does not show the origin of a particular probabilistic distribution. Moreover, the convergence error is $O(M^{-1/2})$ due to the Central Limit Theorem. Therefore, we notice the need to use another numerical approach, the Stochastic Collocation method (SC).

Let us rewrite the definition of the expectation of the velocity defined in (2.51), substituting the probability density (2.53) as

$$\mathbb{E}(v_i) = \int v_i(z, t) \frac{1}{b-a} \chi_{[a,b]}(z) dz = \frac{1}{b-a} \int_a^b v_i(z, t) dz \quad (2.59)$$

numerically the integral can be approximated using the *Gauss-Legendre Formula*.

So, let $\{(z_k, w_k)\}_{k=1}^M$ be a set of nodes in the random space $I_Z = [a, b]$ and their corresponding weights. Solving the deterministic ode for $v_i(z_k, t)$, for each $k = 1, \dots, M$, the integral is approximate as

$$\mathbb{E}(v_i) = \frac{1}{b-a} \int_a^b v_i(z, t) dz \approx \frac{1}{b-a} \sum_{k=1}^M w_k v_i(z_k, t) \quad (2.60)$$

and the variance is calculated using the second moment as

$$\text{Var}(v_i(t)) = \frac{1}{b-a} \int_a^b v_i(z, t)^2 dz - \bar{v}_i(t)^2 \quad (2.61)$$

where $\bar{v}_i(t)$ in (2.61) is obtained with (2.60).

If $Z \sim U[0,1]$

$$\mathbb{E}(v_i) = \int_0^1 v_i(z, t) dz \approx \sum_{k=1}^M w_k v_i(z_k, t) \quad (2.62)$$

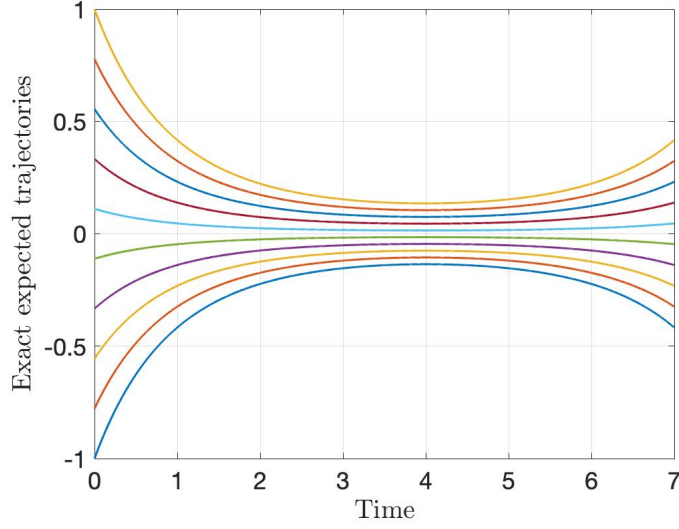


Figure 2.3: *Gaussian case: The evolution of the exact expected trajectories $v_i(t)$ (2.64), with $h(s) = 1$ and $\mu = 1$, $\sigma = 0.5$*

2.6.2 Gaussian case

Let us consider $Z \sim N(\mu, \sigma^2)$, where

$$g_Z(z) = \frac{1}{\sqrt{2\pi\sigma^2}} \exp\left[-\frac{(z-\mu)^2}{2\sigma^2}\right] \quad (2.63)$$

The (2.52) becomes

$$\begin{aligned} \mathbb{E}(v_i) &= V + \frac{(v_i^0 - V)}{\sqrt{2\pi\sigma^2}} \int_{I_Z} \exp\left[-z \int_0^t h(s) ds\right] \exp\left[-\frac{(z-\mu)^2}{2\sigma^2}\right] dz \\ &= V + (v_i^0 - V) \exp\left[\underbrace{-\mu \int_0^t h(s) ds + \frac{\sigma^2}{2} \left(\int_0^t h(s) ds\right)^2}_A\right] \end{aligned} \quad (2.64)$$

Equation (2.64) represents the analytical solution of the mean velocity of the ode system (2.48). Note that

$$e^A \rightarrow 0 \quad \text{for } t \rightarrow +\infty \Leftrightarrow \forall t \quad -\mu \int_0^t h(s) ds + \frac{\sigma^2}{2} \left(\int_0^t h(s) ds\right)^2 < 0 \quad (2.65)$$

that is

$$\int_0^t h(s) ds < \frac{2\mu}{\sigma^2} \quad (2.66)$$

If we suppose $h(t) = 1$ we have that $\int_0^t h(s) ds = t$ and so the solution diverges from

$$t > \frac{2\mu}{\sigma^2} \quad (2.67)$$

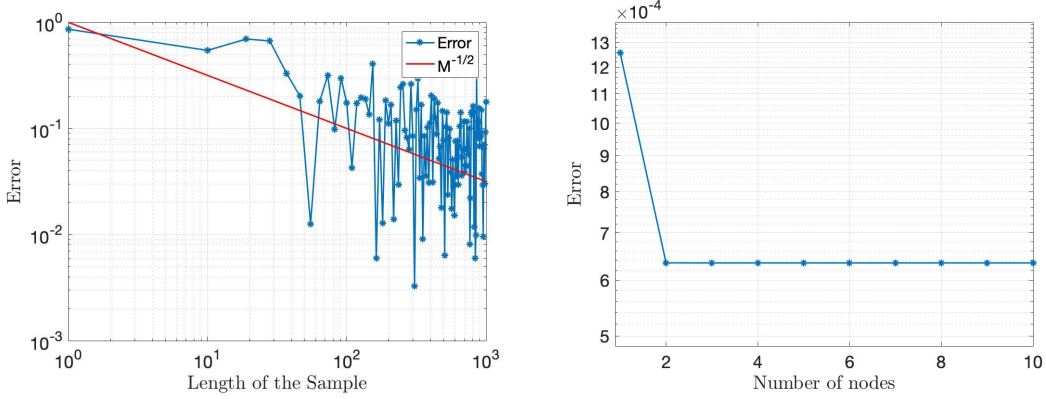


Figure 2.4: *Gaussian case*: The convergence of the error of the MC in loglog scale (on the left), compared with the error in the SC in semilog scale (on the right). Calculated at time $t = 0.1$ with $\mu = 1$, $\sigma = 0.5$

We are therefore observing the following physical phenomenon: an aggregation takes place in the time interval and then a repulsion from $\frac{2\mu}{\sigma^2}$ on, as shown in Fig. 2.3.

The MC method is applied simply using the (2.57)-(2.58) formulas, it is now easy to understand the reason why this approach uses the calculation of the sample mean regardless of the probabilistic distribution; the result is influenced only by the realizations generated by the pseudo-random number simulation algorithms mentioned in the appendix.

The SC method needs a more complete treatment, the (2.51) become

$$\mathbb{E}(v_i(Z, t)) = \int v_i(z, t) \frac{1}{\sqrt{2\pi\sigma^2}} \exp\left[-\frac{(z - \mu)^2}{2\sigma^2}\right] dz \quad (2.68)$$

in the case is exploited the *Gauss-Hermite Formula*. However, we need a variable transformation instead of using the formula explained by (C.39). So we set

$$\zeta = \frac{z - \mu}{\sqrt{2\sigma^2}}, \quad dz = \sqrt{2\sigma^2} d\zeta \quad (2.69)$$

and the (2.68) is transformed as

$$\mathbb{E}(v_i) = \frac{1}{\sqrt{\pi}} \int v_i(\mu + \sqrt{2}\sigma\zeta, t) e^{-\zeta^2} d\zeta \approx \frac{1}{\sqrt{\pi}} \sum_{k=1}^R w_k v_i(\mu + \sqrt{2}\sigma\zeta_k, t) \quad (2.70)$$

and using the transformation to return to the variable Z , we have

$$\mathbb{E}(v_i) \approx \bar{v}_i(t) = \frac{1}{\sqrt{\pi}} \sum_{k=1}^R w_k v_i(z_k, t) \quad (2.71)$$

2.6.3 Exponential case

Let us consider $Z \sim \text{Exp}(\lambda)$ with $\lambda > 0$, where

$$g_Z(z) = \lambda e^{-\lambda z} \quad (z > 0) \quad (2.72)$$

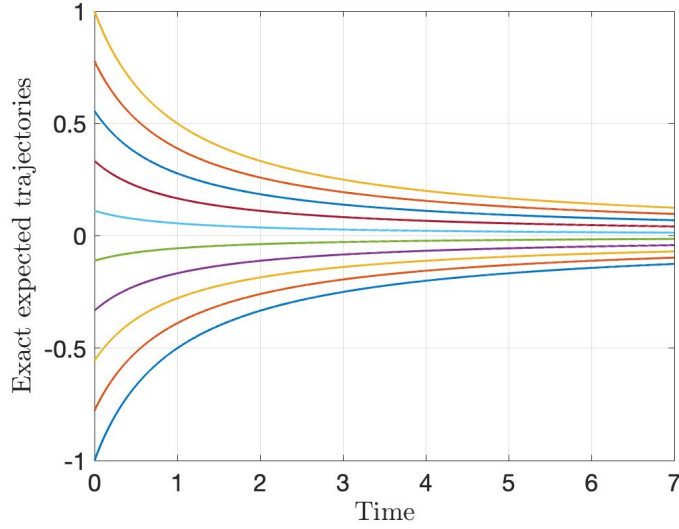


Figure 2.5: *Exponential case: The evolution of the exact expected trajectories $v_i(t)$ (2.73), with $\lambda = 1$.*

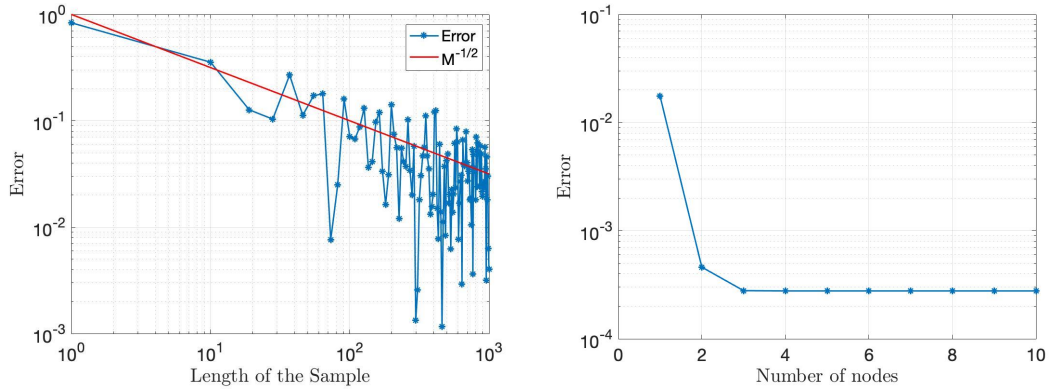


Figure 2.6: *Exponential case: The convergence of the error of the MC in loglog scale (on the left), compared with the error in the SC in semilog scale (on the right). Calculated at time $t = 1$ with $\lambda = 1$*

Setting $h(t) = 1$ the (2.52) becomes

$$\begin{aligned} \mathbb{E}(v_i) &= V + (v_i^0 - V) \int_0^{+\infty} e^{-zt} \lambda e^{-\lambda z} dz \\ &= V + (v_i^0 - V) \frac{\lambda}{\lambda + t}, \quad \forall t \geq 0 \end{aligned} \quad (2.73)$$

note that $\mathbb{E}(v_i) \rightarrow V$ for $t \rightarrow \infty$. Observe that the mean velocity is lower than the Gaussian case. The Monte Carlo method uses (2.57)-(2.58), while the Stochastic Collocation approach exploits

the variable transformation

$$\zeta = \lambda z, \quad dz = \frac{1}{\lambda} d\zeta \quad (2.74)$$

in (2.51) with the exponential probability density as

$$\mathbb{E}(v_i(Z, t)) = \int_0^\infty v_i(z, t) \lambda e^{-\lambda z} dz \quad (2.75)$$

Exploiting the *Gauss-Laguerre Formula* defined in (C.38), we obtain the following expression

$$\mathbb{E}(v_i) = \int_0^\infty v_i(\zeta/\lambda, t) e^{-\zeta} d\zeta \approx \sum_{k=1}^R w_k v_i(\zeta_k/\lambda, t) \quad (2.76)$$

and then the approximation of the expected velocity is

$$\mathbb{E}(v_i) \approx \sum_{k=1}^R w_k v_i(z_k, t) \quad (2.77)$$

Chapter 3

2-Degrees of Freedom

In this chapter we analyze the system composed of seismic mass and test-target, in which 2 degrees of rotational freedom are taken into account. Therefore, a free coordinate represents the rotation angle θ_2 of the seismic mass with respect to the point O, its Center of Gravity (CoG); while the second θ_1 describes the rotation of the test target with respect to its CoG. It must be noted, however, that the angle θ_1 is chosen relative to the upper plane of the seismic mass on which the test article rests. The coil is neglected. The system is represented in Fig. 3.1. To summarize the Lagrangian coordinates are:

- $\theta_1(t)$ which is the rotation of the target mass m around the point C;
- $\theta_2(t)$ which is the rotation of the seismic mass M around the point O;

Is important to understand the reason that leads to introduce a system with only two degrees of freedom (*dof*). As mentioned previously, the numerical technique called *Finite Elements Method* (FEM) exploits the the analysis of systems with many dofs, in systems of this type the analytical analysis is prohibitive. However, we will notice later, and in particular in the next chapter, that some analytical calculations are extremely complex.

This chapter, then, serves as a test in order to understand the rotational behavior of the physical system and to justify some hypothesis which will allow for a complete analysis of the virtual shaker testing of a Space Craft (S/C).

3.1 The Mathematical Model

Let us introduce $\{e_1, e_2, e_3\}$ a mobile reference system, concordant with the rotation $\theta_2(t)$ for $t \geq 0$ of the seismic mass. The relationship between the fixed reference system $\{\hat{i}_1, \hat{i}_2, \hat{i}_3\}$, introduced in the Chapter 1, is described by the rotation matrix:

$$\begin{pmatrix} \hat{i}_1 \\ \hat{i}_2 \end{pmatrix} = \begin{bmatrix} \cos \theta_2 & -\sin \theta_2 \\ \sin \theta_2 & \cos \theta_2 \end{bmatrix} \begin{pmatrix} e_1 \\ e_2 \end{pmatrix}$$

note that $\hat{i}_3 = e_3$.

The aim of this section is to build a mathematical model describing the dynamic behavior of the physical system described in Chapter 1. To do this, we use the theory of Analytical Mechanics presented in Appendix A.

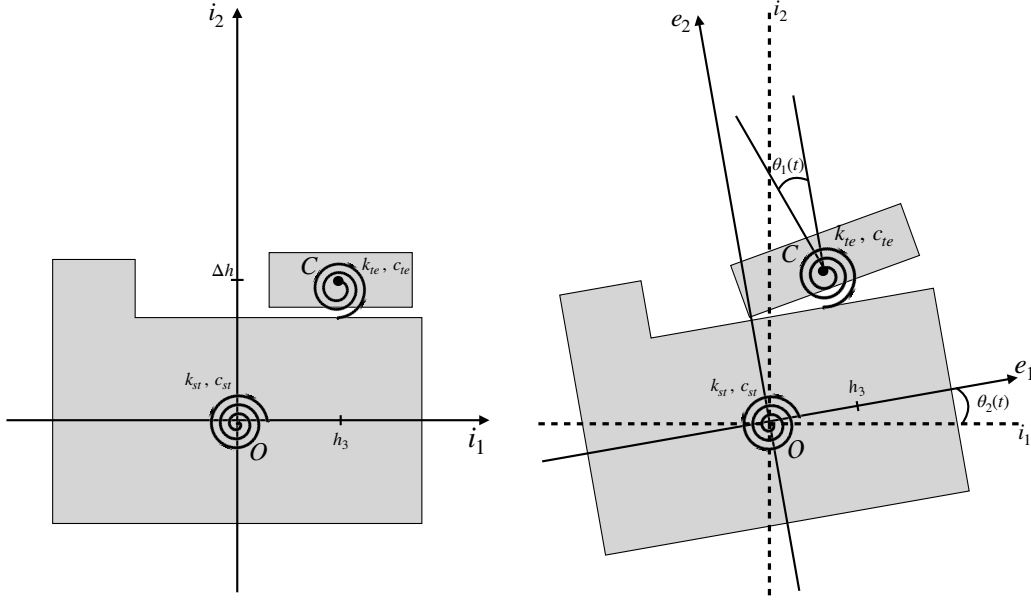


Figure 3.1: The 2dof system at the initial time $t = 0$ (on the left) and the rotated system with the lagrangian coordinates $\theta_1(t)$ and $\theta_2(t)$ for $t > 0$ (on the right).

Our focus will be to have a system of two equations in $\theta_1(t)$ and $\theta_2(t)$.
Let's we start from the *Lagrange equation*:

$$\frac{d}{dt} \left(\frac{\partial}{\partial \dot{q}_k} T \right) - \frac{\partial}{\partial q_k} T = Q_k^{(a)} \quad \text{with } k = 1, 2 \quad (3.1)$$

where T is the *kinetic energy* of the system and Q_k is *generalized Lagrangian force*, and:

$$\{q(t)\} = \{\theta_1(t), \theta_2(t)\}.$$

Compared with the physical system described in the Chapter 1, the coil is neglected. So, observing the Fig. 3.1, the moments generated by the torsional springs are the following

$$\begin{aligned} \mathbf{M}_{te} &= -k_{te}\theta_1\mathbf{i}_3 - c_{te}\dot{\theta}_1\mathbf{i}_3 \\ \mathbf{M}_{st} &= -k_{st}\theta_2\mathbf{i}_3 - c_{st}\dot{\theta}_2\mathbf{i}_3. \end{aligned}$$

They cause the rotations of the two mass m and M as

$$\begin{aligned} \boldsymbol{\varepsilon}_M &= \theta_2\mathbf{i}_3 \\ \boldsymbol{\varepsilon}_m &= (\theta_1 + \theta_2)\mathbf{i}_3. \end{aligned}$$

By using the the approach explained in the appendix A, we could calculate the virtual rotations. Simply differentiating with respect to the Lagrangian coordinates

$$\begin{aligned}\delta\boldsymbol{\varepsilon}_M &= \frac{\partial\boldsymbol{\varepsilon}_M}{\partial\theta_1}\delta\theta_1 + \frac{\partial\boldsymbol{\varepsilon}_M}{\partial\theta_2}\delta\theta_2 \\ &= \delta\theta_2\mathbf{i}_3 \\ \delta\boldsymbol{\varepsilon}_m &= \frac{\partial\boldsymbol{\varepsilon}_m}{\partial\theta_1}\delta\theta_1 + \frac{\partial\boldsymbol{\varepsilon}_m}{\partial\theta_2}\delta\theta_2 \\ &= (\delta\theta_1 + \delta\theta_2)\mathbf{i}_3\end{aligned}$$

Let us define the virtual work as

$$\delta L^{(a)} = \sum_{i=1}^2 M_i^{(a)} \cdot \delta\varepsilon_i \quad \text{where} \quad \delta\varepsilon_i = \sum_{k=1}^2 \frac{\partial\varepsilon_i}{\partial\theta_k} \delta\theta_k \quad (3.2)$$

and it can then be reparametrized by the definition of generalized coordinates (see Appendix A):

$$\delta L^{(a)} = \sum_{i=1}^2 M_i^{(a)} \cdot \left(\sum_{k=1}^2 \frac{\partial\varepsilon_i}{\partial\theta_k} \delta\theta_k \right) = \sum_{k=1}^2 Q_k \cdot \delta\theta_k \quad (3.3)$$

where the *generalized Lagrangian force* is

$$Q_k = \sum_{i=1}^2 M_i^{(a)} \cdot \frac{\partial\varepsilon_i}{\partial\theta_k} \quad \forall k. \quad (3.4)$$

Proceeding in this way, we obtain:

$$\begin{aligned}\delta L^{(a)} &= \mathbf{M}_{st} \cdot \delta\boldsymbol{\varepsilon}_M + \mathbf{M}_{te} \cdot \delta\boldsymbol{\varepsilon}_m - \mathbf{M}_{te} \cdot \delta\boldsymbol{\varepsilon}_M \\ &= [-k_{st}\theta_2 - c_{st}\dot{\theta}_2]\delta\theta_2 \\ &\quad + [-k_{te}\theta_1 - c_{te}\dot{\theta}_1](\delta\theta_1 + \delta\theta_2) \\ &\quad + [k_{te}\theta_1 + c_{te}\dot{\theta}_1]\delta\theta_2\end{aligned}$$

simplifying the expression of the virtual work of the system

$$\begin{aligned}\delta L^{(a)} &= + [-k_{te}\theta_1 - c_{te}\dot{\theta}_1]\delta\theta_1 \\ &\quad + [-k_{st}\theta_2 - c_{st}\dot{\theta}_2]\delta\theta_2\end{aligned}$$

and then we have the *generalized Lagrangian force* as

$$\begin{aligned}Q_{\theta_1}^{(a)} &= -k_{te}\theta_1 - c_{te}\dot{\theta}_1 \\ Q_{\theta_2}^{(a)} &= -k_{st}\theta_2 - c_{st}\dot{\theta}_2\end{aligned}$$

Finally we have to calculate the rotational kinetic energy of the system as the sum of the two component of the physical system m and M

$$T = T_m + T_M = \frac{1}{2}I_M\dot{\theta}_2^2 + \frac{1}{2}I_m(\dot{\theta}_1 + \dot{\theta}_2)^2$$

In conclusion, using the the Lagrangian equation defined in (3.1) we are able to write the equations system

$$\begin{aligned}I_m\ddot{\theta}_1 + I_m\ddot{\theta}_2 + c_{te}\dot{\theta}_1 + k_{te}\theta_1 &= 0 \\ I_m\ddot{\theta}_1 + (I_m + I_M)\ddot{\theta}_2 + c_{st}\dot{\theta}_2 + k_{st}\theta_2 &= 0.\end{aligned} \quad (3.5)$$

Due to the fact that the equations are linear we can be written in the matrix form:

$$[m]\{\ddot{\theta}\} + [c]\{\dot{\theta}\} + [k]\{\theta\} = 0 \quad \{\theta\} = \begin{pmatrix} \theta_1 \\ \theta_2 \end{pmatrix} \quad (3.6)$$

where:

$$[m] = \begin{bmatrix} I_m & I_m \\ I_m & I_m + I_M \end{bmatrix} \quad [c] = \begin{bmatrix} c_{te} & 0 \\ 0 & c_{st} \end{bmatrix} \quad [k] = \begin{bmatrix} k_{te} & 0 \\ 0 & k_{st} \end{bmatrix}$$

It is observed how the equations, although they may seem rather simple, are coupled and this complicates the search for a solution. In order to solve this problem there is the need to introduce a method capable of decoupling equations of the type described by (3.5) and it is called *Modal Analysis*, see [11].

3.1.1 Basic introduction of Modal Analysis

Consider an undamped linear system with multiple degrees of freedom, the equation is:

$$[m]\{\ddot{q}\} + [k]\{q\} = \{0\}. \quad (3.7)$$

We are searching for a solution such that all the masses follow one time function as:

$$\{q(t)\} = \{Q_0\}g(t) \quad (3.8)$$

where $\{Q_0\}$ is a constant non null vector and $g(t)$ is a generic function depending on time. Differentiating with respect to the time, we obtain:

$$[m]\{Q_0\}\ddot{g}(t) + [k]\{Q_0\}g(t) = \{0\} \quad (3.9)$$

Then we multiplying both members for a row vector $\{Q_0\}^T$:

$$\{Q_0\}^T [m] \{Q_0\} \ddot{g}(t) + \{Q_0\}^T [k] \{Q_0\} g(t) = 0 \quad (3.10)$$

Now we could observe that $\{Q_0\}^T [m] \{Q_0\} > 0$ and $\{Q_0\}^T [k] \{Q_0\} \geq 0$, in fact the mass matrix is positive definite and the stiffness one is positive (or semi-positive) definite. Therefore we have

$$\frac{\ddot{g}(t)}{g(t)} = -\frac{\{Q_0\}^T [k] \{Q_0\}}{\{Q_0\}^T [m] \{Q_0\}} = -\omega^2 \leq 0 \quad (3.11)$$

and so we come to the equation

$$\ddot{g}(t) + \omega^2 g(t) = 0 \quad (3.12)$$

and the solution of the (3.7) is

$$\{q(t)\} = \{Q_0\} \cos(\omega t + \varphi) \quad (3.13)$$

and so differentiating two times the (3.13) and substituting in (3.7) we obtain

$$-\omega^2 [m] \{Q_0\} \cos(\omega t + \varphi) + [k] \{Q_0\} \cos(\omega t + \varphi) = \{0\} \quad (3.14)$$

From the equation (3.14) it is easy to have the *eigenvalue problem*:

$$([k] - \omega^2 [m]) \{Q_0\} = \{0\} \quad (3.15)$$

due to the fact that $\{Q_0\}$ is non-zero, it must be true that

$$\det([k] - \omega^2[m]) = 0 \quad (3.16)$$

Note that in a system with n degrees of freedom the condition (3.16) is an algebraic equation of $2n$ -degree in the variable ω (or n -grade in the variable ω^2), this equation takes the name of *characteristic equation*:

$$a_n\omega^{2n} + a_{n-1}\omega^{2n-2} + \dots + a_1\omega^2 + a_0 = 0 \quad (3.17)$$

The zeros of the characteristic polynomial are the *eigenvalues* $\omega_1^2, \dots, \omega_n^2$. The *eigenvalues matrix* is a diagonal matrix containing all the eigenvalues:

$$[\Lambda] = \text{diag}(\omega_r^2) = \begin{bmatrix} \omega_1^2 & 0 & 0 & 0 \\ 0 & \omega_2^2 & 0 & 0 \\ 0 & 0 & \ddots & 0 \\ 0 & 0 & 0 & \omega_n^2 \end{bmatrix} \quad (3.18)$$

the square root of the eigenvalues are called *natural pulses* of the n -dof system. If we substitute all the eigenvalues in the (3.15) and we solve the algebraic system we obtain the eigenvectors, that are called *modal forms*

$$\{\psi_1\}, \dots, \{\psi_n\} \quad (3.19)$$

the *modal matrix* contains all the eigenvector sorted by column

$$[\Psi] = [\{\psi_1\} \dots \{\psi_n\}]. \quad (3.20)$$

Orthogonality of the modal forms

The mass and the stiffness matrix have important characteristics that may result important in the resolution of an n -dof system. In fact as we said previously $[m]$ and $[k]$ are real and symmetric this leads to having real eigenvalues and eigenvectors, while by the fact that the two matrices are positive definite (or semi-definite) we get that the eigenvalues are positive.

However, a crucial property of the eigenvectors is the *orthogonality* with respect to the mass matrix and the stiffness matrix that we will present in this paragraph.

Consider the eigenvalue problem (3.15), for any $r = 1, \dots, n$ we define an eigenvalue ω_r^2 and there is an associated eigenvector $\{\psi_r\}$. If we take $s = 1, \dots, n$ and we have ω_s^2 , we could write the (3.15) problem in this way:

$$\begin{cases} \omega_r^2[m]\{\psi_r\} = [k]\{\psi_r\} \\ \omega_s^2[m]\{\psi_s\} = [k]\{\psi_s\} \end{cases} \quad (3.21)$$

pre-multiplying the first equation of (3.21) by $\{\psi_s\}^T$ and the second by $\{\psi_r\}^T$ we get

$$\begin{cases} \omega_r^2\{\psi_s\}^T[m]\{\psi_r\} = \{\psi_s\}^T[k]\{\psi_r\} \\ \omega_s^2\{\psi_r\}^T[m]\{\psi_s\} = \{\psi_r\}^T[k]\{\psi_s\} \end{cases} \quad (3.22)$$

doing the transposition of the second equation and exploiting the property of symmetry of $[m]$ and $[k]$ we have

$$\omega_s^2\{\psi_s\}^T[m]\{\psi_r\} = \{\psi_s\}^T[k]\{\psi_r\} \quad (3.23)$$

subtracting it from the first equation of (3.22) we obtain

$$(\omega_r^2 - \omega_s^2)\{\psi_s\}^T[m]\{\psi_r\} = 0 \quad (3.24)$$

which leads to

$$\begin{aligned} \text{if } \omega_r \neq \omega_s &\Rightarrow \{\psi_s\}^T[m]\{\psi_r\} = 0 \\ \text{if } \omega_r = \omega_s &\Rightarrow \{\psi_r\}^T[m]\{\psi_r\} = m_r > 0. \end{aligned} \quad (3.25)$$

Note that m_r is called *r-th modal mass* and is positive because $[m]$ is positive definite. It is observed that taking the first equation of (3.22) we have

$$\begin{aligned} \text{if } \omega_r \neq \omega_s &\Rightarrow \{\psi_s\}^T[k]\{\psi_r\} = 0 \\ \text{if } \omega_r = \omega_s &\Rightarrow \{\psi_r\}^T[k]\{\psi_r\} = \omega_r^2 m_r = k_r \geq 0 \end{aligned} \quad (3.26)$$

and k_r is called *r-th modal stiffness*. The second equation of the (3.26) is particularly useful to check out if the orthogonalization was performed correctly, in fact

$$\omega_r^2 = \frac{k_r}{m_r} \quad \forall r = 1, \dots, n. \quad (3.27)$$

To summarize we have proved that

$$\begin{aligned} \{\psi_r\}^T[m]\{\psi_r\} &= \text{diag}(m_r) \\ \{\psi_r\}^T[k]\{\psi_r\} &= \text{diag}(k_r) \end{aligned} \quad (3.28)$$

and so the eigenvectors are said to be *m-orthogonal* and *k-orthogonal*.

Now let us shift the attention to the modal matrix $[\Psi]$. It is constituted by the eigenvectors sorted by column and they are defined up to a constant. Often this constant is chosen in a such way to have all the modal masses equal to 1, however in general if

$$\{\psi_r\}^T[m]\{\psi_r\} = m_r \neq 1 \quad (3.29)$$

so we could *m-normalize* as follows:

$$\{\tilde{\psi}_r\} = \frac{\{\psi_r\}}{\sqrt{m_r}} \quad (3.30)$$

and then we have

$$\begin{aligned} \{\tilde{\psi}_r\}^T[m]\{\tilde{\psi}_r\} &= [I] \\ \{\tilde{\psi}_r\}^T[k]\{\tilde{\psi}_r\} &= \text{diag}(\omega_r^2) = [\Lambda] \end{aligned} \quad (3.31)$$

note that software used for numerical calculations chooses automatically the eigenvectors that make the (3.31) true.

Decoupling of the equation. Proportional damping

Let us consider an unforced viscous dumped system with multi degrees of freedom. The equations that describe this system are the following:

$$[m]\{\ddot{q}\} + [c]\{\dot{q}\} + [k]\{q\} = \{0\}. \quad (3.32)$$

In general these equations are not decoupled and this could make the resolution a bit tricky, so in this paragraph we will describe the decoupling of an n -dof equation exploiting the modal matrix and all the observations that we made previously.

Firstly we have to analyse the undamped system described by the equation (3.15), calculating the eigenvalues, and the associated eigenvectors, we can build the modal matrix $[\Psi]$. Then we define the *modal transformation*

$$\{q(t)\} = [\Psi]\{\phi(t)\} \quad (3.33)$$

where $\{\phi(t)\}$ is the vector of the *modal coordinates* (also called *normal*, *principal* or *natural*). Substituting the (3.33) in (3.32) we have

$$[m][\Psi]\{\ddot{\phi}\} + [c][\Psi]\{\dot{\phi}\} + [k][\Psi]\{\phi\} = \{0\} \quad (3.34)$$

multiplying the latter equation by $[\Psi]^T$ we get

$$[\Psi]^T[m][\Psi]\{\ddot{\phi}\} + [\Psi]^T[c][\Psi]\{\dot{\phi}\} + [\Psi]^T[k][\Psi]\{\phi\} = \{0\} \quad (3.35)$$

using the property described in (3.28) we could re-write (3.35) as

$$\text{diag}(m_r)\{\ddot{\phi}\} + [\Psi]^T[c][\Psi]\{\dot{\phi}\} + \text{diag}(k_r)\{\phi\} = \{0\} \quad (3.36)$$

In general, $[\Psi]^T[c][\Psi]$ is not diagonal and this implies that it is not possible to decouple the equations using the modal analysis, while in an undamped system this problem does not exist. However, there is a solution, it is called *proportional damping* or *Rayleigh damping* [13]. The description of that case is particularly easy, from a mathematical point of view, and every situation with a non-proportional damping but with small entity of damping could be approximated with the proportional one.

The general formula for the viscous proportional damping is called the *Cauchy series*:

$$[c_p] = \sum_{i=0}^{n-1} a_i [m] ([m]^{-1} [k]) \quad (3.37)$$

where n is the number of dofs, while a_i are the possibly null coefficient. Note that a sufficient condition, but not necessary, for having proportional damping is setting every a_i coefficient to zero, except the first two as:

$$[c_p] = \alpha [m] + \beta [k] \quad \Rightarrow \quad \begin{cases} a_0 = \alpha \\ a_1 = \beta \end{cases} \quad (3.38)$$

Now if we suppose $[c] = [c_p]$ we could re-write the (3.36) obtaining

$$\text{diag}(m_r)\{\ddot{\phi}\} + [\Psi]^T(\alpha [m] + \beta [k])[\Psi]\{\dot{\phi}\} + \text{diag}(k_r)\{\phi\} = \{0\} \quad (3.39)$$

and so we could decouple the equations, for every $r = 1, \dots, n$

$$m_r \ddot{\phi}_r + (\alpha m_r + \beta k_r) \dot{\phi}_r + k_r \phi_r = 0. \quad (3.40)$$

At this stage we have built n decoupled equations for the unforced viscous proportional damped system with n degrees of freedom. Dividing for the modal mass we have the canonical form

$$\ddot{\phi}_r + 2\zeta_r \omega_r \dot{\phi}_r + \omega_r^2 \phi_r = 0 \quad (3.41)$$

with the natural pulse ω_r^2 and the damped factor ζ_r defined as

$$\zeta_r = \frac{\alpha}{2} \frac{1}{\omega_r} + \frac{\beta}{2} \omega_r. \quad (3.42)$$

When $\zeta_r < 1$, the r -th mode is said to be *under-damped*. This is a very frequent case, where the zeros of the characteristic polynomial (3.16) are complex conjugated. Due to the under damped hypothesis it is possible to write the analytical solution of (3.41) as:

$$\phi_r(t) = (A_r \cos(\omega_{dr}t) + B_r \sin(\omega_{dr}t))e^{-\zeta_r \omega_r t} \quad (3.43)$$

where:

$$\omega_{dr} = \omega_r \sqrt{1 - \zeta_r^2} \quad (3.44)$$

is the free damped vibration pulse of the r -th mode. A_r and B_r are two constants dependent on the initial conditions $\{q(t=0)\} = \{q_0\}$ and $\{\dot{q}(t=0)\} = \{\dot{q}_0\}$ calculated exploiting the m -orthogonality and the k -orthogonality:

$$\{q(t)\} = [\Psi]\{\phi(t)\} = \sum_{r=1}^n \{\psi_r\} \phi_r(t) = \sum_{r=1}^n \{\psi_r\} (A_r \cos(\omega_{dr}t) + B_r \sin(\omega_{dr}t))e^{-\zeta_r \omega_r t} \quad (3.45)$$

multiplying for $\{\psi_s\}^T[m]$ we have

$$\{\psi_s\}^T[m]\{q(t)\} = \sum_{r=1}^n \{\psi_s\}^T[m]\{\psi_r\} (A_r \cos(\omega_{dr}t) + B_r \sin(\omega_{dr}t))e^{-\zeta_r \omega_r t} \quad (3.46)$$

and setting $t = 0$, we obtain

$$\{\psi_s\}^T[m]\{q_0\} = \sum_{r=1}^n A_r \{\psi_s\}^T[m]\{\psi_r\} = A_s m_s. \quad (3.47)$$

In the same way, differentiating and setting $t = 0$ we get

$$\{\psi_s\}^T[m]\{\dot{q}_0\} = \sum_{r=1}^n (B_r \omega_{dr} - \zeta_r \omega_r A_r) \{\psi_s\}^T[m]\{\psi_r\} = (B_s \omega_{ds} - \zeta_s \omega_s A_s) \quad (3.48)$$

finally we have the constants defined as

$$A_r = \frac{\{\Psi_r\}^T[m]\{q_0\}}{m_r} \quad B_r = \frac{\{\Psi_r\}^T[m]}{\omega_{dr} m_r} (\{\dot{q}_0\} + \zeta_r \omega_r \{q_0\}) \quad (3.49)$$

3.1.2 Application of the modal approach to the 2-dof satellite problem

The linear system of equations obtained describing the rotations of the test article and the seismic mass is

$$[m]\{\ddot{\theta}\} + [c]\{\dot{\theta}\} + [k]\{\theta\} = 0 \quad \{\theta\} = \begin{pmatrix} \theta_1 \\ \theta_2 \end{pmatrix} \quad (3.50)$$

where:

$$[m] = \begin{bmatrix} I_m & I_m \\ I_m & I_m + I_M \end{bmatrix} \quad [c] = \begin{bmatrix} c_{te} & 0 \\ 0 & c_{st} \end{bmatrix} \quad [k] = \begin{bmatrix} k_{te} & 0 \\ 0 & k_{st} \end{bmatrix}$$

As mentioned earlier, the advantage of analyzing a system with few dofs like this one is that we can get an analytical expression of most of the quantities involved in the description. Knowing

these quantities will give us a better understanding of the numerical methods we will be obliged to use later.

Therefore, in this paragraph we try to derive the analytical expression of the pulse frequencies. Firstly, we have to study the undamped system, defining the eigenvalue problem

$$([k] - \omega^2[m])\{\theta_0\} = \{0\} \quad (3.51)$$

The characteristic polynomial obtained is

$$\det([k] - \omega^2[m]) = (k_{te} - \omega^2 I_m)(k_{st} - \omega^2(I_m + I_M)) - (\omega I_m)^2 = 0 \quad (3.52)$$

solving the second order equation for ω^2 yields the two real and positive eigenvalues ω_1^2, ω_2^2 defined as

$$\omega_{1,2}^2 = \frac{I_m k_{st} + (I_m + I_M)k_{te} \pm \sqrt{-4I_m I_M k_{st} k_{te} + (-I_m k_{st} - I_m k_{te} - I_M k_{te})^2}}{2I_m I_M} \quad (3.53)$$

the roots of the eigenvalues are the *natural pulses* for the physical system.

For simplicity we will not explicitly replace the value of the eigenvalues till the end.

The eigenvector is calculated by solving the matrix system:

$$\begin{bmatrix} k_{te} - \omega_1^2 I_m & -\omega_1^2 I_m \\ -\omega_1^2 I_m & k_{st} - \omega_1^2(I_m + I_M) \end{bmatrix} \begin{pmatrix} \psi_{11} \\ \psi_{21} \end{pmatrix} = \begin{pmatrix} 0 \\ 0 \end{pmatrix} \quad (3.54)$$

obtaining the eigenvector associated to the first eigenvalue ω_1^2

$$\psi_{11} = \frac{\omega_1^2 I_m}{k_{te} - \omega_1^2 I_m}, \quad \psi_{21} = 1 \quad (3.55)$$

While solving

$$\begin{bmatrix} k_{te} - \omega_2^2 I_m & -\omega_2^2 I_m \\ -\omega_2^2 I_m & k_{st} - \omega_2^2(I_m + I_M) \end{bmatrix} \begin{pmatrix} \psi_{12} \\ \psi_{22} \end{pmatrix} = \begin{pmatrix} 0 \\ 0 \end{pmatrix} \quad (3.56)$$

we get the eigenvector associated to the second eigenvalue ω_2^2

$$\psi_{12} = 1, \quad \psi_{22} = \frac{\omega_2^2 I_m}{k_{st} - \omega_2^2(I_m + I_M)} \quad (3.57)$$

The modal matrix is built sorting by column the eigenvectors (or *modal forms*) as

$$[\Psi] = \begin{bmatrix} \frac{\omega_1^2 I_m}{k_{te} - \omega_1^2 I_m} & 1 \\ 1 & \frac{\omega_2^2 I_m}{k_{st} - \omega_2^2(I_m + I_M)} \end{bmatrix}$$

Following the steps described in the previous section, we define the modal transformation

$$\{\theta(t)\} = [\Psi]\{\phi(t)\} \quad (3.58)$$

so we can rewrite the system (3.50) multiplying by $[\Psi]^T$

$$[\Psi]^T [m][\Psi]\{\ddot{\phi}\} + [\Psi]^T [c][\Psi]\{\dot{\phi}\} + [\Psi]^T [k][\Psi]\{\phi\} = 0 \quad \{\phi\} = \begin{pmatrix} \phi_1 \\ \phi_2 \end{pmatrix}. \quad (3.59)$$

Using the m -orthogonality and the k -orthogonality we obtain two diagonal matrices. As we know, $[\Psi]^T[c][\Psi]$ is not always diagonal; however, as mentioned in the previous section, we can suppose to have the proportional damping:

$$[c_p] = \alpha[m] + \beta[k] \quad (3.60)$$

We note that $[k]$ is a diagonal matrix while $[m]$ is not; so that to be consistent with the (3.5) we see that:

$$\begin{aligned} \alpha &= 0 \\ \exists \beta > 0 \quad \text{so that} \quad &\begin{cases} c_{te} = \beta k_{te} \\ c_{st} = \beta k_{st} \end{cases} \end{aligned} \quad (3.61)$$

which gives:

$$\begin{aligned} [\Psi]^T[m][\Psi]\{\ddot{\phi}\} + [\Psi]^T(\alpha[m] + \beta[k])[\Psi]\{\dot{\phi}\} + [\Psi]^T[k][\Psi]\{\phi\} &= 0 \\ \text{diag}[m]\{\ddot{\phi}\} + (\beta \text{diag}[k])\{\dot{\phi}\} + \text{diag}[k]\{\phi\} &= 0 \end{aligned} \quad (3.62)$$

For $r = 1,2$ we have the decoupled equations

$$m_r \ddot{\phi}_r + \beta k_r \dot{\phi}_r + k_r \phi_r = 0 \quad (3.63)$$

which can be solved with the resolution methods of systems with a single degree of freedom; moreover, the use of modal analysis also greatly facilitates the resolution using numerical methods of time integration such as the Runge-Kutta or the Euler method.

Dividing by the modal mass m_r , we obtain the canonical form as in (3.41):

$$\ddot{\phi}_r + 2\zeta_r \omega_r \dot{\phi}_r + \omega_r^2 \phi_r = 0 \quad (3.64)$$

with natural pulse ω_r and the damped factor ζ_r for the r -th mode

$$\zeta_r = \frac{\alpha}{2} \frac{1}{\omega_r} + \frac{\beta}{2} \omega_r = \frac{\beta}{2} \omega_r. \quad (3.65)$$

At this point, it is simple to construct the modal matrices m_r and k_r at a theoretical level because we have to follow the steps described above.

The modal stiffness matrix is obtained as:

$$\begin{aligned} [\Psi]^T[k][\Psi] &= \begin{bmatrix} k_{te} \left(\frac{\omega_1^2 I_m}{k_{te} - \omega_1^2 I_m} \right)^2 + k_{st} & 0 \\ 0 & k_{st} \left(\frac{\omega_2^2 I_m}{k_{st} - \omega_2^2 (I_m + I_M)} \right)^2 + k_{te} \end{bmatrix} \\ &= \begin{bmatrix} k_1 & 0 \\ 0 & k_2 \end{bmatrix} \end{aligned} \quad (3.66)$$

while the mass matrix is calculated as follows

$$[\Psi]^T[m][\Psi] = \begin{bmatrix} m_1 & 0 \\ 0 & m_2 \end{bmatrix} \quad (3.67)$$

where:

$$\begin{aligned} m_1 &= \left(\frac{\omega_1^2 I_m}{k_{te} - \omega_1^2 I_m} \right) \left(\frac{\omega_1^2 I_m^2}{k_{te} - \omega_1^2 I_m} + I_m \right) + \left(\frac{\omega_1^2 I_m^2}{k_{te} - \omega_1^2 I_m} \right) + I_m + I_M \\ m_2 &= \left(\frac{\omega_2^2 I_m}{k_{st} - \omega_2^2 (I_m + I_M)} \right) \left(\frac{\omega_2^2 I_m (I_m + I_M)}{k_{st} - \omega_2^2 (I_m + I_M)} + I_m \right) + \left(\frac{\omega_2^2 I_m^2}{k_{st} - \omega_2^2 (I_m + I_M)} \right) + I_m \end{aligned} \quad (3.68)$$

We suppose an under damped mode, so we obtain the solution described by the (3.43), which is the exact solution of the system (3.50)

$$\{\theta(t)\} = [\Psi]\{\phi(t)\} = \sum_{r=1}^2 \{\psi_r\} (A_r \cos(\omega_{dr}t) + B_r \sin(\omega_{dr}t)) e^{-\zeta_r \omega_r t} \quad (3.69)$$

Note that A_r and B_r are two constants depending on the initial conditions defined in the (3.49). Remember that

$$\omega_{dr} = \omega_r \sqrt{1 - \zeta_r^2} \quad (3.70)$$

is the unforced damped vibration pulse of the r -th mode. Therefore, the frequency is defined as

$$f_r = \frac{\omega_r}{2\pi} \quad \text{and so} \quad f_{dr} = f_r \sqrt{1 - \zeta_r^2} \quad (3.71)$$

where f_{dr} is the frequency of vibration of the unforced viscous proportional damped system.

3.2 Numerical Analysis

This section contains the numerical results of the modal analysis of a 2 dof rotational system. The purpose is to compare the exact solution obtained by the equation (3.69) with the numerical one calculated by applying Runge and Kutta on the system (3.63).

Before adding complications to our analysis, we try to better understand the test target behavior in a 2 dof rotational study. The numerical analysis performed on MATLAB is based on two different approaches compared to each other.

The first is to calculate analytically the eigenvalues using the formula (3.53) and then using the (3.55) and (3.57) we obtain the exact values of the eigenvectors. By solving the expression defined in (3.69), we have the exact solution of the displacements $\{\theta(t)\}$.

The numerical approach is based on the MATLAB eigenvalues calculation routine:

```
1 [Psi , Om_q]    = eig(K,M);
2 Om             = sqrt(diag(Om_q));
```

where K is the stiffness matrix, while M is the mass matrix presented in the equation (3.50). In this way, the software solve the eigenvalue problem (3.51), obtaining the modal matrix $[\Psi]$ and the natural pulses ω .

Using the modal analysis, described in the previous section, we are able to build the modal mass and stiffness matrix, useful in the system equations (3.63). In order to solve the system we can exploit any numerical integration method. In this section we used the Runge-Kutta with the fourth-order, meaning that the local truncation error is on the order of $O(h^5)$, while the total accumulated error is on the order of $O(h^4)$, where $h > 0$ is the step size. In the appendix Miscellaneous Topics it is possible to have a description of the algorithm.

The result obtained are represented in Fig. 3.2, from which we can see that there is a good agreement between the numerical and exact solution. This excellent matching is due to the accurate implementation of the MATLAB function **eig**, indeed in Table 3.1 it is possible to observed how the difference between the natural pulses ω_1 and ω_2 calculated through the analytical approach and the numerical ones is negligible. Moreover, this agreement allows us to exchange, in the next analysis, the numerical method with the analytical for the calculation of the eigenvalues (eigenvectors respectively). The physical system with 2 dof allows us to calculate the resonance frequency in a rather simple way, both analytically and numerically. The method is the same

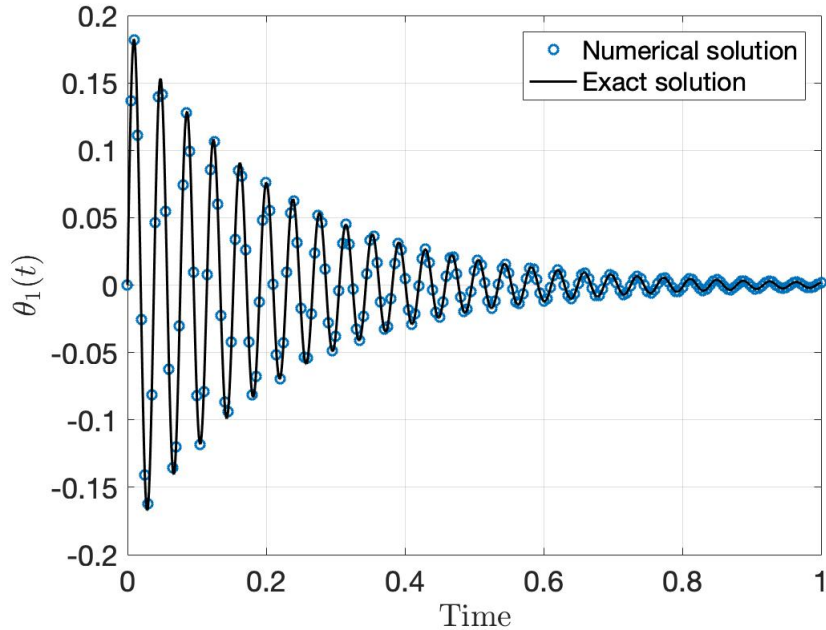


Figure 3.2: The comparison between the numerical solution and the exact solution obtained with (3.69).

	Numerical	Exact	Error
ω_1	0,0046	0,0046	$5.6361 \cdot 10^{-12}$
ω_2	164,5852	164,5852	$1 \cdot 10^{-14}$
f_{dr}	26,1844	26,1844	$1 \cdot 10^{-14}$

Table 3.1: Comparing the eigenvalues (natural pulse) calculated with the numerical and with the (3.53) formula. The resonance frequency f_{dr} is expressed in Hz, while the natural pulses in rad/s.

and is based on the use of (3.71). For the analytical formulation it is sufficient to substitute the natural pulses calculated with (3.53); while for the numerical ones, the values obtained by the **eig** function are used.

We are interested in the damped resonance frequency of the target test which is represented by the second mode; this is due to the construction of the modal matrix. The numerical values are shown in Table 3.1.

3.2.1 Initial Condition

The initial condition of the ordinary differential equation (ODE) system for the angles $\theta_1(0)$, $\theta_2(0)$ are set to zero, indeed in a real base-shake sine test the test article and the seismic mass at $t = 0$ are supposedly stationary while the target movement is generated by the coil that impresses a force applied to the slip table. It has not been imposed an external forcing moment to the test article because it would not be a correct representation of the physical system. For these reasons

the initial condition are

$$\{\theta(0)\} = \begin{pmatrix} 0 \\ 0 \end{pmatrix}, \quad \{\dot{\theta}(0)\} = \begin{pmatrix} \dot{\theta}_0 \\ 0 \end{pmatrix} \quad (3.72)$$

where, in particular, the angular velocity $\dot{\theta}_0$ is equal to 5 Hz (31.41 rad/s).

3.3 2-DOF Stochastic System

The mathematical model associated with the physical system analysed so far is deterministic, in which each quantity is supposedly known or derived from experimental data by the partner company of this thesis. However, in Chapter 1 the focal point has been presented: the randomness of some stiffnesses (and the respective dampings) in the shaker assembly. These elements can change due to temperature and humidity variations in the laboratory. All components of the shaker are scrupulously monitored to avoid any small variation that could compromise the success of the test, but some components are difficult to control, because of their position and/or nature. One of these components is the oil meatus, a pressurized oil with the aim of avoiding the influences created by the vibrations of the seismic mass at the target test.

The use of a purely mechanical deterministic approach is for these reasons, questionable since it cannot take into account the aforementioned factors.

Let us define the stiffness of the oil meatus k_{te} as dependent on a centered random variable Z , i.e $\mathbb{E}(Z) = 0$, as follows:

$$k_{te} = \bar{k}_{te} + \gamma Z \quad (3.73)$$

where \bar{k}_{te} is the experimental data obtained from the partner company assigned in Table 1.1, while γ is a constant called *perturbation size*. Note that k_{te} is a random quantity where $\mathbb{E}(k_{te}) = \bar{k}_{te}$, moreover $k_{te} \geq 0$ and then $0 \leq \gamma \leq \bar{k}_{te}$; the greater the value of γ , the greater the stochastic perturbation in the k_{te} parameter. Moreover, the perturbation of the k_{te} strongly depends on the chosen probability distribution for the random variable Z . So let us suppose that Z has a uniform $U[-1,1]$ distribution. This choice allows us, at least in the first analysis, to assume equally probable any perturbation to the \bar{k}_{te} value.

3.3.1 Monte Carlo method

The first approach used is the Monte Carlo method, already widely described above. Once the sample size M and perturbation size γ have been assigned, pseudo-random numbers, in accordance with the uniform distribution, are generated through pre-implemented algorithms in the used software (in this case MATLAB). Obtaining the random realizations:

$$(k_{te})_k = \bar{k}_{te} + \gamma z_k, \quad k = 1, \dots, M \quad (3.74)$$

	Description	Values	Unit of measure
α	Proportional damping parameter	0	s
β	Proportional damping parameter	$3.379 \cdot 10^{-4}$	s
c_{st}	Torsional M damping	$3.379 \cdot 10^{-3}$	N·m·s
\bar{c}_{te}	Torsional meatus damping	$7.277 \cdot 10^{-4}$	N·m·s

Table 3.2: Table of parameters.

for each value of $(k_{te})_k$ the $[k]$ stiffness matrix and the $[c]$ proportional damping matrix defined in (3.50) are built and using the modal analysis we get M -th systems of equations for the two free coordinates as (3.63). Solving by Runge-Kutta we obtain M -th realizations of the ODE problem solution

$$\theta_r(z_k, t), \quad r = 1, 2 \quad k = 1, \dots, M.$$

However, in experimental tests the satellite displacements are obtained through accelerometers and so the results are in the form of accelerations. Once computed $\{\theta(t)\}$, it is straightforward to calculate the accelerations vector $\{\ddot{\theta}(t)\}$:

$$\ddot{\theta}_r(z_k, t), \quad r = 1, 2 \quad k = 1, \dots, M. \quad (3.75)$$

In this analysis, we set $M = 1000$ samples. We are interested in the quantities related to the test target; so we can calculate the expected acceleration of the test item with the formula similar to (2.57)

$$\ddot{\theta}_1(t) = \frac{1}{M} \sum_{k=1}^M \ddot{\theta}_1(z_k, t), \quad \forall t \geq 0 \quad (3.76)$$

while the respective sample variance is obtained as in (2.58)

$$\hat{\sigma}_{\ddot{\theta}}^2(t) = \frac{1}{M-1} \sum_{k=1}^M (\ddot{\theta}_1(z_k, t) - \ddot{\theta}_1(t))^2, \quad \forall t \geq 0 \quad (3.77)$$

its square root is the standard deviation.

In the absence of details on the nature of the disturbances, it is very difficult to construct useful statistics to describe the phenomenon. So using only the average (3.76), the standard deviation derived from (3.77) and Chebyshev's inequality (B.23). It is possible to construct intervals as the following

$$P\left(|\ddot{\theta}_1 - \ddot{\theta}_1| \geq \lambda \hat{\sigma}\right) \leq \frac{1}{\lambda^2}, \quad \forall t \geq 0 \quad \Rightarrow \quad [\ddot{\theta}_1 - \lambda \hat{\sigma}, \ddot{\theta}_1 + \lambda \hat{\sigma}] \quad (3.78)$$

and they can qualitatively describe a variation interval for the expected solution. Note that the intervals built with the Chebyshev's inequality are weaker than the confidence intervals used in statistical models [12], however those require more information on the perturbation error.

The size of the uncertainty band is affected by varying the perturbation size. For large γ , i.e. 50% of \bar{k}_{te} , the uncertainty band is small around $\ddot{\theta}_1$ for very small times (close to the initial condition) while with the passing of time the band becomes very wide and $\ddot{\theta}_1$ loses oscillatory behavior and stabilizes around zero, see Fig. 3.4. This is due to the fact that a value of γ like this introduces a very high uncertainty on k_{te} , indeed the stiffness of the oil meatus varies between $1.0784 \cdot 10^8$ N·m and $3,2280 \cdot 10^8$ N·m. The oscillations produced by a system with such a wide range of mechanical stiffnesses, lead to cancel the average behaviour of $\ddot{\theta}_1$. However, at large times, the displacement is damped by $c_{te} = \beta k_{te}$ causing the test item to stop.

By varying the perturbation size γ from 20% to 2% of \bar{k}_{te} , it is observed how the uncertainty bands are reduced for a fixed time (e.g. $t = 0.2$ s) around $\ddot{\theta}_1$, while the latter regains physically consistent oscillatory behavior. This is caused by the considerable reduction of the uncertainty on the stiffness, which leads to have vibrational systems more similar to each other, decreasing the flattening of $\ddot{\theta}_1$ oscillations. Exasperating the approach just described, putting γ equal to 1% of \bar{k} , it is observed that it is no longer possible to distinguish the uncertainty band from the mean, in this case the stiffness of the oil meatus varies between $2.1320 \cdot 10^8$ N·m and $2.1750 \cdot 10^8$

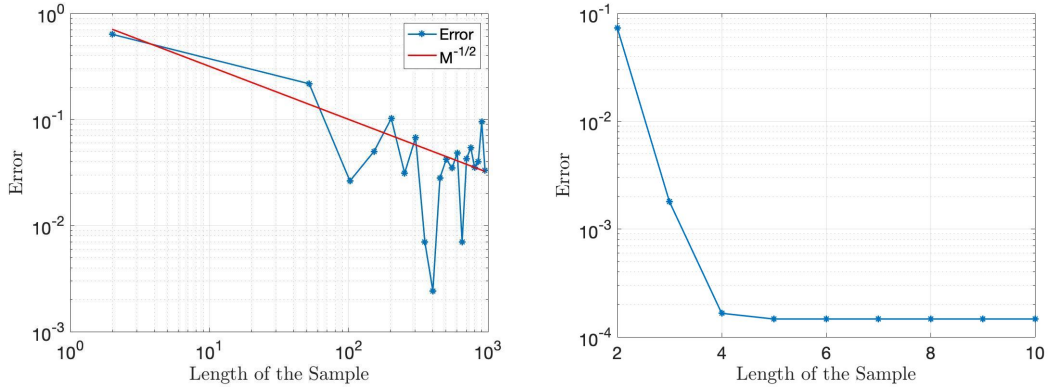


Figure 3.3: The convergence error in Monte Carlo method in loglog scale (on the left), compared with the convergence error of Stochastic Collocation in semilog scale (on the right). $\gamma = \bar{k}_{te}/10$, $t = 0.217$ s.

N·m, see the last figure of Fig. 3.4

The same method can be used to calculate the statistics for the frequencies of vibration of the unforced viscous proportional damped system obtained with (3.71), as follows:

$$\bar{f}_{dr} = \frac{1}{M} \sum_{k=1}^M f_{dr}(z_k), \quad \hat{\sigma}_f^2 = \frac{1}{M-1} \sum_{k=1}^M (f_{dr}(z_k) - \bar{f}_{dr})^2, \quad (3.79)$$

these quantities are, of course, also affected by the perturbation size parameter, indeed with $\gamma = \bar{k}_{te}/2$ we have a resonance of 25.9727 Hz with a standard deviation of 3.7948 Hz; while with the diametrically opposed case $\gamma = \bar{k}_{te}/100$ we obtain $\bar{f}_{dr} = 26.1856$ Hz and $\hat{\sigma}_f = 0.074$ Hz, see Table 3.3 for the other numerical results.

3.3.2 Collocation method

We analyzed in Chapter 2 Monte Carlo methods have a convergence speed of $O(M^{-1/2})$, this is a big limit in our analysis; in order to have an acceptable error we have to work with at least 1000 samples, see Fig 3.3¹. This is not compatible with the experimental reality, indeed, as already mentioned, it is not easy to measure the variations in the physical characteristics of the oil meatus. In order to have such a high number of data, it would be necessary to focus the tests only on the meatus properties, thus diverting the attention to the real aim of the base-shake sine test: the resonance frequency and the vibrational responses of the spacecraft.

For this purpose, as described in the previous chapter we introduce the Stochastic Collocation method, exploiting the generalized polynomial chaos (gPC) theory. The behaviors highlighted in the numerical experiments with SC are equivalent to those of MC, with a remarkable advantage: the convergence rate of collocation methods is higher and it requires few collocation nodes in the $[-1,1]$ range.

¹The figure is obtained assuming that the exact mean of 3.69 can be reached with SC with $R = 30000$ nodes or with the MC with $M = 100000$, however the latter has a computational time of about 6 hours, so it is advisable to use the first method.

	MC				SC			
	\bar{f}_{dr}	$\hat{\sigma}_f$	$(k_{te})_{min}$	$(k_{te})_{max}$	\bar{f}_{dr}	$\hat{\sigma}_f$	$(k_{te})_{min}$	$(k_{te})_{max}$
Deterministic								
$f_{dr} = 26.1844$								
$\bar{k}_{te} = 2.1535$								
Stochastic								
<u>Uniform</u>								
$\gamma = \bar{k}_{te}/2$	25.9727	3.7948	1.0784	3.2280	25.8971	3.8628	1.1495	3.1575
$\gamma = \bar{k}_{te}/5$	26.1677	1.4908	1.7234	2.5833	26.1404	1.5157	1.7519	2.5551
$\gamma = \bar{k}_{te}/10$	26.1868	0.7438	1.9385	2.3684	26.1735	0.7559	1.9527	2.3543
$\gamma = \bar{k}_{te}/25$	26.1879	0.2973	2.0675	2.2395	26.1827	0.3022	2.0732	2.2338
$\gamma = \bar{k}_{te}/50$	26.1866	0.1487	2.1105	2.1965	26.1840	0.1510	2.1133	2.1937
$\gamma = \bar{k}_{te}/100$	26.1856	0.0743	2.1320	2.1750	26.1843	0.0755	2.1334	2.1736

Table 3.3: Table of the results obtained in the various numerical experiments. \bar{f}_{dr} is expected resonance frequency (in Hz), while $\hat{\sigma}_f$ is the deviation standard error (in Hz). $(k_{te})_{min}$ and $(k_{te})_{max}$ are the minimums and maximums perturbed stiffness in N·m. Note: for simplicity of reading the table, the order of magnitude of the stiffnesses has not been reported, it is equal to $\cdot 10^8$.

In Fig. 3.3 we can see that with only 6 nodes the error committed by the method is equal to $1.4673 \cdot 10^{-4}$, while with MC to have the same order convergence error we should work with a number of nodes much higher than the one used in this thesis.

So SC is faster in computational time and accuracy than the MC.

Using the Gauss-Legendre quadrature formula as in (2.60)-(2.61) we are able to approximate the mean and the variance of the $\ddot{\theta}_1(t)$

$$\mathbb{E}(\ddot{\theta}(t)) = \frac{1}{2} \int_{-1}^1 \ddot{\theta}_1(z, t) dz \approx \frac{1}{2} \sum_{k=1}^R w_k \ddot{\theta}_1(z_k, t) = \ddot{\theta}_1(t) \quad \text{and} \quad \hat{\sigma}_{\ddot{\theta}}^2(t) \approx \frac{1}{2} \int_{-1}^1 \ddot{\theta}_1(z, t)^2 dz - \ddot{\theta}_1(t)^2$$

where R is the number of nodes and w_k are the corresponding weights.

In Fig. 3.5 is represented the mean $\ddot{\theta}_1$, when perturbation size γ varies. The behavior in SC is similar to the MC case, we can see how the fluctuation of the uncertainty bands tend to narrow around the expected $\ddot{\theta}_1$ as the perturbation size γ decreases. However, there are a couple of differences.

Firstly, for γ equal to 50% of the value of \bar{k}_{te} , we notice how the mean, unlike MC, loses less its oscillatory behavior; for times between 0.3 and 0.4 s, the uncertainty bands and the expected $\ddot{\theta}_1$ begin to oscillate again, this is due to the fact that the perturbations on the meatus stiffness is smaller, it varies between $1.1495 \cdot 10^8$ N·m and $3.1575 \cdot 10^8$ N·m.

Remember that the damping is proportional and so linearly depending on the stiffness matrix, hence it is perturbed and this influences the behavior for large times. Indeed, we have another difference in the cases γ equal to 20% and 10% for times $t \geq 0.7$ s: in the MC case the oscillatory trend of the average and the respective bands is completely lost, instead it is present in the SC and consistent with the deterministic solution in Fig 3.2.

Decreasing the perturbation size up to the extreme case $\gamma = \bar{k}_{te}/100$, that is equal to 1% of

the stiffness of the oil meatus, observe how it is no longer possible to distinguish, the variability around the expectation.

The resonance frequencies are reported in the Table 3.3 as they vary by γ . The expected frequencies \bar{f}_{dr} are lower and closer to the deterministic value, however the standard deviations are slightly wider. With a perturbation size of γ equals to 2% of k_{te} we get a value of 26.1840 Hz with a deviation of 0.1510 Hz from the higher 26.1866 Hz and 0.1487 Hz in the Monte Carlo method.

With $\gamma = \bar{k}_{te}/100$ the frequency is almost deterministic with a standard deviation of 0.0755 Hz, which means that although the perturbation on k_{te} is not excessively high the resonance frequency for the rotational case at 2 degrees of freedom is not affected drastically.

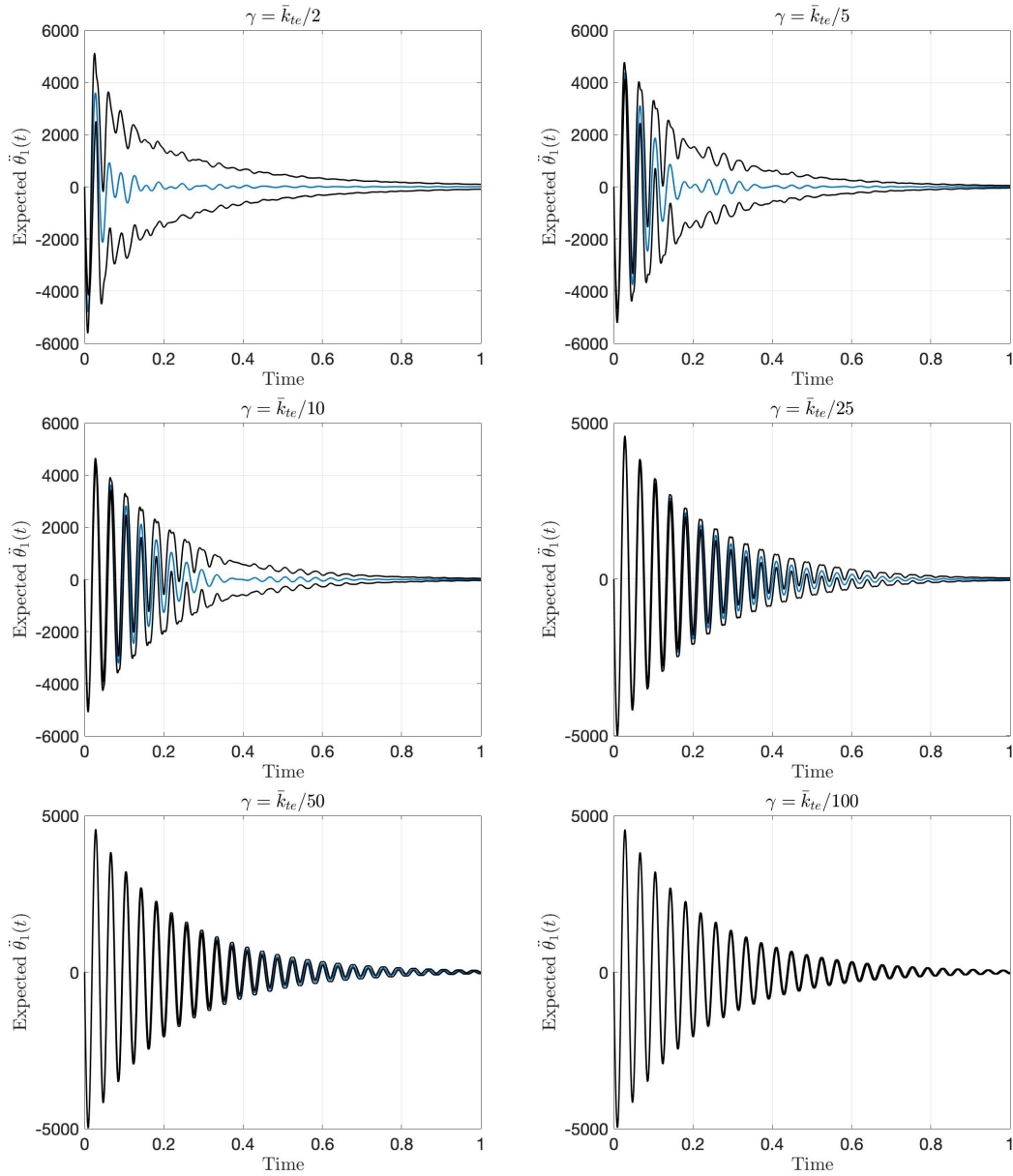


Figure 3.4: Monte Carlo method: representation of the expected $\ddot{\theta}_1$ in rad/s^2 (in blue) with the uncertainty band (in black), varying the perturbation size γ , $M=1000$.

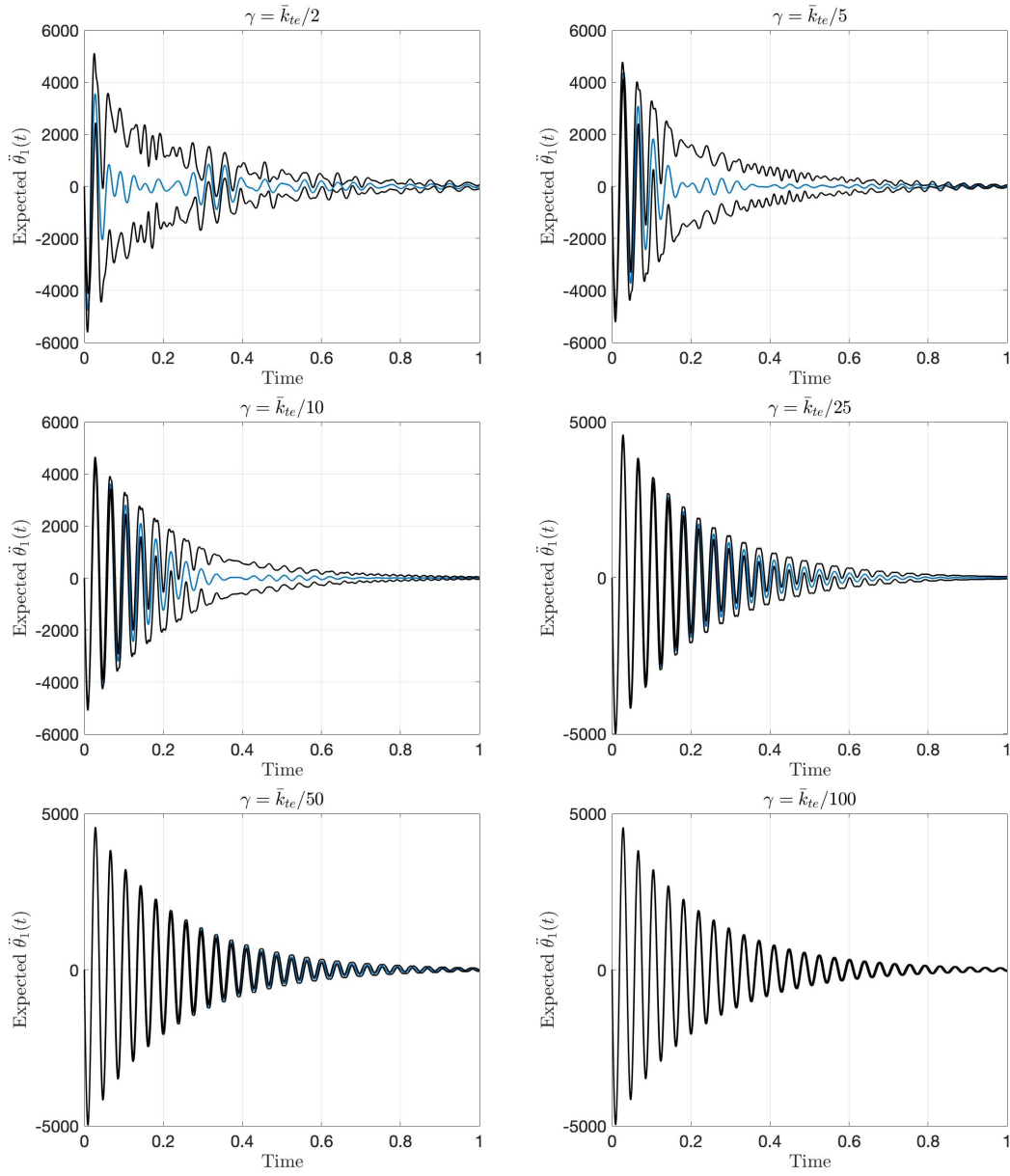


Figure 3.5: Stochastic Collocation method: representation of the expected $\ddot{\theta}_1$ in rad/s^2 (in blue) with the uncertainty band (in black), varying the perturbation size γ , $R=6$.

Chapter 4

3-Degrees of Freedom

In this chapter we continue the analysis of the system composed by the seismic mass and the test article adding a new degree of freedom. The new Lagrangian coordinate x represents the relative horizontal translation of the CoG of the test target. Since the centre of mass at the initial condition is indicated with the point C , the new free coordinate is $x = \overline{C' - C}$, where C' is the CoG for $t \geq 0$.

Thus we define the following coordinates:

- $\theta_1(t)$: the rotation of the target mass m around the point C ;
- $\theta_2(t)$: the rotation of the seismic mass M around the point O ;
- $x(t)$: the relative horizontal translation of the target mass m ;

There is a need to add the external force and the spring, with its damping, which approximate the operation of the coil. All this, together with the addition of a degree of freedom, turns out to be an obvious step for a more in-depth analysis of the physical system. However, this choices bring with them a considerable increase in complications. For the reasons just mentioned, in this chapter it will no longer be possible to calculate analytically the quantities in use, these will be obtained numerically with the same methods used in the previous chapter. This approach is justified by the results of the 2-dof system.

4.1 The Mathematical Model

The mathematical approach applied in this section is similar to the one used in Chapter 3. The aim is to build an ODE system with three equations in such a way to solve it through the modal analysis.

The *Lagrange equation* becomes:

$$\frac{d}{dt} \left(\frac{\partial}{\partial \dot{q}_k} T \right) - \frac{\partial}{\partial q_k} T = Q_k^{(a)} \quad \text{with} \quad \{q(t)\} = \{\theta_1(t), \theta_2(t), x(t)\} \quad (4.1)$$

where T is the *kinetic energy* of the system calculated as follows

$$T = T_m + T_M = \frac{1}{2} I_M \dot{\theta}_2^2 + \frac{1}{2} I_m (\dot{\theta}_1 + \dot{\theta}_2)^2 + \frac{1}{2} m |v_{C'}|^2 \quad (4.2)$$

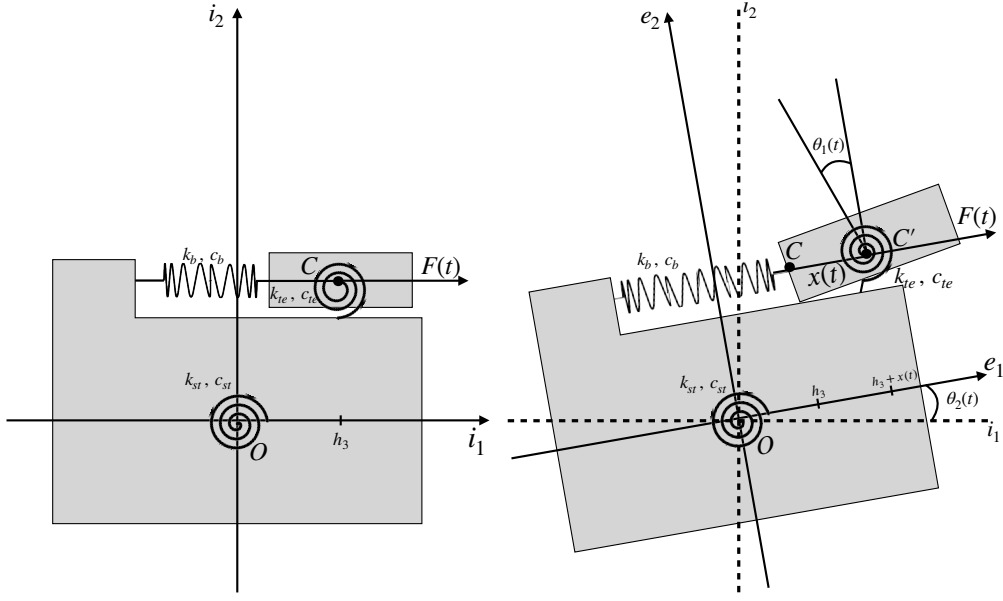


Figure 4.1: The 3 dof system at the initial condition $t = 0$ (on the left) and for $t > 0$ with the three lagrangian coordinate $\{\theta_1(t), \theta_2(t), x(t)\}$ (on the right).

where $v_{C'}$ is the velocity of the CoG of the mass m and is obtained as the time derivative of its coordinates

$$\begin{aligned}
 \Phi_{C'} &= \overline{C' - C} + \overline{C - O} = x\mathbf{e}_1 + h_3\mathbf{e}_1 + \Delta h\mathbf{e}_2 \\
 &= [(x + h_3)\cos\theta_2 - \Delta h\sin\theta_2]\mathbf{i}_1 + [(x + h_3)\sin\theta_2 + \Delta h\cos\theta_2]\mathbf{i}_2 \\
 \Phi_C &= \overline{C - O} = h_3\mathbf{e}_1 + \Delta h\mathbf{e}_2 \\
 &= [h_3\cos\theta_2 - \Delta h\sin\theta_2]\mathbf{i}_1 + [h_3\sin\theta_2 + \Delta h\cos\theta_2]\mathbf{i}_2
 \end{aligned} \tag{4.3}$$

Fig. 4.1 shows the system with the damped springs and the external force applied to the CoG of the test target. Therefore, we can define the angular moments and active force as

$$\begin{aligned}
 \mathbf{M}_{te} &= -k_{te}\theta_1\mathbf{i}_3 - c_{te}\dot{\theta}_1\mathbf{i}_3 \\
 \mathbf{M}_{st} &= -k_{st}\theta_2\mathbf{i}_3 - c_{st}\dot{\theta}_2\mathbf{i}_3 \\
 \mathbf{F}(t) &= F(t)\mathbf{e}_1 = F(t)\cos\theta_2\mathbf{i}_1 + F(t)\sin\theta_2\mathbf{i}_2 \\
 \mathbf{F}_b &= -k_b x - c_b \dot{x}\mathbf{e}_1 \\
 &= -k_b x(\cos\theta_2\mathbf{i}_1 + \sin\theta_2\mathbf{i}_2) - c_b \dot{x}(\cos\theta_2\mathbf{i}_1 + \sin\theta_2\mathbf{i}_2)
 \end{aligned}$$

these angular moments produce the rotations of the masses m and M :

$$\begin{aligned}
 \boldsymbol{\varepsilon}_M &= \theta_2\dot{\mathbf{i}}_3 \\
 \boldsymbol{\varepsilon}_m &= (\theta_1 + \theta_2)\dot{\mathbf{i}}_3
 \end{aligned}$$

and the virtual rotations are obtained as

$$\begin{aligned}\delta\boldsymbol{\varepsilon}_M &= \frac{\partial\boldsymbol{\varepsilon}_M}{\partial x}\delta x + \frac{\partial\boldsymbol{\varepsilon}_M}{\partial\theta_1}\delta\theta_1 + \frac{\partial\boldsymbol{\varepsilon}_M}{\partial\theta_2}\delta\theta_2 \\ &= \delta\theta_2\mathbf{i}_3, \\ \delta\boldsymbol{\varepsilon}_m &= \frac{\partial\boldsymbol{\varepsilon}_m}{\partial x}\delta x + \frac{\partial\boldsymbol{\varepsilon}_m}{\partial\theta_1}\delta\theta_1 + \frac{\partial\boldsymbol{\varepsilon}_m}{\partial\theta_2}\delta\theta_2 \\ &= (\delta\theta_1 + \delta\theta_2)\mathbf{i}_3\end{aligned}$$

We identify the virtual displacement of the CoG of the mass m with the following expression

$$\begin{aligned}\delta\mathbf{C}' &= \frac{\partial\Phi_{C'}}{\partial x}\delta x + \frac{\partial\Phi_{C'}}{\partial\theta_1}\delta\theta_1 + \frac{\partial\Phi_{C'}}{\partial\theta_2}\delta\theta_2 \\ &= [\cos\theta_2\mathbf{i}_1 + \sin\theta_2\mathbf{i}_2]\delta x \\ &\quad + [(-\Delta h \cos\theta_2 - (x + h_3)\sin\theta_2)\mathbf{i}_1 + (-\Delta h \sin\theta_2 + (x + h_3)\cos\theta_2)\mathbf{i}_2]\delta\theta_2\end{aligned}$$

and

$$\begin{aligned}\delta\mathbf{C} &= \frac{\partial\Phi_C}{\partial x}\delta x + \frac{\partial\Phi_C}{\partial\theta_1}\delta\theta_1 + \frac{\partial\Phi_C}{\partial\theta_2}\delta\theta_2 \\ &= [(-\Delta h \cos\theta_2 - h_3 \sin\theta_2)\mathbf{i}_1 + (-\Delta h \sin\theta_2 + h_3 \cos\theta_2)\mathbf{i}_2]\delta\theta_2\end{aligned}$$

The virtual work using the same formula as (3.3) is

$$\begin{aligned}\delta L^{(a)} &= \mathbf{M}_{st} \cdot \delta\boldsymbol{\varepsilon}_M + \mathbf{M}_{te} \cdot \delta\boldsymbol{\varepsilon}_m - \mathbf{M}_{te} \cdot \delta\boldsymbol{\varepsilon}_M + \mathbf{F}(t) \cdot \delta\mathbf{C}' + \mathbf{F}_b \cdot \delta\mathbf{C}' - \mathbf{F}_b \cdot \delta\mathbf{C} \\ &= [-k_{st}\theta_2 - c_{st}\dot{\theta}_2]\delta\theta_2 \\ &\quad + [-k_{te}\theta_1 - c_{te}\dot{\theta}_1]\delta\theta_1 \\ &\quad + F(t)\delta x - \Delta h F(t)\delta\theta_2 \\ &\quad + [-k_b x - c_b \dot{x}]\delta x + [\Delta h(k_b x + c_b \dot{x})]\delta\theta_2 \\ &\quad - [\Delta h(k_b x + c_b \dot{x})]\delta\theta_2\end{aligned}\tag{4.4}$$

which becomes

$$\begin{aligned}\delta L^{(a)} &= +[-k_{te}\theta_1 - c_{te}\dot{\theta}_1]\delta\theta_1 \\ &\quad + [-k_{st}\theta_2 - c_{st}\dot{\theta}_2 - \Delta h F(t)]\delta\theta_2 \\ &\quad + [F(t) - k_b x - c_b \dot{x}]\delta x\end{aligned}\tag{4.5}$$

We recognize the three generalized Lagrangian forces, one for each free coordinate

$$\begin{aligned}Q_{\theta_1}^{(a)} &= -k_{te}\theta_1 - c_{te}\dot{\theta}_1 \\ Q_{\theta_2}^{(a)} &= -k_{st}\theta_2 - c_{st}\dot{\theta}_2 - \Delta h F(t) \\ Q_x^{(a)} &= F(t) - k_b x - c_b \dot{x}\end{aligned}\tag{4.6}$$

Using (4.1) with (4.6) we have the three equations of motion:

$$\begin{aligned}I_m\ddot{\theta}_1 + I_m\ddot{\theta}_2 + k_{te}\theta_1 + c_{te}\dot{\theta}_1 &= 0 \\ m\ddot{x} - m\Delta h\ddot{\theta}_2 - m(h_3 + x)\dot{\theta}_2^2 + k_b x + c_b \dot{x} &= F(t) \\ 2m(h_3 + x)\dot{x}\dot{\theta}_2 - \Delta h m\ddot{x} + I_m\ddot{\theta}_1 + (I_m + I_M + (\Delta h^2 + h_3^2)m + mx(2h_3 + x))\ddot{\theta}_2 \\ + k_{st}\theta_2 + c_{st}\dot{\theta}_2 &= -\Delta h F(t)\end{aligned}\tag{4.7}$$

It is observed that the obtained equations are coupled and non-linear. However, the quantities involved are rather small because it would be physically unacceptable to obtain large angles and displacements. Due to this observation, it is possible to exploit the linearization around the equilibrium configuration of the unforced system (see Appendix A). The latter are simply calculated setting to zero the three Lagrangian forces, and they result:

$$\theta_1^{eq} = \theta_2^{eq} = 0, \quad x^{eq} = 0. \quad (4.8)$$

now defining a auxiliary variable η it is possible to assume the linearized coordinates around the equilibrium points as

$$\begin{aligned} \theta_1(t) &= \theta_1^{eq} + \varepsilon\eta_1(t) = \varepsilon\eta_1(t) \\ \theta_2(t) &= \theta_2^{eq} + \varepsilon\eta_2(t) = \varepsilon\eta_2(t) \\ x(t) &= x^{eq} + \varepsilon\eta_3(t) = \varepsilon\eta_3(t) \end{aligned} \quad (4.9)$$

where $0 < \varepsilon \ll 1$ and $|\eta| = \mathcal{O}(1)$. Moreover we know that $F(t)$ is an oscillating function around the point C , its expression is

$$F(t) = ma_{sw}$$

where a_{sw} is the sine sweep acceleration [20]:

$$a_{sw} = \left(1 - e^{-t/2}\right) \sin\left(2\pi \frac{60f_0}{R_f \cdot \ln 2} \left(2^{\frac{R_f}{60}t} - 1\right)\right)$$

f_0 is the initial frequency and R_f is called the sweep rate. Due to its formulation, we could consider small oscillations around the equilibrium point, so that $F(t)$ can be scaled as $\varepsilon F(t)$.

At this point it is immediate to linearize the equations, simply by replacing the linearized coordinates defined in (4.9) in the system of ordinary differential equations (4.7).

Let us start with the Lagrangian coordinate x , using the Taylor expansion we obtain:

$$m\varepsilon\ddot{\eta}_2 - \Delta hm\varepsilon\ddot{\eta}_2 - m(h_3 + \varepsilon\eta_3)(\varepsilon\dot{\eta}_2)^2 + k_b\varepsilon\eta_3 + c_b\varepsilon\dot{\eta}_3 = \varepsilon F(t) \quad (4.10)$$

by neglecting higher order terms in ε the equation becomes

$$m\varepsilon\ddot{\eta}_2 - \Delta hm\varepsilon\ddot{\eta}_2 + k_b\varepsilon\eta_3 + c_b\varepsilon\dot{\eta}_3 = \varepsilon F(t) \quad (4.11)$$

and then dividing by ε we have the linearized equation for the Lagrangian coordinate η_3

$$m\ddot{\eta}_3 - \Delta hm\ddot{\eta}_2 + k_b\eta_3 + c_b\dot{\eta}_3 = F(t) \quad (4.12)$$

Using the same approach we obtain the linearized equations for η_1 :

$$I_m\ddot{\eta}_1 + I_m\ddot{\eta}_2 + k_{te}\eta_1 + c_{te}\dot{\eta}_1 = 0 \quad (4.13)$$

and for η_2 :

$$I_m\ddot{\eta}_1 - \Delta hm\ddot{\eta}_3 + (I_m + I_M + (\Delta h^2 + h_3^2)m)\ddot{\eta}_2 + k_{st}\eta_2 + c_{st}\dot{\eta}_2 = -\Delta hF(t) \quad (4.14)$$

In conclusion, we are able to write the ODE system for the 3-dof case in a matrix form using the (4.13)-(4.14)-(4.12) as

$$[m]\{\ddot{\eta}\} + [c]\{\dot{\eta}\} + [k]\{\eta\} = \{f(t)\}, \quad \{\eta\} = \begin{pmatrix} \eta_1 \\ \eta_2 \\ \eta_3 \end{pmatrix} \quad (4.15)$$

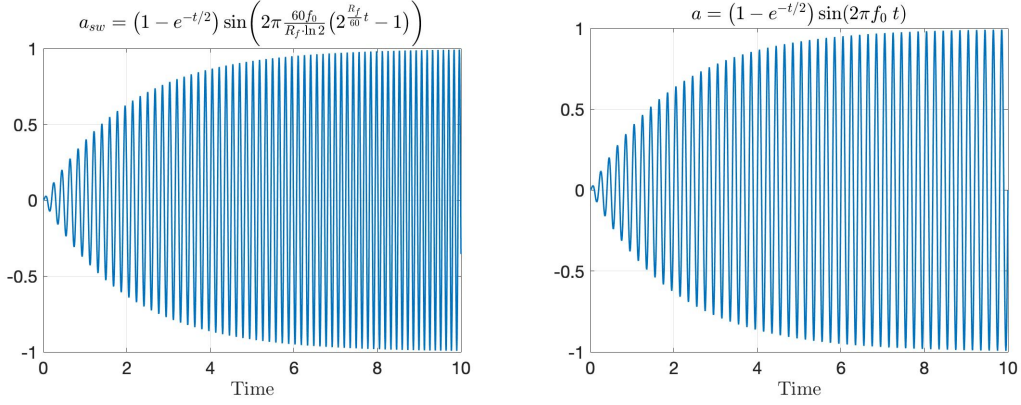


Figure 4.2: The sweep acceleration a_{sw} imposed to the slip table (on the left) compared with its approximation a (on the right). In a_{sw} it is easy to observe the sweep behavior as time progresses.

where:

$$[m] = \begin{bmatrix} I_m & I_m & 0 \\ I_m & I_m + I_M + (\Delta h^2 + h_3^2)m & -m\Delta h \\ 0 & -m\Delta h & m \end{bmatrix}$$

$$[c] = \begin{bmatrix} c_{te} & 0 & 0 \\ 0 & c_{st} & 0 \\ 0 & 0 & c_b \end{bmatrix} \quad [k] = \begin{bmatrix} k_{te} & 0 & 0 \\ 0 & k_{st} & 0 \\ 0 & 0 & k_b \end{bmatrix}$$

while the vector of the external force is:

$$\{f(t)\} = \begin{pmatrix} 0 \\ -\Delta h F(t) \\ F(t) \end{pmatrix}$$

4.1.1 Sweep approximation

Let us assume $F(t)$ as the force applied by the coil to the slip table. Exploiting the assumptions and the hypothesis of Chapter 1, we suppose that the force is applied directly to the point C , the CoG of the S/C+VTA+ST. The expression of the external force is

$$F(t) = ma_{sw} \quad (4.16)$$

where a_{sw} is the sine sweep acceleration:

$$a_{sw} = (1 - e^{-t/2}) \sin\left(2\pi \frac{60f_0}{R_f \cdot \ln 2} (2^{\frac{R_f}{60}t} - 1)\right) \quad (4.17)$$

f_0 is the initial frequency and R_f is called the sweep rate. Note that the first exponential term is used to describe the physical fact that the coil starts from standstill and gradually reaches the regime state and it could be neglected. However, this definition of the sweep acceleration is not in line with the harmonic external force required in some modal analysis tools, such as receptance, so we have to rework the expression.

Firstly we use the Mclaurin expansion of $2^{\frac{R_f}{60}t}$, obtaining:

$$2^{\frac{R_f}{60}t} = 1 + \frac{R_f}{60}t \ln 2 + o(t)$$

and replacing in the (4.17) we redefine the sweep acceleration as:

$$a = \left(1 - e^{-t/2}\right) \sin(2\pi f_0 t) \simeq \sin(2\pi f_0 t) \quad (4.18)$$

A convenient representation of an harmonic function pulse is $\Omega = 2\pi f_0$. It is easy now to write the force vector $\{f(t)\}$ applied to the system, as:

$$\{f(t)\} = \begin{pmatrix} 0 \\ -\Delta h F(t) \\ F(t) \end{pmatrix} \simeq \begin{pmatrix} 0 \\ -m\Delta h \\ m \end{pmatrix} \sin(\Omega t) = \{h(t)\} \quad (4.19)$$

where $\{h(t)\}$ is the harmonic force vector and $\{H_0\} = (0, -m\Delta h, m)^T$.

4.1.2 Application of the modal approach to the 3-dof satellite problem

In case of viscous proportional damping the forced solution could be calculated using the modal transformation $\{\eta\} = [\Psi]\{\phi\}$, calculating the eigenvalues and the eigenvectors of the undamped and unforced system.

Therefore replacing $\{\eta\}$ and applying the $[\Psi]^T$ directly to the equation (4.15), we could exploit the m -orthogonality and the k -orthogonality explained in the previous section, as follows

$$[\Psi]^T [m] [\Psi] \{\ddot{\phi}\} + [\Psi]^T [c] [\Psi] \{\dot{\phi}\} + [\Psi]^T [k] [\Psi] \{\phi\} = [\Psi]^T \{f(t)\} \quad (4.20)$$

that becomes:

$$\text{diag}[m] \{\ddot{\phi}\} + (\beta \text{diag}[k]) \{\dot{\phi}\} + \text{diag}[k] \{\phi\} = [\Psi]^T \{f(t)\} \quad (4.21)$$

if we fix $r = 1, 2, 3$ and $\beta k_r = c_r$, for simplicity of notation, we have:

$$m_r \ddot{\phi}_r + \beta k_r \dot{\phi}_r + k_r \phi_r = \{\Psi_r\}^T \{f(t)\} \quad (4.22)$$

using the sweep approximation defined in (4.18) we have

$$m_r \ddot{\phi}_r + \beta k_r \dot{\phi}_r + k_r \phi_r = \{\Psi_r\}^T \{H_0\} \sin(\Omega t) \quad (4.23)$$

Due to the linearization of the equation we could find a solution at regime as $\{\eta(t)\} = \{\eta_0\} \sin(\Omega t)$, we could note that the modal coordinates will be harmonic at regime as well; that leads to the equation:

$$(k_r - \Omega^2 m_r + \Omega c_r) \phi_r(t) = \{\Psi_r\}^T \{H_0\} \sin(\Omega t) \quad (4.24)$$

and:

$$\{\eta(t)\} = \{\eta_0\} \sin(\Omega t) = \sum_{r=1}^3 \{\Psi_r\} \phi_r(t) = \sum_{r=1}^3 \{\Psi_r\} \phi_{r0} \sin(\Omega t) \quad (4.25)$$

Finally we obtain the amplitude of the oscillation at regime expressed by:

$$\{\eta_0\} = \sum_{r=1}^3 \frac{\{\Psi_r\}^T \{H_0\} \{\Psi_r\}}{k_r - \Omega^2 m_r + \Omega c_r} \quad (4.26)$$

and we could define the receptance as:

$$a_{jk}(\Omega) = \left. \frac{\eta_{j0}}{H_{k0}} \right|_{H_{i0}=0, \forall i \neq k} \quad (4.27)$$

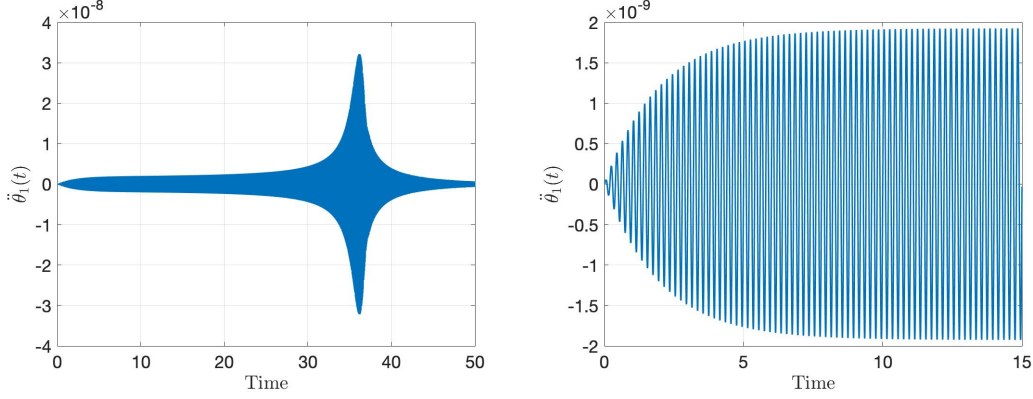


Figure 4.3: The numerical acceleration in rad/s^2 of the forced 3 dof system using Runge-Kutta method on the (4.22) (on the left) and on (4.23) (on the right).

Note that the all forces must be set to zero, except for the k -th degree of freedom.

Using the (4.26) and the (4.27) we are now able to write the expression of the receptance as:

$$a_{jk}(\Omega) = \sum_{r=1}^3 \frac{\Psi_{jr} \Psi_{kr}}{k_r - \Omega^2 m_r + \Omega c_r} = \sum_{r=1}^3 \frac{\tilde{\Psi}_{jr} \tilde{\Psi}_{kr}}{\omega_r^2 - \Omega^2 + 2\zeta_r \Omega \omega_r} \quad (4.28)$$

where $\tilde{\Psi}_r = \Psi_r / \sqrt{m_r}$ is the m -normalized eigenvector.

The receptance is particularly useful to calculate the resonance frequencies of the system, in fact the latter are the frequencies that maximize the modulus of a_{ij} ; note that in general an external force in complex exponential form is $G(t) = G_0 e^{i\Omega t}$ and the receptance will be a complex function, while in this analysis we have that:

$$\{f(t)\} \simeq \{h(t)\} = \{H_0\} \sin(\Omega t) = \Im(\{H_0\} e^{i\Omega t}). \quad (4.29)$$

4.2 Numerical Analysis

In this section the numerical results obtained from the mathematical model will be presented and analyzed.

Firstly we observe that in this system it is no longer possible, with respect to to the previous chapter, to calculate analytically quantities as natural pulse ω and the modal matrix $[\Psi]$. However, thanks to the good results obtained by the two degrees of freedom problem, we can rely on some pre-implemented MATLAB functions. Exploiting the **eig** function, we solve the eigenvalue problem of the 3-dof system undamped and unforced where the stiffness matrix and the mass matrix is defined in (4.15).

In order to obtain the displacement of the target test identified by the coordinate $\theta_1(t)$, there is no need to approximate the sweep acceleration with the equation (4.18), indeed in this phase of the study the theory of modal analysis does not require the harmonicity of the external force. Thus, we use a numerical integration method as Runge-Kutta with the fourth-order of accuracy in order to solve (4.22). Fig. 4.3 represents the angular acceleration $\ddot{\theta}_1(t)$. The acceleration peak at time $t = 36.17$ s corresponds to the attainment of the resonance frequency for the free coordinate θ_1 , this is due to the nature of the force obtained from a sweep-type acceleration, which increases the oscillation frequency with the passage of time [20]. It is important to observe

how the oscillations are so close, this happens because of the small wavelength.

The analytical calculation of the solution according to the theory of the vibration mechanics of forced systems with many degrees of freedom is possible but it is fairly articulate and complex, although the good agreement of the previous chapter allows us to neglect this calculation.

It is important to highlight that to calculate the receptance defined by the (4.28), we have to use the harmonic external force $\{h(t)\}$ in (4.19). So, to get the solution $\theta_1(t)$ and its respective acceleration $\ddot{\theta}_1(t)$ we use the equation (4.22) with the external forces vector $\{f(t)\}$, while to get the resonance frequencies defined in (4.28) we have to approximate the force to the harmonic $\{h(t)\}$. Note that in Fig. 4.3, on the right, it is represented the acceleration $\ddot{\theta}_1(t)$ computed with Runge-Kutta on (4.23). Due to the harmonicity of the force, the acceleration peak is not obtained and a smaller time interval is reported.

In Fig. 4.4 is represented the receptances; we can see the three peaks corresponding to the three resonance frequencies of the 3-dof system. The frequency of interest corresponding to rotation θ_1 of the test target and it is the third.

The resonance frequency of the damped unforced 3-dof is 26,1821 Hz and it is slightly lower than the forced one as 26.9306 Hz. However, the obtained result is in good agreement with the one deduced in the previous chapter, the unforced resonance frequency of the 3-dof system is 0.0023 Hz lower than the 2-dof; thus the addition of a degree of freedom does not drastically affect the unforced resonance of the test article. The results are summarized in Table 4.2.

4.2.1 Initial Conditions

The initial conditions of the ODE for the 3-dof system are set to zero. This is consistent with the experimentation, in fact the system at the initial instant starts from standstill; then it begins to swing, under the effect of the external force exerted by the shaker (coil) at the slip table.

Compared to the previous chapter in which there was no forcing and therefore at a practical level we had to assume a non-zero initial condition for $\dot{\theta}_1(0)$. In this analysis the presence of $\{f(t)\}$ allows us to be more physically consistent for initial conditions, as follows:

$$\{q(0)\} = \begin{pmatrix} 0 \\ 0 \\ 0 \end{pmatrix}, \quad \{\dot{q}(0)\} = \begin{pmatrix} 0 \\ 0 \\ 0 \end{pmatrix} \quad (4.30)$$

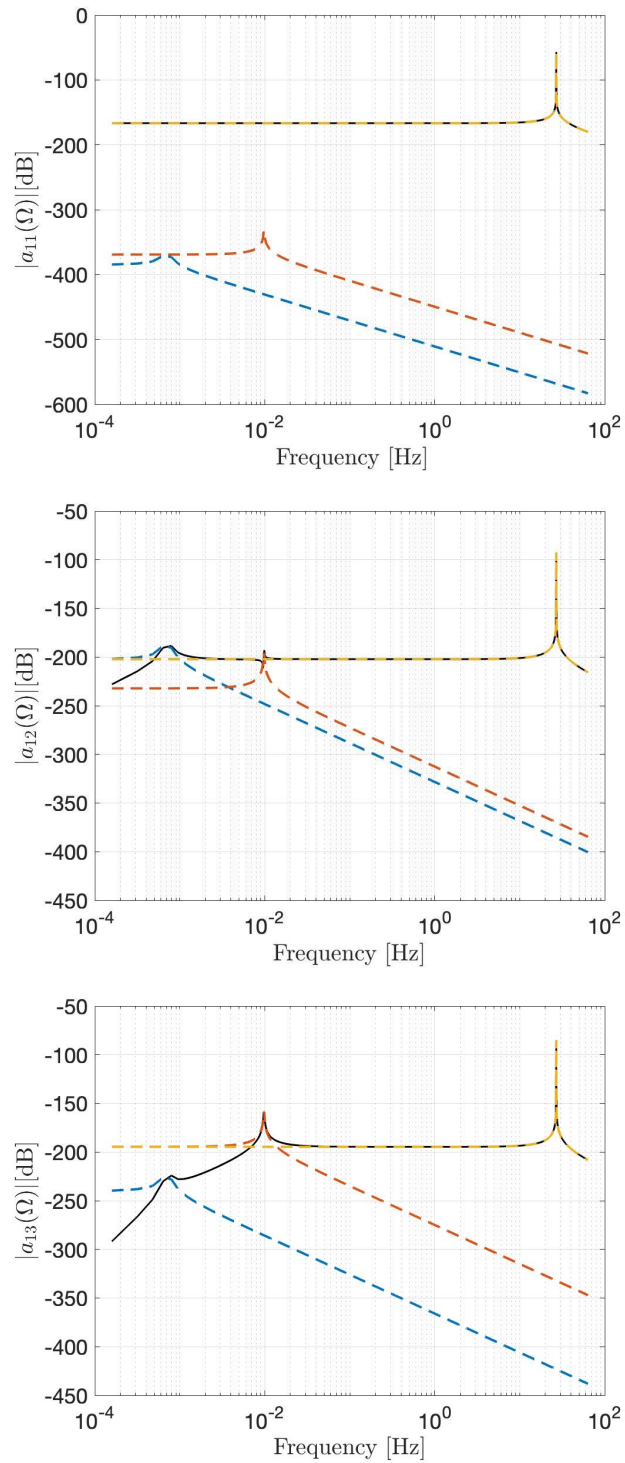


Figure 4.4: The receptances of the deterministic system in semilogarithmic scale. Their modal contributes are represented in dashed lines.

	MC			SC		
	$(k_{te})_{min}$	$(k_{te})_{max}$	Δk_{te}	$(k_{te})_{min}$	$(k_{te})_{max}$	Δk_{te}
Deterministic $\bar{k}_{te} = 2.1535$						
Stochastic						
<u>Uniform</u>						
$\gamma = \bar{k}_{te}/2$	1.0784	3.2280	1.0751	1.1495	3.1575	1.0040
$\gamma = \bar{k}_{te}/5$	1.7234	2.5833	0.4301	1.7519	2.5551	0.4016
$\gamma = \bar{k}_{te}/10$	1.9385	2.3684	0.2150	1.9527	2.3543	0.2008
$\gamma = \bar{k}_{te}/25$	2.0675	2.2395	0.0860	2.0732	2.2338	0.0803
$\gamma = \bar{k}_{te}/50$	2.1105	2.1965	0.0430	2.1133	2.1937	0.0402
$\gamma = \bar{k}_{te}/100$	2.1320	2.1750	0.0215	2.1334	2.1736	0.0201

Table 4.1: *Table stiffness perturbations.* $(k_{te})_{min}$ and $(k_{te})_{max}$ are the minimums and maximums in $N \cdot m$. $\Delta k_{te} = \gamma(z_k)_{max}$, $\forall k$. Note: the order of magnitude of the stiffnesses has not been reported, it is equal to $\cdot 10^8$.

4.3 3-DOF Stochastic System

Let us suppose to have the k_{te} parameter uncertain and perturbed by a centered random Z variable, as follows:

$$k_{te} = \bar{k}_{te} + \gamma Z \quad (4.31)$$

where \bar{k}_{te} is the experimental value in Table 1.1, while γ is the perturbation size mentioned in the previous chapter.

Define $Z \sim U[-1,1]$, we present the analysis of the results obtained from the numerical experiments carried out through the two approaches to ordinary differential equations with an uncertain parameter: the Monte Carlo method (MC) and the Stochastic Collocation method (SC).

We must pay particular attention to the fact that in the 3 degrees of freedom (dof) system the oscillations of the test target are very rapid, see Fig. 4.3, this is due to the presence of the external force $\{f(t)\}$ or its approximation $\{h(t)\}$.

4.3.1 Monte Carlo method

Let us fix the sample size M and the perturbation size γ , then we can generate the realizations of the stiffness perturbed by a random variable with known distribution:

$$(k_{te})_k = \bar{k}_{te} + \gamma z_k, \quad k = 1, \dots, M$$

as already described in Chapter 3 for each $(k_{te})_k$ value we have to build the $[k]$ stiffness matrix and the respective $[c]$ damping matrix. By using the `eig` function, we get the natural pulses ω_k , where the index $k = 1, \dots, M$ represents the dependence on the random realizations, and the respective modal eigenvectors.

By using the equation (3.71) we obtain the resonance frequency of the $f_{dr}(z_k)$ of the M deterministic systems, while through the formula of the receptance (4.28), we obtain the resonance frequencies $f_r(z_k)$ of the forced system (4.23). We are interested in the resonance frequency of

the test-target, so we are referring to the case with $r = 3$, which is the third mode in (3.71) and the third peak in the receptance (4.28). The mean and the variance are computed with the formulas:

$$\bar{f}_{dr} = \frac{1}{M} \sum_{k=1}^M f_{dr}(z_k), \quad \hat{\sigma}_f^2 = \frac{1}{M-1} \sum_{k=1}^M (f_{dr}(z_k) - \bar{f}_{dr})^2. \quad (4.32)$$

and

$$\bar{f}_r = \frac{1}{M} \sum_{k=1}^M f_r(z_k), \quad \hat{\sigma}_f^2 = \frac{1}{M-1} \sum_{k=1}^M (f_r(z_k) - \bar{f}_r)^2. \quad (4.33)$$

The results obtained are in line with those of the 2-dof system. We observe how, for γ equal to 50% of \bar{k}_{te} there is a rather high standard deviation in both forced and unforced case, which tends to go down as the perturbation size decreases. Notice that the values of the standard deviations of the \bar{f}_{dr} frequencies are almost equal to those of the 2-dof system in the Table 3.3, which means that, for the same range of γ , the frequency deviations are the same.

Solving by Runge-Kutta with the fourth-order of accuracy the ODE system (4.22) we obtain the M -th realizations:

$$\theta_r(z_k, t), \quad k = 1, \dots, M$$

and respective accelerations

$$\ddot{\theta}_r(z_k, t), \quad k = 1, \dots, M$$

The mean and the variance of the test-item acceleration are computed as in Chapter 3 in (3.76)-(3.77):

$$\bar{\ddot{\theta}}_1(t) = \frac{1}{M} \sum_{k=1}^M \ddot{\theta}_1(z_k, t), \quad \hat{\sigma}_{\ddot{\theta}}^2(t) = \frac{1}{M-1} \sum_{k=1}^M (\ddot{\theta}_1(z_k, t) - \bar{\ddot{\theta}}_1(t))^2, \quad \forall t \geq 0 \quad (4.34)$$

In Fig. 4.5 are represented the accelerations and uncertainty bands (3.78) when the perturbation size γ varies.

We observe that, with γ small the uncertainty band becomes very tight around the mean value $\bar{\ddot{\theta}}_1$, for this reason in the extreme case $\gamma = \bar{k}_{te}/100$ a zoom of the peak obtained at time $t \simeq 36$ s has been added, that shows how the uncertainty band maintains the oscillatory behavior with a different wavelength.

In the case with $\gamma = \bar{k}_{te}/2$, we observe that the uncertainty band has a very wide wavelength compared to the mean value $\bar{\ddot{\theta}}_1$, the latter due to the stiffness variability of the oil meatus tends zero by losing the peak of maximum amplitude oscillation. This is consistent with the larger standard deviation in the frequency \bar{f}_r , see Table 4.2, in fact the peak in the amplitude oscillation represent the achievement by the satellite of the resonance frequency. The range the stiffness k_{te} , see Table 4.1, leads to different time-instants resonance peaks, creating a more streamlined form of the mean acceleration. The same behaviour occurs with $\gamma = \bar{k}_{te}/5$, but the standard deviation of frequency is smaller and this is also noticeable with the uncertainty band in Fig. 4.5, where the number of resonance peaks are in a shorter time interval that goes from $t = 30$ s to $t = 40$ s. This characteristic does not happen with a smaller range values of k_{te} where the standard frequency deviation is lower allowing the expected acceleration to have a more pronounced resonance peak. So the main effect of the uncertainties is the smoothing of the resonance point making it less sharper and abrupt than in cases with a lower perturbation size.

The number of samples used in this analysis is quite elevated ($M = 1000$) however, as in the case of two degrees of freedom the error and computational time can be high, the time taken for each numerical experiment is about 30 min. Moreover, as already mentioned, it would be

	MC				SC			
	\bar{f}_{dr}	$\hat{\sigma}_f$	\bar{f}_r	$\hat{\sigma}_f$	\bar{f}_{dr}	$\hat{\sigma}_f$	\bar{f}_r	$\hat{\sigma}_f$
Deterministic								
$f_{dr} = 26,1821$								
$f_r = 26.9306$								
Stochastic								
<u>Uniform</u>								
$\gamma = \bar{k}_{te}/2$	25.9704	3.7944	26.7233	4.0094	25.8948	3.8624	26.6440	4.0809
$\gamma = \bar{k}_{te}/5$	26.1654	1.4907	26.9156	1.5769	26.1381	1.5156	26.8867	1.6031
$\gamma = \bar{k}_{te}/10$	26.1845	0.7437	26.9338	0.7868	26.1712	0.7559	26.9197	0.7997
$\gamma = \bar{k}_{te}/25$	26.1856	0.2973	26.9344	0.3146	26.1804	0.3021	26.9289	0.3196
$\gamma = \bar{k}_{te}/50$	26.1843	0.1486	26.9330	0.1573	26.1817	0.1511	26.9302	0.1598
$\gamma = \bar{k}_{te}/100$	26.1833	0.0743	26.9319	0.0786	26.1820	0.0755	26.9305	0.0799

Table 4.2: Table of the results obtained in the various numerical experiments. \bar{f}_{dr} is the expected resonance frequency and its standard deviation (in Hz) for the unforced system; while \bar{f}_r is the expected frequency with its deviation (in Hz).

rather difficult to obtain 1000 numerical values of the rigidity of the oil meatus, for this reason we present the results with the second analysis approach chosen for the thesis.

4.3.2 Collocation Method

The Stochastic Collocation methods exploit the gPC projection and the quadrature rules in order to approximate the quantities of interest. The main advantage of the SC methods is that it does not require an excessive number of collocation points R , i.e. we will use $R = 6$ nodes, as in the 2-dof case. Moreover the computational time is reduced, the time taken for each numerical experiments is about 10 seconds.

The mean and the standard deviation are obtained using the approximation of Lebesgue's integral using Gauss-Legendre's formula (since $Z \sim U[-1,1]$) for the vibration frequency of the 3 dof system without the external force, as follows

$$\mathbb{E}(f_{dr}) = \frac{1}{2} \int_{-1}^1 f_{dr}(z) dz \approx \frac{1}{2} \sum_{k=1}^R w_k f_{dr}(z_k) = \bar{f}_{dr} \quad \text{and} \quad \hat{\sigma}_f^2 \approx \frac{1}{2} \int_{-1}^1 f_{dr}^2(z) dz - (\bar{f}_{dr})^2$$

while for the resonance frequency of the 3 dof system with the external force, with the following formula

$$\mathbb{E}(f_r) = \frac{1}{2} \int_{-1}^1 f_r(z) dz \approx \frac{1}{2} \sum_{k=1}^R w_k f_r(z_k) = \bar{f}_r \quad \text{and} \quad \hat{\sigma}_f^2 \approx \frac{1}{2} \int_{-1}^1 f_r^2(z) dz - (\bar{f}_r)^2$$

In Table 4.2 we observe that with a high perturbation size, equal to $\bar{k}_{te}/2$, the standard deviation $\hat{\sigma}_f$ is high. By lowering the perturbation size the deviation tends to decrease, moreover the difference between the deterministic value of f_{dr} (and f_r , respectively) with the mean value \bar{f}_{dr}

(and \bar{f}_r , respectively) obtain in the numerical experiments decrease, until you have a difference of $1 \cdot 10^{-4}$ Hz. Because of the greater accuracy of the SC method, see figure 3.3 of the 2-dof case, we can say that the presence of a very low uncertainty represented by a perturbation size as small as $\gamma = \bar{k}_{te}/100$ allows to obtain an average value very close to the deterministic one with a standard deviation of 0.0755 Hz.

Using the same approach, exploiting the Gauss-Legendre's quadrature formula we can approximate the mean value and the variance of the test-target acceleration:

$$\mathbb{E}(\ddot{\theta}(t)) = \frac{1}{2} \int_{-1}^1 \ddot{\theta}_1(z, t) dz \approx \frac{1}{2} \sum_{k=1}^R w_k \ddot{\theta}_1(z_k, t) = \ddot{\theta}_1(t) \quad \text{and} \quad \hat{\sigma}_{\ddot{\theta}}^2(t) \approx \frac{1}{2} \int_{-1}^1 \ddot{\theta}_1(z, t)^2 dz - \ddot{\theta}_1(t)^2$$

the standard deviation is obtain with the square root of the variance.

In Fig. 4.6 the expected acceleration and the uncertainty band are represented.

The main difference is highlighted in cases with high perturbation size (γ equal to 50% and 20% of the value of \bar{k}_{te}) where we have a more edgy and less smooth trend than the Monte Carlo method both for the $\ddot{\theta}_1$ and for uncertainty band. This affects the variance deviation (and the associated standard deviation) of the resonance frequency which is 4.0809 Hz for case $\gamma = \bar{k}_{te}/2$ and 1.6031 for case $\gamma = \bar{k}_{te}/5$.

Particularly interesting, can be observed that in the Fig. 4.6 for the case with a γ equal to 50% of the \bar{k}_{te} , a zoom of the oscillations in the first time instants has been added to point out that the uncertainty bands follow the oscillatory behavior of the mean acceleration with a higher wavelength. Moreover, it is observed that the uncertainty in the first time instants is smaller for small γ values and it is almost impossible to recognize the uncertainty band and the expected acceleration.

The uncertainty band in the case $\gamma = \bar{k}_{te}/25$ is clearly visible in the time interval between $t = 33$ s and $t = 39$ s, thanks to the zoom placed in Fig 4.6. We can make the same observation in the extreme case $\gamma = \bar{k}_{te}/100$; only by zooming in on the zone of maximum acceleration amplitude we can see the difference between the uncertainty band and the $\ddot{\theta}_1$, this proximity between the two quantities leads to a resonance frequency $\bar{f}_r = 26.9305$ Hz, which is very close to the deterministic one, $f_r = 26.9306$ Hz, with a standard deviation of 7.9 %.

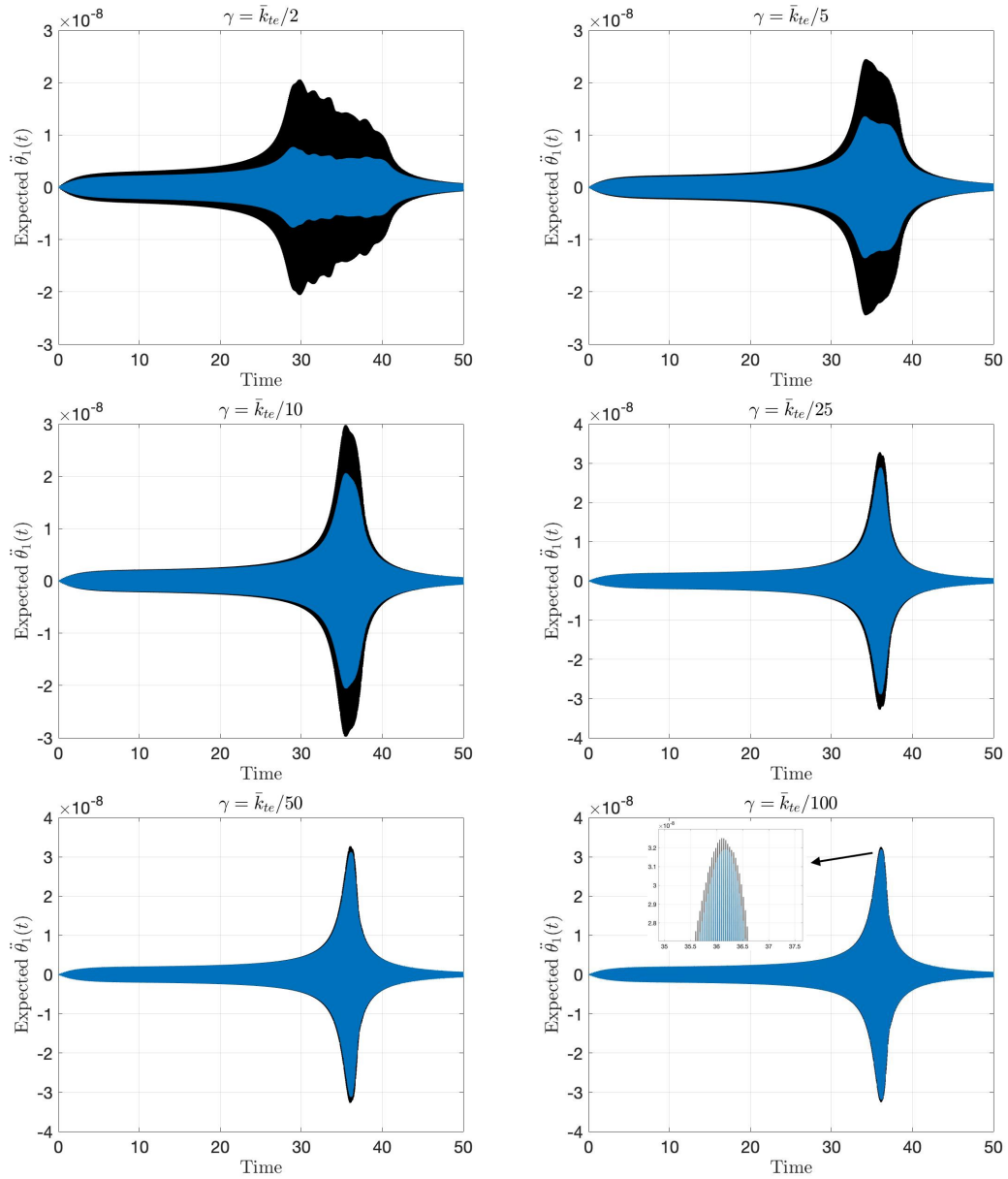


Figure 4.5: Monte Carlo method: representation of the expected $\ddot{\theta}_1$ in rad/s^2 (in blue) with the uncertainty band (in black), varying the perturbation size γ , $M=1000$.

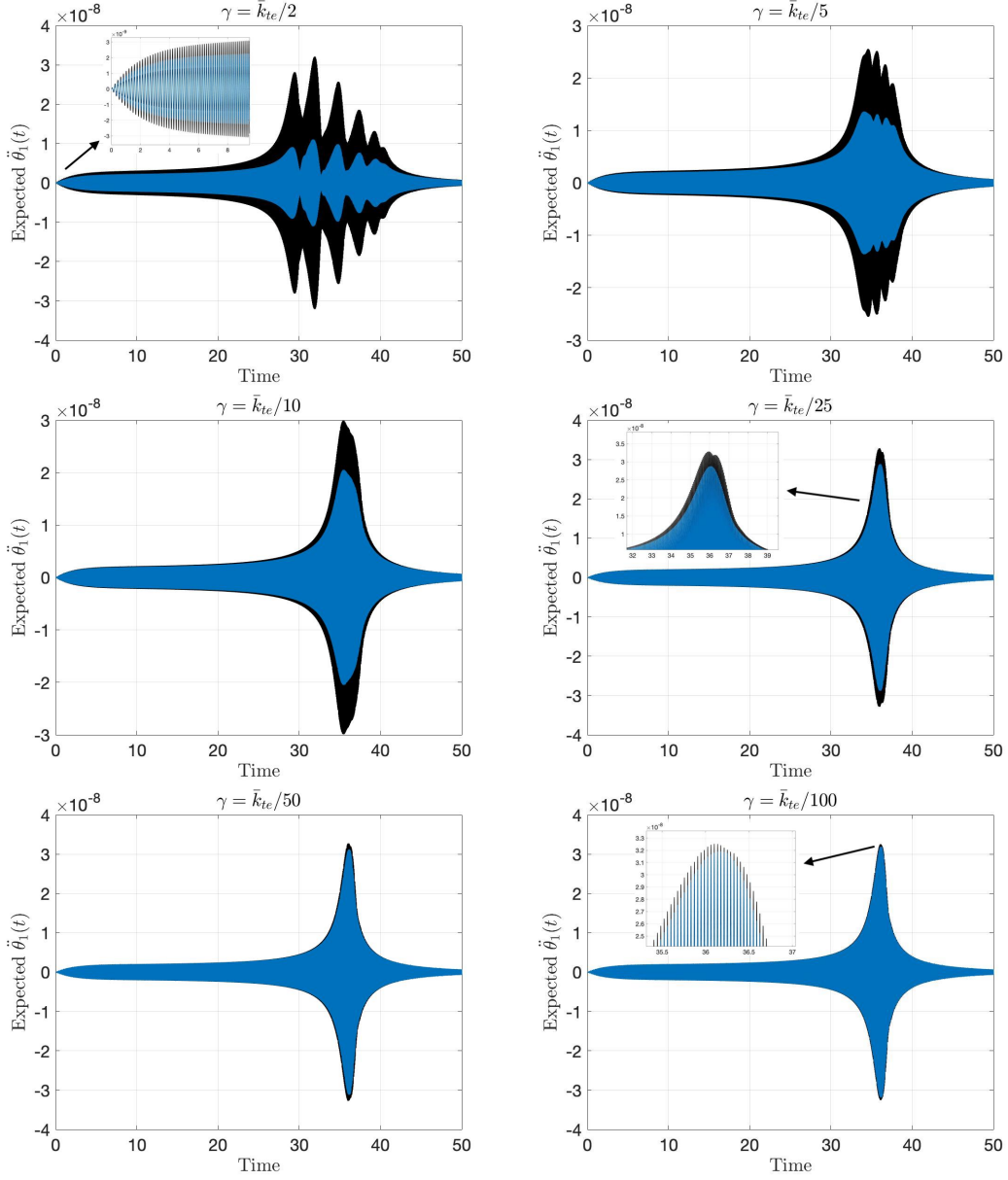


Figure 4.6: Stochastic Collocation method: representation of the expected $\ddot{\theta}_1$ in rad/s^2 (in blue) with the uncertainty band (in black), varying the perturbation size γ , $R=6$.

Chapter 5

Outcomes and future developments

The aim of this thesis was to analyze how unpredictable perturbations on the mechanical stiffness of the components of a shaker assembly could influence the resonance frequency and dynamic characteristics of a satellite.

In order to manage stochastic perturbations, it was necessary to introduce ordinary differential equations with uncertain parameters and then present solving methods clarifying their advantages and disadvantages with numerical experiments.

In the aerospace field, some studies are progressing in the area of uncertainty quantification and these are based on the Monte Carlo (MC) method [9]. In this thesis, we have shown that the MC method has a fairly simple mathematical formulation and also does not require information on the probability distribution of uncertainty. This is certainly an advantage when the distribution is not known and only the experimental data are available; but as we proved in this thesis in particular with the convergence graphs 3.3 and the various numerical results, the Monte Carlo method requires a very high sample number M . The results presented in this thesis are obtained by setting $M = 1000$, despite the high number of sample the error committed in the approximation of the mean value is about $M^{-1/2} \simeq 0.0316$ which is definitely too high considering the orders of magnitude taken into account in this thesis. Moreover, as already mentioned above, supposing to have 1000 experimental values of oil meatus stiffness is wrong because this would shift the attention to the real aim of the base-shake sine test: the resonance frequency and the vibrational responses of the satellite.

For these reasons we presented an alternative method based on the generalized polynomial chaos (gPC) [4]-[15], the Stochastic Collocation (SC) method [2]-[3]. An advantage of the SC lies in a higher convergence rate with a smaller R , collocation nodes, requests; in this thesis, we have shown that with $R = 6$ the approximation error is about $1.4673 \cdot 10^{-4}$, see Fig. 3.3. However, the formulation of the method requires the knowledge of the uncertainty probability distribution, improving the approximation of the quantities of interest.

This thesis presents two case studies: the 2-degrees of freedom without an external force and the 3-degrees of freedom with a sine sweep external force; whose results are summarized in Table 5.1. Note that in Appendix D the results obtained with the 1-dof system are reported.

Using the descriptions of the sine-shake test bases in the literature [18]-[19] and under the supervision of Thales Alenia Space's engineers, a mathematical model was built using Analytical Mechanics. Once the motion equation (3.50) and (4.22)-(4.15) were obtained, the uncertain parameter, i.e. the stiffness of the oil meatus represented by the torsional equivalent rigidity k_{te} ,

	1DOF		2DOF		3DOF			
	Unforced		Unforced		Unforced		Forced	
	\bar{f}_{dr}	$\hat{\sigma}_f$	\bar{f}_{dr}	$\hat{\sigma}_f$	\bar{f}_{dr}	$\hat{\sigma}_f$	\bar{f}_r	$\hat{\sigma}_f$
Deterministic	25.9623		26.1844		26.1821		26.9306	
Stochastic								
<u>Uniform</u>								
$\gamma = \bar{k}_{te}/2$	25.6774	3.8301	25.8971	3.8628	25.8948	3.8624	26.6440	4.0809
$\gamma = \bar{k}_{te}/5$	25.9186	1.5029	26.1404	1.5157	26.1381	1.5156	26.8867	1.6031
$\gamma = \bar{k}_{te}/10$	25.9515	0.7495	26.1735	0.7559	26.1712	0.7559	26.9197	0.7997
$\gamma = \bar{k}_{te}/25$	25.9606	0.2996	26.1827	0.3022	26.1804	0.3021	26.9289	0.3196
$\gamma = \bar{k}_{te}/50$	25.9619	0.1498	26.1840	0.1510	26.1817	0.1511	26.9302	0.1598
$\gamma = \bar{k}_{te}/100$	25.9622	0.0749	26.1843	0.0755	26.1820	0.0755	26.9305	0.0799

Table 5.1: *SC: Table of the results. \bar{f}_{dr} represents the resonance frequency and $\hat{\sigma}_f$ is its deviation standard error (in Hz). \bar{f}_r is the frequency for the forced system and its deviation standard (in Hz).*

was perturbed with a random variable.

Based on the value of the perturbation size γ various numerical results were obtained comparing the Monte Carlo method with the Stochastic collocation method, proving the effectiveness and accuracy of the latter. Moreover, these results show how the oil meatus influenced the resonance frequencies and the dynamic properties of the satellite. About concerning the influence of oil meatus in the resonance frequency, Table 5.1 shows that, for example, if the perturbation size γ is equal to the 10% of the value of \bar{k}_{te} then the mechanical rigidity varies between $1.9527 \cdot 10^8$ N·m and $2.3543 \cdot 10^8$ N·m and the resonance frequencies have a standard deviation of about 80%. In the literature, the stiffness values used in numerical simulations can change a lot, so a choice of such a perturbation size may not be excessive. However, the influences due to the physical perturbations of the pressurized oil can hardly exceed the value of $\gamma = \bar{k}_{te}/10$, but since there are no studies focused on the perturbations of the mechanical stiffness of the oil meatus, we decided to present also the two extreme cases ($\gamma = \bar{k}_{te}/2$, $\gamma = \bar{k}_{te}/5$) where the standard deviation of the frequency is much higher.

The results, although preliminary, shown in this thesis and the interest of the European Space Agency (ESA) [9] in the field of uncertainty quantification (UQ) make the work done particularly interesting with possible developments.

A first improvement may be to develop the stochastic collocation approach in engineering simulations based on Finite Element method (FEM). This, however, has a major limitation at implementation level, in fact, numerical simulations are performed on commercial software that does not involve the use of collocation methods, so we should implement a code that is able to include this type of models. The second improvement lies in this last observation, in fact to improve the reliability of numerical experiments it would be interesting to make some tests on the variation of the oil meatus rigidity, obtaining more experimental data and with the statistical models present in the literature, see some in [12], it would be possible to have more information on the probability distributions of the uncertainty so as to build *ad hoc* numerical methods.

At the scientific level, in conclusion, it can be interesting and useful to better understand the uncertainty fluctuations of the satellite physical properties, both by performing more targeted tests for the oil meatus and by building more complex numerical simulation codes using innovative stochastic approaches that allow to reduce the computational costs that are fundamental in the company.

Appendix A

Analytical Mechanics

In this chapter we introduce some of the basic concepts of Analytical Mechanics, which give us a rigorous procedure to build a mathematical model for the satellite physical system. The material presented is based on [1].

A.1 Free coordinates and virtual displacements

Let us define *free coordinate system* for a set of configurations \mathcal{C} , the correspondence that associates a set of real numbers $(q_1, \dots, q_N) \in \mathcal{U} \subseteq \mathbb{R}^N$, at each instant of time t , to a configuration in \mathcal{C} . The set \mathcal{U} has to be connected and open. The function

$$P(q_1, \dots, q_N; t) \tag{A.1}$$

assigns the *position* of the point when the parameters (q_1, \dots, q_N) change. The corresponding motion of P depends on the N -functions $q_k(t)$, with $k = 1, \dots, N$

$$P(t) = P(q_1(t), \dots, q_N(t); t) \tag{A.2}$$

By differentiating the position in time it is possible to obtain the velocity of a generic point P

$$\mathbf{v}_P = \frac{dP}{dt} = \sum_{k=1}^N \frac{\partial P}{\partial q_k} \dot{q}_k + \frac{\partial P}{\partial t} \tag{A.3}$$

which implies

$$dP = \mathbf{v}_P dt = \sum_{k=1}^N \frac{\partial P}{\partial q_k} dq_k + \frac{\partial P}{\partial t} dt \tag{A.4}$$

Finally we define the *virtual displacement* (velocity, respectively) as the displacement (velocity, respectively) instantaneously consistent with the constraint, and their expressions are

$$\delta P = \sum_{k=1}^N \frac{\partial P}{\partial q_k} \delta q_k, \quad \mathbf{v}'(P) = \sum_{k=1}^N \frac{\partial P}{\partial q_k} \nu_k \tag{A.5}$$

Note that δP is used to indicate the virtual displacement and to distinguish it from the infinitesimal displacement dP . While δq_k are the virtual increments of the Lagrangian coordinates and ν_k are the virtual variations in time of the Lagrangian coordinates. In both cases, the compatibility with system constraints is taken into account, but this does not necessarily refer to the displacement of point P .

A.1.1 Work

Let us suppose that the active force $\mathbf{F}(P, \mathbf{v}, t)$ and the corresponding motion $P(t)$ are known. Then we define the differential form of the *work* as

$$dL = \mathbf{F}(P(t), \mathbf{v}_P(t), t) \cdot \mathbf{v}_P(t) dt = \Pi(t) dt \quad (\text{A.6})$$

where

$$\Pi = \mathbf{F} \cdot \mathbf{v}_P \quad (\text{A.7})$$

is the *power*. If we consider a system of forces \mathbf{F}_i applied to the points $\{P_i\}$, with $i = 1, \dots, n$, described by the (q_1, \dots, q_N) free coordinates, we call *elementary work*

$$dL = \sum_{i=1}^n \mathbf{F}_i \cdot dP_i \quad (\text{A.8})$$

and *virtual work*

$$\delta L = \sum_{i=1}^n \mathbf{F}_i \cdot \delta P_i \quad (\text{A.9})$$

and using the (A.5) we obtain

$$\delta L = \sum_{i=1}^n \mathbf{F}_i \cdot \left(\sum_{k=1}^N \frac{\partial P}{\partial q_k} \delta q_k \right) = \sum_{k=1}^N \sum_{i=1}^n \left(\mathbf{F}_i \cdot \frac{\partial P}{\partial q_k} \right) \delta q_k = \sum_{k=1}^N Q_k \delta q_k \quad (\text{A.10})$$

where $\mathbf{Q} = \{Q_k\}_{k=1}^N$ is the *generalized force* and its components are the *lagrangian components of the active force*.

If the system of forces is conservative with potential U then the elementary work becomes an exact differential $\delta L = \delta U$, and $dL = dU$. From the previous expressions we have that

$$Q_k = \frac{\partial U}{\partial q_k}, \quad k = 1, \dots, N \quad (\text{A.11})$$

A.2 Static and virtual work principle

The laws of mechanics make it possible to study every type of motion, once the forces and the initial conditions are known. Let us introduce the equation

$$m\mathbf{a} = \mathbf{F}(P, \mathbf{v}). \quad (\text{A.12})$$

Definition A.1. A configuration P^* is called an *equilibrium* if

$$\mathbf{F}(P^*, 0) = 0. \quad (\text{A.13})$$

where $P(t) = P^*$, for each $t \geq t_0$, is a constant solution of (A.12), and it corresponds to the initial conditions $P(t_0) = P^*$, $\mathbf{v}(t_0) = 0$.

Definition A.2. The ideal constraints are those capable of performing the systems of constraining reactions Φ such that

$$\delta L^{(c)} = \Phi \cdot \delta P \geq 0, \quad \forall \delta P$$

starting from an equilibrium configuration.

Definition A.3. A constraint is called *bilateral* if each virtual displacement (or velocity) is reversible. While a bilateral constraint that can be expressed as

$$f(q_1, \dots, q_N; t) = 0$$

is called *holonomic*.

In order to characterize the equilibrium configurations of a generic mechanical system, it is important to present a fundamental theorem, see [1] for the proof.

Theorem A.1 (Virtual Work Theorem). *Let $\delta L^{(a)}$ be the virtual work obtained by active force. The necessary and sufficient condition so that a configuration \mathcal{C} is in equilibrium for a mechanical system with ideal constraints, is that*

$$\delta L^{(a)} \leq 0, \quad \forall \delta P \text{ from } \mathcal{C} \quad (\text{A.14})$$

or

$$\delta L^{(a)} = 0, \quad \forall \delta P \text{ reversible from } \mathcal{C} \quad (\text{A.15})$$

A.3 Kinetic Energy

The *kinetic energy* is the scalar defined as

$$T = \frac{1}{2} \sum_{i=1}^n m_i v_i^2 \quad (\text{A.16})$$

while for a general material system is expressed

$$T = \frac{1}{2} m v_G^2 + T^{(G)} \quad (\text{A.17})$$

i.e. the sum of the kinetic energy of the CoG and the kinetic energy of the system in a relative motion with respect to the CoG. Moreover, if we substitute the definition of the velocity v_i (A.3)

$$v_i = \sum_{k=1}^N \frac{\partial P_i}{\partial q_k} \dot{q}_k + \frac{\partial P}{\partial t} \quad (\text{A.18})$$

the kinetic energy becomes

$$\begin{aligned} T &= \frac{1}{2} \sum_{i=1}^n m_i v_i^2 = \frac{1}{2} \sum_{i=1}^n m_i \left(\sum_{k=1}^N \frac{\partial P_i}{\partial q_k} \dot{q}_k + \frac{\partial P}{\partial t} \right) \cdot \left(\sum_{h=1}^N \frac{\partial P_i}{\partial q_h} \dot{q}_h + \frac{\partial P}{\partial t} \right) \\ &= \sum_{k=1}^N \sum_{h=1}^N \left(\sum_{i=1}^n \frac{1}{2} m_i \frac{\partial P_i}{\partial q_k} \frac{\partial P_i}{\partial q_h} \right) \dot{q}_k \dot{q}_h + \sum_{k=1}^N \left(\sum_{i=1}^n m_i \frac{\partial P_i}{\partial q_k} \frac{\partial P}{\partial t} \right) \dot{q}_k + \sum_{i=1}^n \frac{1}{2} m_i \frac{\partial P_i}{\partial t} \frac{\partial P_i}{\partial t} \\ &= \frac{1}{2} \sum_{k,h=1}^N a_{kh} \dot{q}_k \dot{q}_h + \sum_{k=1}^N b_k \dot{q}_k + c \end{aligned} \quad (\text{A.19})$$

The matrix

$$A = \begin{bmatrix} a_{11} & \dots & a_{1N} \\ \vdots & & \vdots \\ a_{N1} & \dots & a_{NN} \end{bmatrix} \text{ where } a_{kh} = \sum_{i=1}^n m_i \frac{\partial P_i}{\partial q_k} \frac{\partial P_i}{\partial q_h}, \quad k, h = 1, \dots, N$$

is called *mass matrix*.

A.4 Lagrangian Mechanics

In the previous section we introduced the virtual works principle, which is a procedure capable of forming equilibrium equations in constrained systems. We have to define the dynamic equivalent, *the d'Alembert Principle*.

Let us introduce the dragging force

$$\mathbf{F}_\tau = -m\mathbf{a} \quad (\text{A.20})$$

and it is called *inertia force*, then the fundamental law of the relative dynamics becomes

$$(\mathbf{F} - \mathbf{F}_\tau) + \phi = (\mathbf{F} - m\mathbf{a}) + \phi = \mathbf{0} \quad (\text{A.21})$$

where \mathbf{F} indicates the resultant of active forces, while ϕ is the resultant of the binding reactions. It can be generalized in

Theorem A.2 (The d'Alembert Principle). *Let us suppose that a system of $k \leq n$ active forces \mathbf{F}_i is applied to a system of material points $\{(P_i, m_i)\}$, with $i = 1, \dots, n$. So it is possible to pass from static equations*

$$\sum_{i=1}^k \mathbf{F}_i = \mathbf{0} \quad (\text{A.22})$$

to the dynamic equations, provided that all the inertia forces are included in the active forces as

$$\sum_{i=1}^k (\mathbf{F}_i - m_i \mathbf{a}_i) - \sum_{i=k+1}^n m_i \mathbf{a}_i = \mathbf{0}. \quad (\text{A.23})$$

If we apply the d'Alembert principle to the virtual work principle we obtain a fundamental concept of the Lagrangian mechanics

Theorem A.3 (Symbolic relation of dynamic). *Let $\{(P_i, m_i)\}$, with $i = 1, \dots, n$ be a system of free material points or subject to ideal constraints. The system $\{(P_i, \mathbf{F}_i)\}$, with $i = 1, \dots, n$ is a set of active forces applied to the points P_i . Necessary and sufficient condition for the set of accelerations $\{(P_i, \mathbf{a}_i)\}$, with $i = 1, \dots, n$, to provide system motion is that*

$$\sum_{i=1}^n (\mathbf{F}_i - m_i \mathbf{a}_i) \cdot \delta P_i \leq 0 \quad (\text{A.24})$$

while if the constraints are ideal and bilateral

$$\sum_{i=1}^n (\mathbf{F}_i - m_i \mathbf{a}_i) \cdot \delta P_i = 0 \quad (\text{A.25})$$

for each $\{(P_i, \delta P_i)\}_{i=1}^n$ admissible virtual displacement.

A.4.1 The Lagrange Equations

Let us consider a system with holonomic, ideal and bilateral constraints. Using the equation (A.5) in the (A.25) we obtain

$$\begin{aligned} \sum_{i=1}^n (\mathbf{F}_i - m_i \mathbf{a}_i) \cdot \delta P_i &= \sum_{i=1}^n (\mathbf{F}_i - m_i \mathbf{a}_i) \cdot \sum_{k=1}^N \frac{\partial P_i}{\partial q_k} \delta q_k = \\ \sum_{k=1}^N \left(\sum_{i=1}^n (\mathbf{F}_i - m_i \mathbf{a}_i) \cdot \frac{\partial P_i}{\partial q_k} \right) \delta q_k &= \sum_{k=1}^N (Q_k - \tau_k) \delta q_k = 0 \end{aligned} \quad (\text{A.26})$$

where τ_k are the *lagrangian components of the opposite of the inertial forces*. Let T be the kinetic energy then it is possible to prove that [1]

$$\tau_k = \frac{d}{dt} \left(\frac{\partial T}{\partial \dot{q}_k} \right) - \frac{\partial T}{\partial q_k}, \quad \forall k = 1, \dots, N. \quad (\text{A.27})$$

Therefore, substituting the (A.27) in (A.27) we obtain the *Lagrange equations*

$$\frac{d}{dt} \left(\frac{\partial T}{\partial \dot{q}_k} \right) - \frac{\partial T}{\partial q_k} = Q_k, \quad \forall k = 1, \dots, N \quad (\text{A.28})$$

A.4.2 Lagrangian Determinism

The motion equations (A.28) are second order differential equations in time. The Cauchy theorem guarantees the existence of one and only one solution to the initial-values problem, where position and velocity are assigned for each $t \geq 0$, as long as the forces are sufficiently regular on position and velocity.

Definition A.4. The function $f : D \subset \mathbb{R}^n \rightarrow \mathbb{R}$ is *Lipschitz continuous* in one or more variables (e.g. $x_1 \in [a, b]$) if there exists a constant K such that

$$|f(x_1'', \dots, x_n) - f(x_1', \dots, x_n)| \leq K|x_1'' - x_1'|, \quad \forall x_1', x_1'' \in [a, b], \quad \forall x_2, \dots, x_n. \quad (\text{A.29})$$

The Lagrange equations are *deterministic*, i.e. the knowledge of the act of motion in a certain time instant t_0 guarantees the complete characterization of the motion for some $t \geq t_0$. In fact it is possible to state the following theorem:

Theorem A.4. *Let us consider holonomous system with ideal and bilateral constraints, (q_1, \dots, q_N) are the free coordinates. The Cauchy problem, for each $k = 1, \dots, N$*

$$\begin{cases} \frac{d}{dt} \left(\frac{\partial T}{\partial \dot{q}_k} \right) - \frac{\partial T}{\partial q_k} = Q_k \\ q_k(t_0) = q_{k0} \quad \dot{q}_k(t_0) = \dot{q}_{k0} \end{cases} \quad (\text{A.30})$$

admits one and only one solution in at least an interval $t \in [t_0, t_1]$, with $t_1 > t_0$, if the Lagrangian components are Lipschitz continuous functions of the free coordinates and time derivatives.

If all the forces applied to system are conservative, their Lagrangian components may be expressed with the potential as (A.11). Moreover, due to the fact that the conservative forces are always positional, Q_k does not depend either on velocity or on time, we define the *Lagrange function* as $\mathcal{L}(q, \dot{q}, t) = T(q, \dot{q}, t) + U(q, \dot{q}, t)$ where

$$\frac{\partial \mathcal{L}}{\partial \dot{q}_k} = \frac{\partial(T + U)}{\partial \dot{q}_k} = \frac{\partial T}{\partial \dot{q}_k} \quad (\text{A.31})$$

and so the (A.28) becomes

$$\frac{d}{dt} \left(\frac{\partial \mathcal{L}}{\partial \dot{q}_k} \right) - \frac{\partial \mathcal{L}}{\partial q_k} = 0, \quad \forall k = 1, \dots, N \quad (\text{A.32})$$

Note that if there are both conservative (with potential U) and non conservative forces it is possible to define the Lagrange equations with the Lagrange function as

$$\frac{d}{dt} \left(\frac{\partial \mathcal{L}}{\partial \dot{q}_k} \right) - \frac{\partial \mathcal{L}}{\partial q_k} = Q_k^{n.c.}, \quad \forall k = 1, \dots, N \quad (\text{A.33})$$

where $Q_k^{n.c.}$ is the non conservative Lagrangian force.

A.5 Linearization of the motion equations

Let us define $q^0 = (q_1^0, \dots, q_N^0)$ the free coordinates corresponding to the equilibrium configurations. Using a variable transformation we write the free coordinates $q_k(t)$ close to q_k^0 as

$$q_k(t) = q_k^0 + \varepsilon \eta_k(t), \quad \forall k = 1, \dots, N \quad (\text{A.34})$$

where $0 < \varepsilon \ll 1$ and $|\eta| = \mathcal{O}(1)$. By substituting the variable transformation in the Lagrange equations we are able to linearize the motion equations.

Let us fix k , the Lagrange equation becomes

$$\frac{d}{dt} \left(\frac{\partial T}{\partial \dot{q}_k} \right) - \frac{\partial T}{\partial q_k} = \frac{\partial U}{\partial q_k} \quad (\text{A.35})$$

then, the linearized kinetic energy defined by (A.19) is

$$T = \frac{1}{2} \sum_{i,j} a_{ij}(q) \dot{q}_i \dot{q}_j = \frac{\varepsilon^2}{2} \sum_{i,j} a_{ij}(q_k^0 + \varepsilon \eta) \dot{\eta}_i \dot{\eta}_j = \frac{\varepsilon^2}{2} \dot{\eta}_i \cdot A(q_k^0 + \varepsilon \eta) \cdot \dot{\eta}_j \quad (\text{A.36})$$

and so the (A.35) is rewritten as

$$\varepsilon^2 \frac{d}{dt} \left(\sum_{j=1}^N a_{jk} \dot{\eta}_j \right) = \frac{\varepsilon^2}{2} \sum_{i,j=1}^N \left[\frac{\partial}{\partial \eta_k} a_{ij}(q_k^0 + \varepsilon \eta) \right] \dot{\eta}_i \dot{\eta}_j + \frac{\partial}{\partial \eta_k} U(q_k^0 + \varepsilon \eta) \quad (\text{A.37})$$

it is observed that all the terms are at least of the second order in the variable ε . Let us use the Taylor series in ε on the potential U as

$$\begin{aligned} U(q^0 + \varepsilon \eta) &= U(q^0) + \varepsilon \sum_{j=1}^N \left. \frac{\partial U}{\partial q_j} \right|_{q=q^0} \eta_j + \frac{\varepsilon^2}{2} \sum_{i,j=1}^N \left. \frac{\partial^2 U}{\partial q_j \partial q_i} \right|_{q=q^0} \eta_j \eta_i + o(\varepsilon^2) \\ &= U(q^0) + \frac{\varepsilon^2}{2} \sum_{i,j=1}^N b_{ij}^0 \eta_j \eta_i + o(\varepsilon^2) = U(q^0) + \frac{\varepsilon^2}{2} \eta \cdot B^0 \cdot \eta + o(\varepsilon^2) \end{aligned} \quad (\text{A.38})$$

note that the first sum is set to zero due to the stationary potential Theorem, see [1]. Differentiating (A.38), we obtain

$$\frac{\partial}{\partial \eta_k} U(q^0 + \varepsilon \eta) = \varepsilon^2 \sum_{j=1}^N b_{kj}^0 \eta_j + o(\varepsilon^2) \quad (\text{A.39})$$

Let us use the first order Taylor series in ε for the mass matrix A as

$$a_{ij}(q^0 + \varepsilon \eta) = a_{ij}(q^0) + \varepsilon \sum_{k=1}^N \left. \frac{\partial a_{ij}}{\partial q_k} \right|_{q=q^0} \eta_k + o(\varepsilon) \quad (\text{A.40})$$

hence

$$\frac{\partial}{\partial \eta_k} a_{ij}(q^0 + \varepsilon \eta) = \varepsilon \left. \frac{\partial a_{ij}}{\partial q_k} \right|_{q=q^0} \eta_k + o(\varepsilon) \quad (\text{A.41})$$

The partial derivatives are at least of the first order in ε and, therefore, the first term of the (A.37) is of order ε^3 , and it may be neglected. A similar consideration is made for the left-hand side of (A.37):

$$\begin{aligned} \varepsilon^2 \frac{d}{dt} \left(\sum_{j=1}^N a_{jk}(q^0 + \varepsilon\eta) \dot{\eta}_j \right) &= \varepsilon^2 \frac{d}{dt} \left(\sum_{j=1}^N a_{jk}(q^0) \dot{\eta}_j + O(\varepsilon) \right) \\ &= \varepsilon^2 \frac{d}{dt} \sum_{j=1}^N a_{jk}(q^0) \ddot{\eta}_j + O(\varepsilon) \end{aligned} \tag{A.42}$$

In conclusion, by combining the above observations we obtain the motion equations approximated to the second order

$$\begin{aligned} \sum_{j=1}^N A_{jk}^0 \ddot{\eta}_j &= \sum_{j=1}^N b_{jk}^0 \eta_j \\ A^0 \ddot{\eta} &= B^0 \eta \end{aligned} \tag{A.43}$$

where A^0 , B^0 are the mass matrix and the Hessian matrix of the potential U , respectively, both computed in equilibrium configuration q^0 .

Appendix B

Essentials of Probability Theory

In this chapter we will present some basic concepts of probability [2]-[8] and statistics computation [12].

B.1 Random variable

Firstly, we start with a collection of definitions and properties of the *measure theory* that will be useful later on.

Definition B.1. Let Σ be a non-empty set and $\mathcal{P}(\Sigma)$ a partition set of Σ . A set $\mathcal{A} \subseteq \mathcal{P}(\Sigma)$ is called a σ -algebra if

- $\Sigma \in \mathcal{A}, \emptyset \in \mathcal{A}$
- if $A \in \mathcal{A}$ then $A^c \in \mathcal{A}$
- $\forall (A_n)_{n \in \mathbb{N}}$ countable family of elements of \mathcal{A} then

$$\bigcup_{n \in \mathbb{N}} A_n \in \mathcal{A} \quad \text{and} \quad \bigcap_{n \in \mathbb{N}} A_n = \left(\bigcup_{n \in \mathbb{N}} A_n^c \right)^c \in \mathcal{A}$$

Note that if we take $\epsilon \subset \mathcal{P}(\Sigma)$ a collection of subset of Σ the intersection of all the σ -algebras (or σ -fields) which contains ϵ is the smallest σ -algebra containing ϵ . So $\sigma(\epsilon)$ is called σ -algebra generated by ϵ .

If Σ is a topological space, then the smallest σ -algebra on *Sigma* containing all open sets (or, equivalently, all closed sets) is called Borel σ -algebra.

Definition B.2. Let \mathcal{A} be a σ -algebra and $\mu : \mathcal{A} \rightarrow [0, \infty]$ a function such that $\mu(\emptyset) = 0$. μ is called a *measure* if it is σ -additive, which means that for all countable family $(A_n)_{n \in \mathbb{N}}$ of pairwise disjoint elements of \mathcal{A} we have that

$$\mu\left(\bigcup_{n \in \mathbb{N}} A_n\right) = \sum_n \mu(A_n)$$

Observe that if $\mu(\Sigma) = 1$ then μ is called a *probability measure*.

Note that the triplet $(\Sigma, \mathcal{A}, \mu)$, with \mathcal{A} a σ -algebra, is called a *measure space*, and each element of \mathcal{A} is a *measurable set*. While (Ω, \mathcal{F}, P) is a *probability space*, where \mathcal{F} is the σ -algebra of events and Ω is the a sample space which represents the possible results of a random phenomenon. Finally we can define $X : \Omega \rightarrow \mathbb{R}$ a *random variable* if

$$\{X \leq x\} = \{\omega \in \Omega : X(\omega) \leq x\} \in \mathcal{F}, \quad \forall x \in \mathbb{R} \quad (\text{B.1})$$

B.2 Probability Distributions

The concept of probability is used to measure the likelihood of the occurrence of certain events.

Definition B.3. Let the triplet (Ω, \mathcal{F}, P) be *probability space* and X a random variable. The function

$$F_X(x) = P(X \leq x) = P(\{\omega \in \Omega : X(\omega) \leq x\}), \quad x \in \mathbb{R} \quad (\text{B.2})$$

is the *distribution function* of X .

Some elementary properties of probability measures are easily summarized. For events $A, B \in \mathcal{F}$,

$$P(A \cup B) = P(A) + P(B) - P(A \cap B),$$

and if A and B are independent

$$P(A \cap B) = P(A) \cdot P(B)$$

Moreover

$$P(A^c) = 1 - P(A), \quad P(\Omega) = 1, \quad P(\emptyset) = 0.$$

B.2.1 Discrete Distributions

Let us take a countable set of values $\{x_1, \dots, x_k, \dots\}$. Suppose $X \in \{x_1, \dots, x_k, \dots\}$ is random variable then the sets

$$\{X = x_i\} \quad i = 1, 2, \dots$$

are events and so we can write

$$\{X \leq x\} = \bigcup_{x_i \leq x} \{X = x_i\}.$$

Now defining $p : \mathbb{R} \rightarrow \mathbb{R}^+$ as $p_i = p(x_i) = P(X = x_i)$, p enjoys the same properties as probabilities

$$0 \leq p(x_i) \leq 1, \quad \forall i, \quad \sum_i p(x_i) = 1 \quad (\text{B.3})$$

and so it is called a *probability density*, while the distribution is defined as

$$F_X(x) = \sum_i p_i = \sum_i p(x_i) \quad (\text{B.4})$$

and it is called a *discrete* distribution. The random variable X with a distribution like (B.4) is a discrete random variable.

In probability literature, there are two important discrete distributions:

- *Binomial* distribution $B(n, p)$ with $n \in \mathbb{N}_0$ and $p \in [0, 1]$ where

$$P(X = x_k) = \binom{n}{x_k} p^{x_k} (1-p)^{(n-x_k)}, \quad x_k \in \{0, 1, 2, \dots\}; \quad (\text{B.5})$$

- *Poisson* distribution $P(\lambda)$ with parameter $\lambda > 0$ and

$$P(X = x_k) = \frac{e^{-\lambda}}{x_k!} \lambda^{x_k}, \quad x_k \in \{0, 1, 2, \dots\}. \quad (\text{B.6})$$

B.2.2 Continuous Distributions

In contrast to discrete distributions and random variables taking values in a numerable set, we define a distribution and random variables which may take on values in \mathbb{R} . These types of variables are called *continuous* variable and distribution.

The probability density of a continuous random variable X is a non-negative function $f_X(x) \geq 0$ such that

$$P(X \in A) = \int_A f_X(x) dx, \quad A \in B(\mathbb{R}) \quad (\text{B.7})$$

where $B(\mathbb{R})$ is the Borel σ -algebra. A continuous random variable takes any precise value with probability 0

$$P(X = x) = 0, \quad \forall x \in \mathbb{R}. \quad (\text{B.8})$$

The distribution of a continuous random variable is defined as

$$F_X(x) = P(X \leq x) = \int_{-\infty}^x f(x) dx, \quad x \in \mathbb{R} \quad (\text{B.9})$$

Definition B.4. Let us define two random variables X and Y . They are *independent* if and only if

$$F_{(X,Y)}(x, y) = F_X(x)F_Y(y), \quad \forall x, y \in \mathbb{R} \quad (\text{B.10})$$

where $F_{(X,Y)}(x, y)$ is the *joint distribution function* and $F_X(x)$ and $F_Y(y)$ are their *marginal distribution function*.

We will deal here with three important continuous distributions

- *Uniform* distribution $U(a, b)$ with density

$$f_X(x) = \frac{1}{b-a} \chi_{(a,b)}(x) \quad (\text{B.11})$$

where $\chi_{(a,b)}(x)$ is called the characteristic function and is 1 when $x \in (a, b)$, 0 otherwise.

- *Exponential* distribution $Exp(\lambda)$ with $\lambda > 0$, where

$$f_X(x) = \lambda e^{-\lambda x}, \quad x > 0. \quad (\text{B.12})$$

- *Gaussian* or *Normal* distribution $N(\mu, \sigma^2)$ and

$$f_X(x) = \frac{1}{\sqrt{2\pi\sigma^2}} \exp\left[-\frac{(x-\mu)^2}{2\sigma^2}\right], \quad \mu \in \mathbb{R}, \quad \sigma > 0 \quad (\text{B.13})$$

note that $N(0,1)$ is called standard Gaussian

B.2.3 Expectation and Moments Theory

Let us take (Ω, \mathcal{F}, P) a probability space and continuous random variable X with density f_X . We can define $g : \mathbb{R} \rightarrow \mathbb{R}$ a measurable function such that

$$g \circ X \in L^1((\Omega, \mathcal{F}, P)) \Leftrightarrow g \in L^1((\mathbb{R}, B(\mathbb{R}), f_X)) \quad (\text{B.14})$$

the integral

$$\mathbb{E}(g(X)) = \int_{-\infty}^{\infty} g(x) f_X(x) dx \quad (\text{B.15})$$

is defined as the *expectation* or *mean value* of $g(X)$. Note that if $X \in L^1((\Omega, \mathcal{F}, P))$ then the mean value of the continuous random variable X is

$$\mathbb{E}(X) = \int_{-\infty}^{\infty} x f_X(x) dx \quad (\text{B.16})$$

while if $X \in L^m((\Omega, \mathcal{F}, P))$ we can define the *moment* of order m of X as

$$\mathbb{E}(X^m) = \int_{-\infty}^{\infty} x^m f_X(x) dx \quad (\text{B.17})$$

the integral

$$\mathbb{E}((X - \mathbb{E}(X))^m) = \int_{-\infty}^{\infty} (x - \mathbb{E}(X))^m f_X(x) dx \quad (\text{B.18})$$

is called the centered moment of order m . The centered moment of order 2 is called *variance*

$$\text{Var}(X) = \mathbb{E}((X - \mathbb{E}(X))^2) = \int_{-\infty}^{\infty} (x - \mathbb{E}(X))^2 f_X(x) dx \quad (\text{B.19})$$

and its square root is the *deviation error*, in fact the latter represents the deviation from the mean value.

Similarly, for a discrete random variable X with probability $p_i = P(X = x_i)$, we have

$$\begin{aligned} \mathbb{E}(X) &= \sum_{i=1}^n x_i p_i \\ \text{Var}(X) &= \mathbb{E}((X - \mathbb{E}(X))^2) = \sum_{i=1}^n (x_i - \mathbb{E}(X))^2 p_i \end{aligned} \quad (\text{B.20})$$

Here we present some important properties of the expectations, let us take two random variables X, Y , we have:

- *Linearity*: $\mathbb{E}(aX + bY) = a\mathbb{E}(X) + b\mathbb{E}(Y)$
- *Product*: $\mathbb{E}(XY) = \mathbb{E}(X)\mathbb{E}(Y)$ if X, Y are independent
- *Jensen inequality*: If g is a convex function

$$\mathbb{E}(g(X)) \geq g(\mathbb{E}(X)) \quad (\text{B.21})$$

- *Markov inequality*: if X is a non-negative random variable, then for all $r > 0$

$$P(X \geq r) \leq \frac{\mathbb{E}(X)}{r} \quad (\text{B.22})$$

- *Chebyshev inequality*: if X random variable with mean μ and finite variance σ^2 , then for all $r > 0$

$$P(|X - \mu| \geq r) \leq \frac{\sigma^2}{r} \quad (\text{B.23})$$

Definition B.5. Let (Ω, \mathcal{F}, P) be a probability space and X a random variable. We can define the *characteristic function* of X , the complex valued function

$$\phi_x(t) = \mathbb{E}(e^{itx}) = \int_{-\infty}^{\infty} e^{itx} f_X(x) dx, \quad \forall t \in \mathbb{R} \quad (\text{B.24})$$

Note that all the definitions and properties can be extended to $\mathbf{X} = (X_1, \dots, X_n)$ n -dimensional random vector.

B.2.4 Convergence of Random Variables and Limit Theorems

Let (Ω, \mathcal{F}, P) be a probability space and $(X_n)_{n \in \mathbb{N}}$ a sequence of random variables.

Definition B.6. The sequence $(X_n)_{n \in \mathbb{N}}$ converges *almost surely* (or *a.s.*) to X if

$$P(\{\omega \in \Omega : X_n(\omega) \rightarrow X(\omega)\}) = P(X_n \rightarrow X) = 1, \quad n \rightarrow \infty \quad (\text{B.25})$$

can be written as $X_n \xrightarrow{a.s.} X$

Definition B.7. The sequence $(X_n)_{n \in \mathbb{N}}$ converges in *probability* to X if $\forall \varepsilon > 0$

$$\lim_{n \rightarrow \infty} P(|X_n - X| > \varepsilon) = \lim_{n \rightarrow \infty} P(\{\omega \in \Omega : |X_n(\omega) - X(\omega)| > \varepsilon\}) = 0 \quad (\text{B.26})$$

it is written as $X_n \xrightarrow{P} X$

Definition B.8. The sequence $(X_n)_{n \in \mathbb{N}}$ with $X \in L^p(\Omega, \mathcal{F}, P)$, $p \geq 1$, converges in *p -th mean* (or in norm L^p) to X if

$$\|X_n - X\|_{L^p(\Omega, \mathcal{F}, P)}^p = \mathbb{E}(|X_n - X|^p) \rightarrow 0, \quad n \rightarrow \infty \quad (\text{B.27})$$

it is written as $X_n \xrightarrow{L^p} X$.

We have to observe that if we set $q < p$ ($L^q \subset L^p$), if $X_n \xrightarrow{L^p} X$ then $X_n \xrightarrow{L^q} X$. Moreover let $p = 2$ if $X_n \xrightarrow{L^2} a$ then $\mathbb{E}(X_n) \rightarrow a$ and $\text{Var}(X_n) \rightarrow 0$, where a is a constant.

Convergence in p -th mean implies convergence in probability, while the viceversa is true if the sequence is uniformly bounded as $|X_n| \leq M, \forall n$. Convergence in probability does not imply a.s. convergence, whereas the opposite is true. However, if $X_n \xrightarrow{P} X$ then $X_{n_k} \xrightarrow{a.s.} X$ for a suitable subsequence (X_{n_k}) .

Definition B.9. Let $\mu_n, n \in \mathbb{N}$, and μ be a finite measure on $(\mathbb{R}, B(\mathbb{R}))$. It is said that $(\mu_n)_n$ converges *weakly* to μ if, $\forall f \in C_b(\mathbb{R})$ (continuous and bounded)

$$\int_{\mathbb{R}} f d\mu_n \rightarrow \int_{\mathbb{R}} f d\mu, \quad n \rightarrow \infty \quad (\text{B.28})$$

where these are the *Lebesgue* integrals. It is written as $X_n \rightharpoonup X$

Definition B.10. The sequence $(X_n)_{n \in \mathbb{N}}$ converges in law (or in *distribution*) to X if the sequence of the laws P_{X_n} converges weakly to the law P_X , or $\forall f \in C_b(\mathbb{R})$

$$\int_{\mathbb{R}} f dP_{X_n} \rightarrow \int_{\mathbb{R}} f dP_X \Leftrightarrow \mathbb{E}(f(X_n)) \rightarrow \mathbb{E}(f(X)), \quad n \rightarrow \infty \quad (\text{B.29})$$

it is written as $X_n \xrightarrow{d} X$. Note that

$$X_n \xrightarrow{d} X \quad \text{if and only if} \quad F_{X_n}(x) \rightarrow F_X(x), \quad n \rightarrow \infty \quad (\text{B.30})$$

for all points x where the distribution function F_X is continuous.

We have to observe that if $X_n \xrightarrow{P} X$ then $X_n \xrightarrow{d} X$.

This overview of definitions is preparatory to understand one of the most important theorems of probabilistic literature: *Central Limit Theorem*, the proof is not reported (see [2]); the latter will be necessary to understand the characteristics of the methods in previous chapters. Firstly we have to state a theorem that we present without proof.

Theorem B.1 (Paul Lévy). *Let $(X_n)_{n \in \mathbb{N}}$ a sequence of real random variables with characteristic function $(\phi_{X_n})_n$ so*

- If $X_n \xrightarrow{d} X$ then $\forall t \in \mathbb{R}$

$$\lim_{n \rightarrow \infty} \phi_{X_n}(t) = \phi_X(t) \quad (\text{B.31})$$

with ϕ_X characteristic function of the random variable X

- If $\forall t \in \mathbb{R}$

$$\lim_{n \rightarrow \infty} \phi_{X_n}(t) = \varphi(t) \quad (\text{B.32})$$

with φ continuous in 0, then there exists a random variable X such that $\varphi = \phi_X$ and then $X_n \xrightarrow{d} X$.

Note that the two items of this theorem correspond to the necessary and sufficient condition to make the theorem true.

Central Limit Theorem

Theorem B.2. *Let $(X_n)_{n \in \mathbb{N}}$ be a sequence of independent real random variable in $L^2(\Omega, \mathcal{F}, P)$ with mean value μ and variance σ^2 .*

Set $S_n = \sum_{i=1}^n X_i$ and S_n^ its standardization with null mean and unitary variance. Then it can be stated that*

$$S_n^* \xrightarrow{d} N(0,1), \quad n \rightarrow \infty \quad (\text{B.33})$$

Note that the theorem could be re-written as

$$\sqrt{n}(\bar{X}_n - \mu) \xrightarrow{d} N(0, \sigma^2) \quad (\text{B.34})$$

where $\bar{X}_n = \frac{S_n}{n}$ is called the *sample mean*.

B.3 Simulation of Random Variables

Let F_X be the distribution function of a random variable X . One of the basic tasks in a stochastic simulation is to generate x_1, \dots, x_N realizations from the i.i.d. variables X_1, \dots, X_N ¹ with F_X . Note that x_1, \dots, x_N are just numbers, however the tricky part of this problem is to generate N numbers that well represent the distribution assigned experimentally.

Before going further in the analysis of the statistical simulation we have to present some definitions and properties.

Definition B.11. Let X be a random variable with distribution function F_X . The *quantile function* is defined as

$$Q : u \in (0,1) \mapsto Q(u) = \inf\{x : u \leq F_X(x)\} \quad (\text{B.35})$$

For a fixed u , $Q(u)$ is called the *u-quantile*.

It should be noted that the quantile function Q for a random variable X is a non-decreasing and left continuous function. It has jump points at constant traits of F_X . For each $u \in (0,1)$ and $x \in \mathbb{R}$ the following conditions are equivalent:

$$Q(u) \leq x, \quad u \leq F_X(x) \quad (\text{B.36})$$

and so if the distribution function is invertible, then $Q = F_X^{-1}$.

We observe that if the variable X has quantile function Q and U is a uniform random variable in $(0,1)$, then X and $Q(U)$ have the same distribution, in fact

$$P(Q(U) \leq x) = P(U \leq F_X(x)) = \int_0^{F_X(x)} du = F_X(x). \quad (\text{B.37})$$

Some sort of inverse property can be proved, indeed if X has a continuous distribution function F_X in each x then the random variable $F_X(X)$ is a $U(0,1)$:

$$P(F_X(X) \leq u) = P(X \leq Q(u)) = F_X(Q(u)) = u \quad (\text{B.38})$$

Now we have all the tools to generate a *simulation flux*, which is the numerical sequence x_1, \dots, x_N artificially generated as realizations of random variables X_1, \dots, X_N i.i.d. with distribution F_X . This problem could be split in two sub-problems:

1. Generate a numerical flux u_1, \dots, u_N from a $U(0,1)$;
2. Obtain x_1, \dots, x_N from u_1, \dots, u_N .

To solve the first sub-problem there are many available algorithms that could generate a "random" sequence of uniformly distributed values in the interval $[0,1]$; however these algorithms use a deterministic implementation to generate them, as recursion. For this reason the sequence of outputs u_1, \dots, u_N is called a sequence of *pseudorandom numbers*.

It is clear now the use of the words "artificially generated", in fact the uniform flux is generated by a computer which uses algorithms, the latter are not specifically analysed here, see [12].

The second sub-problem, we can use the definitions and properties explained previously. In fact we can generate x_1, \dots, x_N realizations with distribution F_X using the quantile function

$$x_1 = Q(u_1), x_2 = Q(u_2), \dots, x_N = Q(u_N). \quad (\text{B.39})$$

¹independent and identically distributed

Note that for each distribution F_X *ad hoc* algorithms have been studied which could exploit the properties of the distribution functions. For example, to generate two random realizations z_1, z_2 from a $N(0,1)$ there is the *Box-Muller* algorithm, see [12].

Multivariate simulation

In the previous section we described the univariate simulation, using a pseudorandom numerical flux u_1, \dots, u_N to rebuild the realizations x_1, \dots, x_N of random variables X_1, \dots, X_N with F_X . This is granted in \mathbb{R} , however is no longer valid in \mathbb{R}^n because this space is not sorted. Often a multivariate random generation is based on multiples univariate simulations. For example, if the distribution of the variable \mathbf{X} , which is a random vector, permit the representation with DAG². We can use the conditional densities to generate the numerical flux desired.

B.4 Statistical Tools

Suppose we are on the opposite side of what has been described above. We have experimental data which are the representation of a random variable with an unknown distribution. In this case it is easy to imagine we have to build some methods or models which allow us to calculate quantities useful for the analysis and the well understanding of the data behavior.

Definition B.12. A *sample* is a random variable $\{X_1, \dots, X_n\}$ represented by data, or by experimental observations. A *statistics* is a function $S = T(X_1, \dots, X_n)$ and its distribution is called a *sample distribution*.

It is important to understand that a statistics is a function of data only and is not a random variable. The most used statistics are the *sample mean*, defined as

$$\bar{X} = \frac{1}{n} \sum_{i=1}^n X_i \tag{B.40}$$

and the *sample variance*

$$S^2 = \frac{1}{n-1} \sum_{i=1}^n (X_i - \bar{X})^2 \tag{B.41}$$

It is not easy to obtain the sample distribution of a statistics, there are basically two alternatives: the exact calculus and the approximated one. The first way uses probability methods to calculate exactly the distribution, however this approach is not always possible or it proves to be exaggeratedly difficult. So often, in mathematical statistics, the approximation with the Central Limit Theorem is used obtaining the *asymptotic distribution*. This method applies for large n and is based on substituting the sample distribution with its limit value. For example, let X_1, \dots, X_n be a sample of a random variable with mean μ , such that $\mu \neq 0$ and with finite fourth moment $\mu_4 = \mathbb{E}((X - \mu)^4)$; for the central limit theorem we have that

$$\sqrt{n}(\bar{X}_n - \mu) \xrightarrow{d} N(0, \sigma^2) \tag{B.42}$$

and

$$\sqrt{n}(S_n^2 - \sigma^2) \xrightarrow{d} N(0, \mu_4 - \sigma^2) \tag{B.43}$$

²Directional Acyclic Graph

Appendix C

Integral calculus and Orthogonal Polynomials

C.1 Introduction to numerical integral calculus

In this chapter we will analyse how to evaluate numerically definite integrals [10]

$$I(f) = \int_a^b f(x)dx \quad (\text{C.1})$$

Often the analytic way may results impossible or unnecessarily complex; moreover, if the function $f(x)$ is known by points or evaluable for each x with a routine, the analytical approach has to be discarded.

Suppose to know the function $f(x)$ by points $\{x_i\}$, chosen arbitrarily or calculated. We examine the construction of the *quadrature formulas* as

$$\int_a^b f(x)dx \approx \sum_{i=1}^n w_i f(x_i) \quad (\text{C.2})$$

where x_i are called *nodes*, while w_i are the *weights* of the quadrature formula.

Assign distinct nodes $\{x_i\}$ and suppose the interval $[a, b]$ limited, we could approximated the function $f(x)$ with a polynomial $L_{n-1}(f; x)$ with $n-1$ degree, it is the only one who interpolates the function in the nodes:

$$\int_a^b f(x)dx = \int_a^b [L_{n-1}(f; x) + E_n(f; x)]dx = \int_a^b L_{n-1}(f; x)dx + \int_a^b E_n(f; x)dx$$

with

$$L_{n-1}(f; x) = f(x_i) \quad i = 1, \dots, n \quad (\text{C.3})$$

Suppose now that we represent $L_{n-1}(f; x)$ with the Lagrange form

$$L_{n-1}(f; x) = \sum_{i=1}^n l_i(x) f(x_i) \quad (\text{C.4})$$

we obtain

$$\int_a^b f(x)dx = \sum_{i=1}^n w_i f(x_i) + R_n(f) \quad (\text{C.5})$$

where

$$w_i = \int_a^b l_i(x) dx \tag{C.6}$$

while

$$R_n(f) = \int_a^b E_n(f; x) dx \tag{C.7}$$

represent the error of the quadrature formula. Note that this type of formulas are called *interpolatory*. They are considered to be exact, which means the error $R_n(f)$ is null, whenever $f(x)$ is a polynomial with degree lower or equals to $n - 1$.

A useful concept for comparing the accuracy degree of different quadrature formulas is the precision degree.

A quadrature formula has a *precision degree* d if it is exact when the integrand function $f(x)$ is a polynomial with degree lower or equals to d and there is at least one $d + 1$ polynomial for which the error is not null.

Suppose now we want to evaluate the integral $I(f)$ where the function $f(x)$ is factorized as

$$f(x) = w(x)g(x) \tag{C.8}$$

where $w(x)$ is a function which contains the singularity of $f(x)$, while $g(x)$ is the regular part of $f(x)$. We can generalize the approach defined in (C.5) and (C.6) so as to build an interpolation formula for the integral

$$\int_a^b w(x)g(x) dx \tag{C.9}$$

where (a, b) could be illimited.

Using Lagrange form, we have

$$g(x) = \sum_{i=1}^n l_i(x)g(x_i) + E_n(g; x) \tag{C.10}$$

and we obtain

$$\int_a^b w(x)g(x) dx = \sum_{i=1}^n w_i g(x_i) + R_n(g) \tag{C.11}$$

where

$$w_i = \int_a^b w(x)l_i(x) dx \tag{C.12}$$

and

$$R_n(f) = \int_a^b w(x)E_n(g; x) dx \tag{C.13}$$

The function $w(x)$ must be such as to permit the existence of the integrals and to permit the construction of the weights w_i . The formula (C.11) has at least a degree of accuracy equal to $n - 1$.

In order to have the (C.2) defined with a "good" *discretization* of the integral is necessary that

$$\lim_{n \rightarrow \infty} \sum_{i=1}^n w_i f(x_i) = \int_a^b f(x) dx \tag{C.14}$$

in that case we said that the formula is *convergent*. There are many condition that ensure the convergence. For example, if the interval (a, b) is limited and $f \in C[a, b]$ the convergence is guaranteed if

$$\sum_{i=1}^n |w_i| \leq K \tag{C.15}$$

where K is an independent constant from n . Note that the only condition that we imposed until now is that the nodes $\{x_i\}$ are supposed to be distinct, however it is possible to build different quadrature formulas choosing other approaches:

- equidistant nodes, Newton-Cotes Formulas ¹;
- nodes that are the zeros of orthogonal polynomials, Gaussian Formulas

C.2 Orthogonal Polynomials

Lets define a not negative and not null weight function $w(x)$ in the interval (a, b) that could be finite or infinite, then suppose that all the moment

$$m_k = \int_a^b w(x)x^k dx \quad k = 0, 1, \dots \tag{C.16}$$

exist. Define a polynomial system as

$$\{P_0(x), P_1(x), \dots, P_n(x), \dots\} \tag{C.17}$$

where

$$P_n(x) = k_{n,0}x^n + k_{n,1}x^{n-1} + \dots + k_{n,n} \quad \text{and} \quad k_{n,0} \neq 0 \tag{C.18}$$

is called a *Orthogonal polynomial* in (a, b) with respect to the weight function $w(x)$ if

$$\int_a^b w(x)P_n(x)P_m(x)dx = h_n\delta_{nm} \tag{C.19}$$

where δ_{nm} is the kronecker delta, note that

$$h_n = \int_a^b w(x)P_n^2(x)dx > 0 \quad n = 1, 2, \dots \tag{C.20}$$

and if $h_n = 1$ is called a *orthonormal polynomial*.

The interval (a, b) and the weight function $w(x)$ uniquely define the polynomials $P_n(x)$, up to not null constant. This concept is well explained in this theorem, which we report without proof.

Theorem C.1. *Each orthogonal polynomials system $\{P_n(x)\}$ satisfies a three-term recurrence relationship as:*

$$P_{n+1}(x) = (A_n x + B_n)P_n(x) - C_n P_{n-1}(x), \quad n = 1, 2, \dots \tag{C.21}$$

with $C_n > 0$. Where

$$A_n = \frac{k_{n+1,0}}{k_{n,0}} \quad B_n = A_n \left(\frac{k_{n+1,1}}{k_{n+1,0}} - \frac{k_{n,1}}{k_{n,0}} \right) \quad C_n = \frac{A_n}{A_{n-1}} \frac{h_n}{h_{n-1}}.$$

¹not taken into account here

This result allowed us to state that the system $\{P_n(x)\}$ defined by the couple $\{(a, b), w(x)\}$ could be uniquely identified by the coefficients $\{(A_n, B_n, C_n)\}$. For each $n > 1$ the orthogonal polynomial $P_n(x)$ has n real and distinct roots in the interval (a, b) . Moreover, the zeros of $P_n(x)$ alternate with those of $P_{n-1}(x)$. Then we can define another theorem.

Theorem C.2. For each polynomial $q(x)$ with degree lower or equals to $n - 1$ we have

$$\int_a^b w(x)P_n(x)q(x)dx = 0 \quad (\text{C.22})$$

In particular

$$\int_a^b w(x)P_n(x)x^k dx = 0 \quad k = 0, 1, \dots, n - 1 \quad (\text{C.23})$$

this last equation defined uniquely the orthogonal polynomial.

In literature are known some orthogonal polynomial that are called *classic*, here we see the most used:

- Legendre Polynomials $P_n(x)$: $w(x) = 1$, $(a, b) = (-1, 1)$

$$\begin{cases} P_0(x) = 1, & P_1(x) = x \\ (n + 1)P_{n+1}(x) = (2n + 1)xP_n(x) - nP_{n-1}(x), & n = 1, 2, \dots \end{cases} \quad (\text{C.24})$$

$$k_{n,0} = \frac{(2n)!}{2^n(n!)^2}, \quad h_n = \frac{2}{2n + 1}$$

- Laguerre Polynomials $L_n(x)$: $w(x) = e^{-x}$, $(a, b) = (0, \infty)$

$$\begin{cases} L_0(x) = 1, & L_1(x) = 1 - x \\ (n + 1)L_{n+1}(x) = (2n + 1 - x)L_n(x) - nL_{n-1}(x), & n = 1, 2, \dots \end{cases} \quad (\text{C.25})$$

$$k_{n,0} = \frac{(-1)^n}{n!}, \quad h_n = 1$$

- Hermite Polynomials $H_n(x)$: $w(x) = e^{-x^2}$, $(a, b) = (-\infty, \infty)$

$$\begin{cases} H_0(x) = 1, & H_1(x) = 2x \\ H_{n+1}(x) = 2xH_n(x) - 2nH_{n-1}(x), & n = 1, 2, \dots \end{cases} \quad (\text{C.26})$$

$$k_{n,0} = 2^n, \quad h_n = \sqrt{\pi}2^n n!$$

- Jacobi Polynomials $P_n^{\alpha, \beta}(x)$: $w(x) = (1 - x)^\alpha(1 + x)^\beta$, $\alpha, \beta > -1$, $(a, b) = (-1, 1)$

$$\begin{cases} P_0(x) = 1, & P_1(x) = [1 + \frac{1}{2}(\alpha + \beta)]x + \frac{1}{2}(\alpha - \beta) \\ 2(n + 1)(n + \alpha + \beta + 1)(2n + \alpha + \beta)P_{n+1}^{\alpha, \beta}(x) = \\ (2n + \alpha + \beta + 1)[(\alpha^2 - \beta^2) + (2n + \alpha + \beta + 2)(2n + \alpha + \beta)x]P_n^{\alpha, \beta}(x) - \\ 2(n + \alpha)(n + \beta)(2n + \alpha + \beta + 2)P_{n-1}^{\alpha, \beta}(x), & n = 1, 2, \dots \end{cases} \quad (\text{C.27})$$

$$k_{n,0} = 2^n \left[\binom{n + \alpha}{n} + \binom{n + \beta}{n} \right],$$

$$h_n = \frac{2^{\alpha + \beta + 1}}{2n + \alpha + \beta + 1} \cdot \frac{\Gamma(n + \alpha + 1)\Gamma(n + \beta + 1)}{n!\Gamma(n + \alpha + \beta + 1)}$$

C.3 Gaussian quadrature

In the previous section we proof that with n distinct nodes $\{x_i\}$ is possible to build a quadrature formula as (C.11) with at least a degree of accuracy equal to $n - 1$. However, we would like to choose a more convenient node assignment mode. So we suppose that :

- the weight function $w(x)$ has to be $w(x) \neq 0$ and $w(x) \geq 0$ in (a, b)
- all the moments exist, as $m_k = \int_a^b w(x)x^k < \infty$, with $k = 0, 1, \dots$

Firstly we have to observe that $2n - 1$ is the maximum precision degree reachable from a formula with n real nodes. In fact if we suppose by absurd that we could reach a precision degree of $2n$, we could define

$$f(x) = \prod_{i=1}^n (x - x_i)^2 \in \mathbb{P}_{2n} \tag{C.28}$$

so we have that

$$0 < \int_a^b w(x) \prod_{i=1}^n (x - x_i)^2 dx = \sum_{i=1}^n w_i \cdot 0 + R_n(f) = 0 \tag{C.29}$$

which is the absurd.

Therefore, we can state that the necessary and sufficient condition for the formula

$$\int_a^b w(x)f(x)dx = \sum_{i=1}^n w_i f(x_i) + R_n(f) \tag{C.30}$$

has precision degree equals to $2n-1$, and it is called *Gaussian*. Due to its precision degree, belongs to the class of interpolation formulas, while the nodes $\{x_i\}$ are the n zeros of the polynomial $P_n(x)$, with n degree, in (a, b) orthogonal to the weight function $w(x)$.

Let us try to find a representation of the weight w_i , so lets take in the equation (C.30)

$$f(x) = \frac{P_n(x)}{x - x_k} = \prod_{\substack{i=1 \\ i \neq k}}^n (x - x_i) \tag{C.31}$$

we obtain

$$\int_a^b w(x) \frac{P_n(x)}{x - x_k} dx = w_k P_n'(x_k) \tag{C.32}$$

and so

$$w_k = \frac{1}{P_n'(x_k)} \int_a^b w(x) \frac{P_n(x)}{x - x_k} dx \quad k = 1, 2, \dots, n \tag{C.33}$$

However, this expression does not highlights some important characteristics of the weight function, moreover it does not use the property of the Gaussian formulas, and so if we choose

$$f(x) = \left[\frac{P_n(x)}{x - x_k} \right]^2 \in \mathbb{P}_{2n-2} \tag{C.34}$$

we obtain

$$w_k = \frac{1}{[P_n'(x_k)]^2} \int_a^b w(x) \left[\frac{P_n(x)}{x - x_k} \right]^2 dx \quad k = 1, 2, \dots, n \tag{C.35}$$

this expression proof that the weights $\{w_i\}$ of the Gauss formulas are all positive, and this property in a limited interval (a, b) guarantees the convergence of the quadrature formulas for all $f(x) \in C[a, b]$, in fact it is easy to see that if we set $f(x) = 1$

$$\sum_{i=1}^n |w_i| = \sum_{i=1}^n w_i = \int_a^b w(x) dx < \infty. \quad (\text{C.36})$$

If we associate the *classic* orthogonal polynomial to the quadrature formula we obtain the *Classic Gaussian* formulas:

- *Gauss-Legendre* formula

$$\int_{-1}^1 f(x) dx \approx \sum_{i=1}^n w_i f(x_i) \quad (\text{C.37})$$

where $k_{n,0} \prod_{i=1}^n (x - x_i) = P_n(x)$ is the Legendre polynomial.

- *Gauss-Laguerre* formula

$$\int_0^\infty e^{-x} f(x) dx \approx \sum_{i=1}^n w_i f(x_i) \quad (\text{C.38})$$

where $k_{n,0} \prod_{i=1}^n (x - x_i) = L_n(x)$ is the Laguerre polynomial.

- *Gauss-Hermite* formula

$$\int_{-\infty}^\infty e^{-x^2} f(x) dx \approx \sum_{i=1}^n w_i f(x_i) \quad (\text{C.39})$$

where $k_{n,0} \prod_{i=1}^n (x - x_i) = H_n(x)$ is the Hermite polynomial.

- *Gauss-Jacobi* formula

$$\int_{-1}^1 (1-x)^\alpha (1+x)^\beta f(x) dx \approx \sum_{i=1}^n w_i f(x_i), \quad \alpha, \beta > -1 \quad (\text{C.40})$$

where $k_{n,0} \prod_{i=1}^n (x - x_i) = P_n^{(\alpha, \beta)}(x)$ is the Hermite polynomial.

C.4 Error estimation

Let we suppose that we have built a quadrature formula as

$$Q_n(f) = \sum_{i=1}^n w_i f(x_i) \quad (\text{C.41})$$

that approximate the integral

$$I(f) = \int_{-1}^1 w(x) f(x) dx \quad (\text{C.42})$$

For the interpolation formulas we have defined a representation of the integral error

$$R_n(f) = I(f) - Q_n(f) \quad (\text{C.43})$$

however this expression has only theoretical importance, usually you take another formula $Q_m(f)$ with more nodes ($m > n$), that is more precise and so

$$|R_n(f)| \approx |Q_m(f) - Q_n(f)| \tag{C.44}$$

where normally $m = n + 1$ when $f(x)$ is sufficiently regular, while $m \approx 2n$ in other cases. The couple $\{(Q_m(f), Q_n(f))\}$ costs $n + m$ evaluations of the function $\{f(x_i)\}$. If we take a Gaussian quadrature formula as

$$G_n(f) = \sum_{i=1}^n w_i f(x_i) \tag{C.45}$$

assuming

$$|R_n(f)| \approx |G_n(f) - G_{n+1}(f)| \tag{C.46}$$

we impose the calculus of $2n + 1$ values of $\{f(x_i)\}$, in fact $G_n(f)$ and $G_{n+1}(f)$ have not any nodes in common. Moreover, the degree of precision more accurate of the formula $G_{n+1}(f)$ is $2n + 1$.

Appendix D

Miscellaneous Topics

D.1 Runge-Kutta Method

In this section we describe briefly the Runge-Kutta method [10] for solving an ordinary differential equation system (ode) as

$$\begin{cases} \dot{y} &= f(x, t) \\ y(0) &= y_0 \end{cases} \quad (\text{D.1})$$

the algorithm is

$$\begin{aligned} y_{n+1} &= y_n + \frac{1}{6}(k_1 + 2k_2 + 2k_3 + k_4) \\ t_{n+1} &= t_n + h \end{aligned} \quad (\text{D.2})$$

for $n = 0, 1, 2, \dots$, where

$$\begin{aligned} k_1 &= hf(t_n, y_n) \\ k_2 &= hf\left(t_n + \frac{h}{2}, y_n + \frac{k_1}{2}\right) \\ k_3 &= hf\left(t_n + \frac{h}{2}, y_n + \frac{k_2}{2}\right) \\ k_4 &= hf(t_n + h, y_n + k_3) \end{aligned} \quad (\text{D.3})$$

D.2 Beta distribution and Gauss-Jacobi formula

Let us define X a random variable with general Beta distribution with probability density, [17]:

$$f_X(x) = \frac{(b-x)^\alpha (x-a)^\beta}{(b-a)^{(\alpha+\beta+1)} B(\alpha+1, \beta+1)}, \quad x \in [a, b], \quad \alpha, \beta > -1$$

where

$$B(\alpha+1, \beta+1) = \frac{\Gamma(\alpha+1)\Gamma(\beta+1)}{\Gamma(\alpha+\beta+2)}, \quad \text{note that } \Gamma(\alpha+1) = \alpha!$$

The Gauss-Jacobi formula to approximate the integral calculus is

$$\int_{-1}^1 (1-x)^\alpha (1+x)^\beta g(x) dx \approx \sum_{i=1}^n w_i g(x_i), \quad \alpha, \beta > -1$$

it is easy to note that the weight function of the Jacobi orthogonal polynomial is similar to the density function of a Beta distribution. Therefore, in order to calculate the mean of $g(Z)$, where $Z \sim \text{Beta}(\alpha, \beta)$ in $[a, b] = [-1, 1]$, we exploits the gPC Jacobi as

$$\begin{aligned} E(g(Z)) &= \frac{2^{-(\alpha+\beta+1)}}{B(\alpha+1, \beta+1)} \int_{-1}^1 (1-z)^\alpha (1+z)^\beta g(z) dx \\ &\approx \frac{2^{-(\alpha+\beta+1)}}{B(\alpha+1, \beta+1)} \sum_{i=1}^n w_i g(z_i) \\ &= \frac{\alpha! \beta!}{(\alpha+\beta+1)!} 2^{-(\alpha+\beta+1)} \sum_{i=1}^n w_i g(z_i), \quad \alpha, \beta > -1 \end{aligned}$$

D.3 1-Degree of Freedom

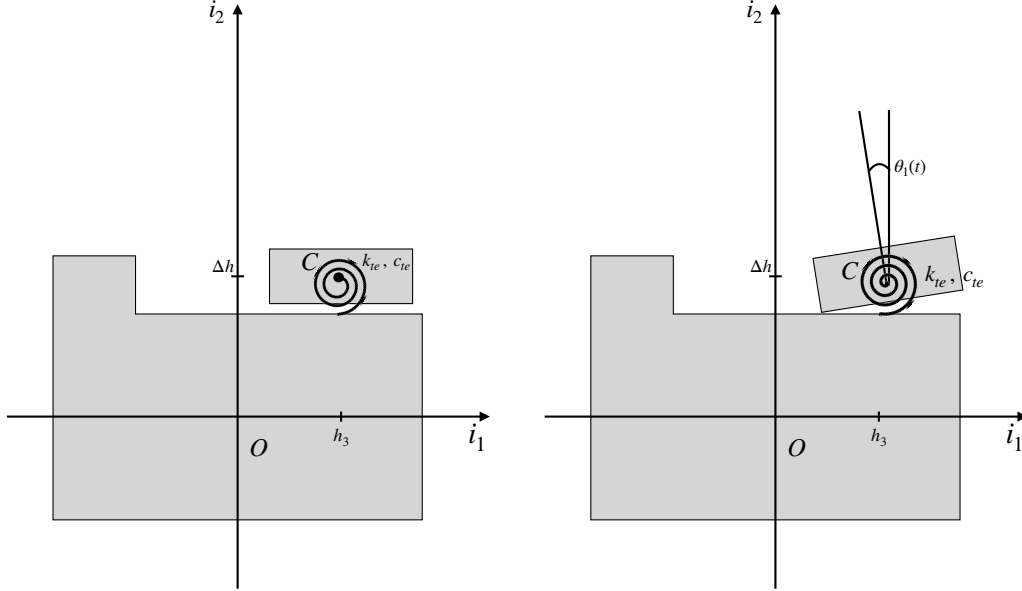


Figure D.1: *The single dof system at the initial condition $t = 0$ (on the left) and for $t > 0$ the free coordinate $\theta_1(t)$ (on the right) .*

Let us analyze the case with a single rotational degree of freedom of the system defined in Fig. 1.4. The free coordinate θ_1 is the rotation of the test article with respect to the plane of the fixed seismic mass. This study is trivial exercise of vibration mechanics [11] where the mass m can rotate and its motion is influenced by a torsional spring with damping (the oil meatus). From Fig. D.1, it is simple to get the equation of motion

$$I_m \ddot{\theta}_1 + c_{te} \dot{\theta}_1 + k_{te} \theta = 0 \quad (\text{D.4})$$

which is a second order ODE.
The characteristic polynomial

$$I_m s^2 + c_{te} s + k_{te} = 0,$$

whose roots are

$$s_{1,2} = \frac{-c_{te} \pm \sqrt{c_{te}^2 - 4k_{te}I_m}}{2I_m}.$$

Therefore, if

$$c_{te}^2 > -4k_{te}I_m, \quad (\text{D.5})$$

the solution of (D.4) writes

$$\theta_1(t) = A_1 e^{s_1 t} + A_2 e^{s_2 t}$$

where the constants A_1, A_2 are obtained through the initial conditions. We denote by $c_{cr} = 2\sqrt{k_{te}I_m}$ the *critical damping* and by $\zeta = c_{te}/c_{cr}$ the *damping factor*.

The natural pulse is defined as:

$$\omega = \sqrt{\frac{k_{te}}{I_m}}$$

while the pulse of the damped free oscillations is obtained with the formula

$$\omega_d = \omega \sqrt{1 - \zeta^2}.$$

provided $\zeta < 1$, which is consistent with the previous requirement (D.5). Using (3.71) we have the frequency of the free and damped oscillations:

$$f = \frac{\omega}{2\pi}, \quad f_d = f \sqrt{1 - \zeta^2}.$$

From this equation it can be seen that assuming k_{te} perturbed by a random variable Z , it is immediate to calculate the perturbed $f_d(Z)$, its mean value and the respective standard deviation. Note that with a small abuse of notation in the thesis we refer to f_d as f_{dr} because, with a number of degrees of freedom greater than one, the index r indicates the r -th mode, however in the sigle dof $r = 1$.

D.4 Equivalent oil meatus stiffness

The index of k_{te} stands for "*torsional equivalent*" stiffness of the spring, and its damping, which in the thesis represents the oil meatus. However, it is important to specify that this definition is a small abuse of notation, in fact the spring identified by k_{te} is actually obtained from the serial composition of two other springs with their stiffness, as follows:

$$k_{te} = \frac{k_t k_m}{k_t + k_m}$$

where $k_m = 2.7489 \cdot 10^9$ N·m is the rigidity of the oil meatus and $k_t = 2.3365 \cdot 10^8$ N·m is the torsional stiffness of the S/C. The technique of assigning a rigidity to the spacecraft corresponds to the same trick used in the k_{st} definition, these values are useful to make the study more similar to the experimental results [18]-[19].

The use in the thesis of k_{te} stiffness, for the analysis of the stochastic perturbations, does not bring either errors or binding suppositions.

Observe that in the thesis we assumed that the uncertainty perturbations are on the torsional equivalent stiffness k_{te} and not exactly on the rigidity of the oil meatus k_m . A possible improvement of the thesis, could be to perturb the k_m parameter and do the same calculations.

Bibliography

- [1] P. Biscari, T. Ruggeri, G. Saccomandi, M. Vianello - *Meccanica Razionale*, Springer - Verlag Italia (2014)
- [2] D. Xiu - *Numerical Methods for Stochastic Computations - A Spectral Method Approach*, Princeton University Press (2010)
- [3] D. Xiu, J. S. Hesthaven - High-Order Collocation Method for Differential Equations with Random Input - *SIAM J. SCI. COMPUT.* Vol. 27, No. 3, pp. 1118–1139, Society for Industrial and Applied Mathematics (2005)
- [4] D. Xiu, G. Em Karniadakis - The Wiener–Askey Polynomial Chaos for Stochastic Differential Equation - *SIAM J. SCI. COMPUT.* Vol. 24, No. 2, pp. 619–644, Society for Industrial and Applied Mathematics (2002)
- [5] D. Xiu - Efficient Collocational Approach for Parametric Uncertainty Analysis - *Commun. Comput. Phys.* Vol. 2, No. 2, pp. 293-309 (2007)
- [6] G. Zhang, M. Gunzburger - Error analysis of a stochastic collocation method for parabolic partial differential equations with random input data - *SIAM J. NUMER. ANAL.* Vol. 50, No. 4, pp. 1922–1940 (2012)
- [7] Y. Ma, X. Shen - Approximation Of Beta-jacobi Ensembles By Beta-laguerre Ensembles - *arXiv: 1807.03446*
- [8] R. E. Caflisch - Monte Carlo and quasi-Monte Carlo methods - *Acta Numerica*, pp . 1-49, (1998)
- [9] A. Calvi - Uncertainty-based loads analysis for spacecraft: Finite element model validation and dynamic responses - *Computers and Structures* 83, 1103–1112, (2005)
- [10] G. Monegato - *Metodi e algoritmi per il calcolo numerico*, C.L.U.T. Editrice (2008)
- [11] A. Fasana, S. Marchesiello - *Meccanica delle vibrazioni*, C.L.U.T. Editrice (2016)
- [12] M. Gasparini - *Modelli probabilistici e statistici - con temi d'esame*, C.L.U.T. Editrice (2014)
- [13] MSC Nastran - *Dynamic Analysis User's Guide* (2012)
- [14] L. A. Grzelak, J. A. S. Witteveen, M. Suárez-Taboada and C. W. Oosterlee - The stochastic collocation Monte Carlo sampler: highly efficient sampling from ‘expensive’ distributions, *Quantitative Finance*, 19:2, 339-356, (2019)

- [15] N. Wiener - The Homogeneous chaos - *American Journal of Mathematics*, Vol. 60, No. 4 , pp. 897-936 (Oct., 1938)
- [16] J.A. Carrillo, M. Zanella - Monte Carlo gPC Methods for Diffusive Kinetic Flocking Models with Uncertainties - *Vietnam Journal of Mathematics*, (Nov. 2019)
- [17] D. Sanjel, N. Balakrishnan - Jacobi and Laguerre polynomial approximations for the distributions of statistics useful in testing for outliers in exponential and gamma samples - *Journal of Statistical Computation and Simulation*, 82:3, 463-473, (2012)
- [18] P. Nali, A. Calvi, C. Casagrande, L. Caccamo, V. Di Pietro, P. Ladisa, G. Bitetti, F. Lumaca - From Virtual Shaker Testing to a handy analytical formulation for calculating the frequency down-shift of the S/C main lateral mode - *Proceedings of the Aerospace Testing Seminar*, Los Angeles, California, U.S.A., Oct. 2018
- [19] P. Nali, A. Calvi - A lower bound analytical estimation of the fundamental lateral frequency down-shift of items subjected to sine testing - *Advances in Aircraft and Spacecraft Science*, Vol. 7, No. 1 (2020) 79-90
- [20] E. Sauter - Sine Sweep Vibration Testing for Modal Response Primer - Department of Optical Sciences, University of Arizona, Tuscon, (2013)
- [21] V994 product data by Brüel and Kjær and Sound Vibration Measurement A/S · DK-2850 Nærum - Denmark, checked 8th February 2020
<https://www.bksv.com/en/products/shakers-and-exciter/LDS-shaker-systems/high-force-shakers/V994>
- [22] F. Giordano, M. N. Mazziotta, S. Rainò - Engineering Model Tower – Vibration Test Procedure - November 3, 2003 - LAT-TD-2363
- [23] Thales Alenia Space choose LDS V994 Shaker for Satellite Testing - 16th May 2011, checked 8th February 2020
<https://www.militarysystems-tech.com>